Molecular basis of IgE specificity and effector functions in allergic diseases

Dissertation

zur Erlangung des Doktorgrades der Naturwissenschaften

der Fakultät für Mathematik, Informatik und Naturwissenschaften
der Universität Hamburg

vorgelegt von

Frederic Jabs

aus Münster

Hamburg

2017

The experimental part of this work was performed from June 2014 until September 2017 in the group of Assoc. Prof. Dr. Edzard Spillner at the Department of Engineering at Aarhus University, Denmark.

Gutachter der Dissertation: Assoc. Prof. Dr. Edzard Spillner

Prof. Dr. Bernd Meyer

Gutachter der Disputation: Assoc. Prof. Dr. Edzard Spillner

Prof. Dr. Wolfgang Maison

Dr. Thomas Hackl

Datum der Disputation und Druckfreigabe der Dissertation: 26.01.2018

Für meine Eltern

Silvia & Hans-Ulrich Jabs

Publication list

"Trapping IgE in a closed conformation by mimicking CD23 binding prevents and disrupts interaction with FcεRI."
Jabs, F., Plum, M., Laursen, N.S., Jensen, R.K., Mølgaard B., Miehe, M., Mandolesi, M., Rauber, M.M., Pfützner, W., Jakob, T., Möbs, C., Andersen, G.R., Spillner, E.
Nature Communications, accepted **2017**.

"Phospholipase A1-based cross-reactivity among venoms of clinically relevant Hymenoptera from Neotropical and temperate regions."
Perez-Riverol, A., Romani Fernandes, L.G., Musacchio Lasac, A., dos Santos-Pintod, J.R.A., Moitinho Abramb, D., Izuka Moraesa, G.D., **Jabs, F.**, Miehe, M., Seismann, H., Palmad, M.S., de Lima Zollner, R., Spillner, E., Brochetto-Braga, M.R.
Molecular Immunology, 93, 87-93, **2017**.

"ATTACK, a novel bispecific T cell-recruiting antibody with trivalent EGFR binding and monovalent CD3 binding for cancer immunotherapy."
Lykke Harwood, S., Alvarez de Cienfuegos, A., Nuñez del Prado, N., Compte, M., Hernández Pérez, S., Merino, N., Bonet, J., Navarro, R., Bergen en Henegouwen, P., Lykkemark, S., Mikkelsen, K., Molgaard, K., **Jabs, F.**, Sanz, L., Blanco, F., Roda-Navarro, P., Alvarez-Vallina, L.
OncoImmunology, DOI: 10.1080/2162402X.2017.1377874, **2017**.

"Human IgE is efficiently produced in glycosylated and biologically active form in lepidopteran cells."
Bantleon F., Wolf S., Seismann H., Dam S., Lorentzen A., Miehe M., **Jabs F.**, Jakob T., Plum M., Spillner E.
Molecular Immunology, 72, 49-56, **2016**.

"Venoms of Neotropical wasps lack cross-reactive carbohydrate determinants enabling reliable protein-based sIgE determination."
Perez-Riverol, A., Miehe, M., **Jabs, F.**, Seismann, H., Romani Fernandes, L.G., de Lima Zollner, R., Brochetto-Braga, M.R., Spillner, E.
Submitted.

"**Red meat-allergic patients exhibit IgE reactivities to α-Gal and additional carbohydrate antigens with variant fine specificities**."

Jabs, F., Miehe, M., van Hage, M., Hoffmann, H.-J., Nentvic, I., Jappe, U., Seismann, H., Jakob, T., Plum, M., Spillner, E.

Submitted.

Table of Contents

I. Abbreviations

Å	Ångström
A	adenine
ABTS	2,2'-azino-bis(3-ethylbenzthiazoline-6-sulphonic acid)
ADAM	a disintegrin and metalloproteinase
ADCC	antibody-dependent cell-mediated cytotoxicity
ADCP	antibody-dependent cellular phagocytosis
alpha-Gal	galactose-α-1,3-galactose
AP	alkaline phosphatase
APC	antigen presenting cells
Api m	*Apis mellifera*
APS	ammonium persulfate
ATP	adenosine triphosphate
BAT	basophil activation test
BCIP	5-bromo-4-chloro-3-indolyl phosphate
Bet v	*Betula verrucosa*
bp	base pair
BSA	bovine serum albumin
C	cytosine
CCD	cross-reactive carbohydrate determinant
CD	cluster of differentiation
CDR	complementarity determining regions
CH	constant heavy chain
CHO	Chinese hamster ovary
CL	constant light chain
Ctrl	control
CV	column volume

DARPin	designed ankyrin repeat protein
DC	dendritic cell
ddH$_2$O	double distilled water
DMEM	Dulbecco's modified eagle medium
DMSO	dimethyl sulfoxide
DNA	deoxyribonucleic acid
dNTP	deoxynucleoside triphosphate
dpi	dots per inch
DTT	dithiothreitol
EBV	Epstein-Barr virus
E. coli	*Escherichia coli*
EDTA	ethylenediaminetetraacetic acid
e.g.	*exempli gratia* (for example)
EAACI	European Academy for Allergy and Clinical Immunology
ELIFAB	enzyme-linked immunosorbent facilitated antigen binding
ELISA	enzyme-linked immunosorbent assay
EM	electron microscopy
ER	endoplasmic reticulum
ESI	electrospray ionisation
TOF	time of flight
et al.	*et alii* (and others)
EU	European Union
Fab	fragment antigen binding
Fc	fragment crystallisable
FCS	foetal calf serum
FDA	Food and Drug Administration
Fig.	figure

FRET	Förster resonance energy transfer
FT	flow-through
Fuc	fucose
G	guanine
Gal	galactose
Glc	glucose
GlcNAc	*N*-acetyl-D-glucosamine
HCAbs	heavy chain antibodies
HEK	human embryonic kidney
HEPES	4-(2-hydroxyethyl)-1-piperazineethanesulphonic acid
HIC	hydrophobic interaction chromatography
His	histidine
HIV	human immunodeficiency virus
HRP	horseradish peroxidase
HSA	human serum albumin
hu	human
IC_{50}	half-maximal inhibitory concentration
IEX	ion exchange chromatography
Ig	immunoglobulin
IL	interleukin
ILC2	type 2 innate lymphoid cells
IMAC	immobilized metal ion affinity chromatography
IPTG	isopropyl β-D-1-thiogalactopyranoside
ITAM	immunoreceptor tyrosine-based activation motif
IU	international unit
K_d	dissociation constant
kDa	kilodalton

kUA	kilo units of antibody
m/z	mass-to-charge ratio
Man	mannose
MHC	major histocompatibility complex
MS	mass spectrometry
MW	molecular weight
MWCO	molecular weight cut off
NBT	nitro blue tetrazolium chloride
Neu5Ac	*N*-acetylneuraminic acid
Neu5Gc	*N*-glycolylneuraminic acid
Ni-NTA	nickel nitrilotriacetic acid
NMR	nuclear magnetic resonance
o/n	overnight
OD	optical density
PAGE	polyacrylamid gel electrophoresis
PAMP	pathogen-associated molecular patterns
PBS	phosphate-buffered saline
PCR	polymerase chain reaction
PDB	protein data base
PEG	polyethylene glycol
pH	potential of hydrogen
pI	isoelectric point
pNAG	4-nitrophenyl *N*-acetyl-β-D-glucosaminide
pNPP	*p*-nitrophenyl phosphate
RBL	rat basophilic leukaemia
rpm	rounds per minute
SAXS	small angle X-ray scattering

sdab	single domain antibody
SDS	sodium dodecyl sulphate
SEC	size exclusion chromatography
Sf	*Spodoptera frugiperda*
sIgE	specific immunoglobulin E
SIT	specific immune therapy
SN	supernatant
SPR	surface plasmon resonance
T	thymine
Taq	*Thermus aquaticus*
TEMED	tetramethylethylenediamine
tIgE	total immunoglobulin E
TRIS	2-amino-2-(hydroxymethyl)propane-1,3-diol
TSLP	thymic stromal lymphopoietin
U	unit
UHPLC	ultra high-performance liquid chromatography
UV	ultraviolet
v/v	volume per volume
Ves v	*Vespula vulgaris*
V_H	variable heavy chain
V_L	variable light chain
w/v	weight per volume
wt	wild type
x g	times gravity
Xyl	xylose
Zeo	zeocin

II. Abstract

Allergic disorders are increasingly prevalent in the developed world with more than one-quarter of affected individuals in industrialised countries [1]. The identification of IgE antibodies as a therapeutical target in allergic diseases has been known for many years, but the difficulty has been to develop novel immunological drugs that are able to block their effect [2]. Omalizumab is the only anti-IgE antibody approved for treatment of moderate to severe asthma and chronic idiopathic urticaria [3]. Other anti-IgE molecules are under development, and some of them are in clinical trials such as the IgG1 antibody ligelizumab [4].

In this thesis, the mode of action of two anti-IgE antibodies should be investigated by structural and functional approaches. For the first time, the structure of the single domain antibody IgE026 in complex with human IgE Fc Cε3-4 was determined revealing an entirely new mechanism in anti-IgE therapy. The epitope of the anti-IgE single domain antibody showed minor overlap with the high-affinity IgE receptor (FcεRI) binding site but a significant overlap with the binding site of CD23. IgE026 acted as a functional homologue of CD23 and induced conformational changes into the closed IgE Fc conformation incompatible with FcεRI binding. For the first time, small angle X-ray data documented substantial conformational rearrangements of the IgE Fc upon anti-IgE binding in solution. Mutational analysis and inhibition studies corroborated the obtained data. Notably, the antibody was able to displace IgE from both CD23 and FcεRI on human basophils and thereby abrogated allergen-mediated activation. The discovered unique inhibitory mechanism opens up for the future development of novel anti-IgE therapeutics for the treatment of allergic diseases.

Furthermore, ligelizumab Fab was crystallised in complex with IgE Fc and an anti-IgE sdab for the first time. The resolution of 7.1 Å was not sufficient to determine the structure, but optimization of the crystallisation conditions could result in better diffracting crystals in the future and provide first insights into the binding mechanism of ligelizumab.

The second part of this thesis addressed the analysis of fine specificity and recognition of alpha-Gal by red meat allergic patients. The disaccharide galactose-α-1,3-galactose (alpha-Gal) is a ubiquitous carbohydrate in cells and tissues of most non-primate mammals and New World monkeys [5]. Hence, alpha-Gal is an

immunogenic glycan for humans, because of the lack of the α-1,3-galactosyltransferase gene [6]. The sensitization mechanism of alpha-Gal is not entirely understood and the delayed, pronounced allergic reactions remain enigmatic [7]. Thus, understanding the molecular basis for alpha-Gal-mediated allergies demands knowledge on patients' IgE response to alpha-Gal and carbohydrates in general. Therefore, the fully functional alpha-Gal-specific chimeric mouse/human M86 IgE antibody was obtained from *Sf*9 insect cells. The antibody exhibited intrinsic potential to activate effector cells by cross-linking the FcεRI with anti-IgE, which was not translated to an antigen-dependent manner suggesting a more complex mechanism in carbohydrate-specific activation of effector cells. Additionally, the M86 Fab was successfully crystallised providing structural insights into an alpha-Gal-specific antibody for the first time.

Furthermore, the IgE-specific response in red meat allergic patients was investigated using glycan arrays covering a broad panel of potential carbohydrate IgE epitopes. Compared to the alpha-Gal-specific recombinant M86huIgE, sera of red meat allergic patients with elevated levels of sIgE to alpha-Gal exhibited IgE reactivity with varying fine specificity to different alpha-Gal structures. Moreover, the sera displayed additional IgE reactivities to structurally related and non-related carbohydrates such as milk oligosaccharides or blood group antigens. These results suggest a patient-specific signature of carbohydrate recognition beyond alpha-Gal with potential relevance for the elucidation of the alpha-Gal sensitization mechanism.

In general, the results in this thesis provide detailed information regarding the molecular basis of IgE specificity and effector functions with major implications for the therapeutic targeting of IgE.

III. Zusammenfassung

Allergische Erkrankungen betreffen etwa ein Viertel aller Individuen in Industrienationen und die Prävalenz ist stetig steigend [1]. Das Potential von IgE-Antikörpern als therapeutische Zielstruktur in allergischen Erkrankungen ist seit langem bekannt, jedoch ist Omalizumab derzeit der einzige anti-IgE-Antikörper, der für die Behandlung von moderatem bis schwerem Asthma und chronisch idiopathischer Urtikaria zugelassen ist [2,3]. Deshalb ist es notwendig, neue immunologische Arzneimittel zur Inhibition von IgE-Antikörpern zu entwickeln [2]. Andere anti-IgE-Moleküle sind zurzeit noch in der Entwicklung, wobei einige in klinischen Studien sind, wie der IgG1-Antikörper Ligelizumab [4].

In der vorliegenden Doktorarbeit sollte der Bindungsmechanismus von zwei anti-IgE-Antikörpern mit strukturbasierten und funktionellen Methoden untersucht werden. Hierbei konnte erstmalig der Komplex zwischen dem Einzeldomänenantikörper IgE026 und dem humanen IgE Fc Cε3-4 kristallisiert, die Struktur aufgeklärt und ein neuer, einzigartiger Mechanismus in der anti-IgE-Therapie ermittelt werden. Das Epitop des anti-IgE-Einzeldomänenantikörpers zeigte zwar nur minimale Überlappungen mit der Bindungsstelle für den hoch-affinen IgE-Rezeptor (FcεRI), jedoch signifikante Überlappungen mit der Bindungsstelle von CD23. IgE026 agiert somit als ein funktionelles Homolog von CD23 und induziert eine strukturelle Änderung zu der geschlossenen IgE-Fc-Konformation. So vorliegend kann der FcεRI nicht binden und wird somit indirekt blockiert. Zusätzlich konnten Röntgenkleinwinkelstreuungsexperimente (SAXS) erstmalig eine substantielle Konformationsänderung des von IgE026 gebundenen IgE Fcs in Lösung aufzeigen. Mutations- und Inhibitionsstudien bestätigten die vorliegenden Ergebnisse. Bemerkenswerterweise war IgE026 dazu fähig, IgE von CD23 sowie FcεRI auf humanen Basophilen zu verdrängen und die allergen-induzierte Aktivierung zu verhindern. Die Entdeckung dieses einzigartigen Inhibitionsmechanismus' ermöglicht die zukünftige Entwicklung von neuen anti-IgE-Therapeutika für die Behandlung von allergischen Erkrankungen. Des Weiteren konnte Ligelizumab Fab im Komplex mit humanem IgE-Fc erstmalig kristallisiert werden, jedoch war die Auflösung von 7.1 Å zu niedrig, um die Struktur zu lösen. Die Optimierung der Kristallisationskonditionen kann vermutlich zu besser diffraktierenden Kristallen führen und einen ersten Einblick in den Bindungsmechanismus von Ligelizumab geben.

Der zweite Teil dieser Arbeit beschäftigte sich mit der Analyse der Spezifität und Erkennung von alpha-Gal durch Patienten mit einer Allergie auf rotes Fleisch. Das Disaccharid Galaktose-α-1,3-Galaktose (alpha-Gal) ist ein ubiquitäres Kohlenhydrat, welches in Zellen und Geweben der meisten nicht zu den Primaten gehörenden Säugetieren und Neuweltaffen vorkommt [5]. Aufgrund des fehlenden α-1,3-Galaktosyltransferasegens stellt alpha-Gal ein immunogenes Glykan für den Menschen dar [6]. Der Sensibilisierungsmechanismus konnte noch nicht vollständig aufgeklärt werden und die verzögerte, ausgeprägte allergische Reaktion bleibt weiterhin rätselhaft [7]. Deswegen ist es notwendig die IgE-Reaktivität von Patienten gegen alpha-Gal und andere Kohlenhydrate detaillierter zu untersuchen, um die molekularen Grundlagen der alpha-Gal-vermittelten Allergie zu verstehen. Hierfür konnte ein voll funktionaler alpha-Gal spezifischer chimärer murin/human M86-IgE Antikörper in *Sf*9-Insektenzellen exprimiert werden. Der Antikörper zeigte intrinsisches Potential Effektorzellen zu aktivieren, welche mit einem anti-IgE kreuzvernetzt wurden. Diese Beobachtung konnte nicht auf eine Antigen-abhängige Methode übertragen werden, was auf einen weit komplexeren Mechanismus in der Kohlenhydrat-spezifischen Aktivierung von Effektorzellen schließen lässt. Zusätzlich konnte das M86 Fab erfolgreich kristallisiert werden, was erstmalig Einblicke in die Struktur von alpha-Gal-spezifischen Antikörpern erlaubt. Die IgE-spezifische Immunantwort in Patienten mit einer Allergie gegen rotes Fleisch wurde mit Hilfe von Glykanarrays, welche eine Vielzahl von potentiellen Kohlenhydrat-IgE-Epitopen abdecken, analysiert. Hierbei besitzen Seren von Allergikern mit erhöhten sIgE-Werten zu alpha-Gal variierende Spezifitäten zu verschiedenen alpha-Gal Strukturen, verglichen mit dem alpha-Gal spezifischen, rekombinanten M86huIgE. Zusätzlich konnten IgE-Reaktivitäten zu strukturell verwandten und nichtverwandten Kohlenhydraten wie Milcholigosacchariden oder Blutgruppenantigenen beobachtet werden. Diese Ergebnisse zeigen ein Patienten-spezifisches Muster bei der Erkennung von Kohlenhydraten jenseits von alpha-Gal mit einer potentiellen Relevanz für die Aufklärung des alpha-Gal-Sensibilisierungsmechanismus'.

Zusammenfassend liefern die Ergebnisse dieser Arbeit detaillierte Informationen über die molekulare Grundlage der IgE-Spezifität und -Effektorfunktionen mit wichtigen Erkenntnissen für das therapeutische Targeting von IgE.

1. Introduction

1.1 Allergy

The term allergy (derived from two Greek words: *allos* "other, different, strange" and *érgon* "(re)activity") was coined by the Austrian paediatrician CLEMENS FREIHERR VON PIRQUET to discriminate between a beneficial and a harmful immune response in 1906 [8,9]. Today allergy comprises an abnormal adaptive immune response against non-infectious, harmless, exogenous, environmental substances called allergens [1]. Generally, these allergens are proteins, glycoproteins or peptides which derive from grass and tree pollens, animal dander, house dust mite faecal particles, specific food, latex, some medicines and insect venoms [1]. Allergic disorders like allergic rhinitis, atopic dermatitis, allergic asthma and anaphylaxis are increasingly prevalent in the developed world, and more than 25% of individuals in industrialised countries are affected [1]. The European Academy of Allergy and Clinical Immunology (EAACI) estimates that more than 150 million Europeans suffer from chronic allergic diseases and more than 50% of the population of Europe will suffer from at least one type of allergy by 2025 [10]. Besides the limited quality of life of allergic patients, the high health care costs are a tremendous economic problem (55 - 151 billion €/annum for allergy treatment in the EU), and the need for curative and preventative treatments remains high [10,11].

In 1963 GELL and COOMBS proposed a classification of hypersensitivity reactions based on the different immunopathologic mechanisms underlying the disease [12]. Four types of hypersensitivity reactions, designated type I, II, III, and IV, are distinguished.

Type I reactions in this classification are immediate hypersensitivity reactions mediated by immunoglobulin E (IgE) antibodies bound to tissue mast cells and blood basophils. In order to trigger an allergic reaction against a given antigen, the individual has first to be exposed to the antigen [13]. During the primary response to the antigen, which is known as sensitization, the antigen promotes the differentiation of $CD4^+$ T cells into T_H2 cells during priming [14]. Notably, not all encounters with a potential allergen will lead to sensitization, and not all sensitization will result in a symptomatic allergic response, even in atopic individuals [13]. The term atopy is often used when describing IgE-mediated diseases and characterises the genetic predisposition to become sensitized to environmental allergens [15].

Sensitization starts with the allergen uptake by antigen presenting cells (APCs) like dendritic cells (DC) in the airway lumen or in the tissue entering through epithelium disruption (Fig. 1a) [1,14]. The allergen is endocytosed by the APCs, processed, and the resulting peptides are presented by the major histocompatibility complex II (MHCII) to naïve T cells in the lymph nodes [1]. In order to induce the differentiation of naïve T cells to T_H2 cells, a T_H2 promoting milieu is essential, which is generated by the secretion of epithelial cell-derived cytokines, like interleukin (IL)-25, IL-33 and thymic stromal lymphopoietin (TSLP) [16]. These cytokines are released during tissue damage, pathogen recognition or allergen exposure [16]. The activated T_H2 cells express and secrete other cytokines like IL-4, IL-5, IL-9 and IL-13, which, notably IL-4 and IL-13, induce the class switch recombination in stimulated B cells and the subsequent secretion of IgE antibodies [13,16]. Typically, the IgE serum concentration is low because most IgE is bound to receptors on mast cells or basophils, but after allergen contact, the IgE levels and the sensitivity of the individual to the specific allergen are enhanced [1,13,14]. The increased IgE level and the presence of IL-4 upregulate the expression of the IgE high-affinity receptor (FcεRI) on the surface of mast cells [17].

Re-exposure to the allergen results in the cross-linking of allergen-specific IgE bound to the FcεRI and the aggregation of surface FcεRI [18]. This leads to the activation and degranulation of mast cells and basophils followed by the secretion of preformed mediators, newly synthesised lipid mediators, cytokines/chemokines and growth factors into the extracellular environment (Fig. 1b) [17]. The inflammatory mediators, e.g. histamine affect the smooth muscles, endothelial cells, nerve endings and mucous secretion [17].
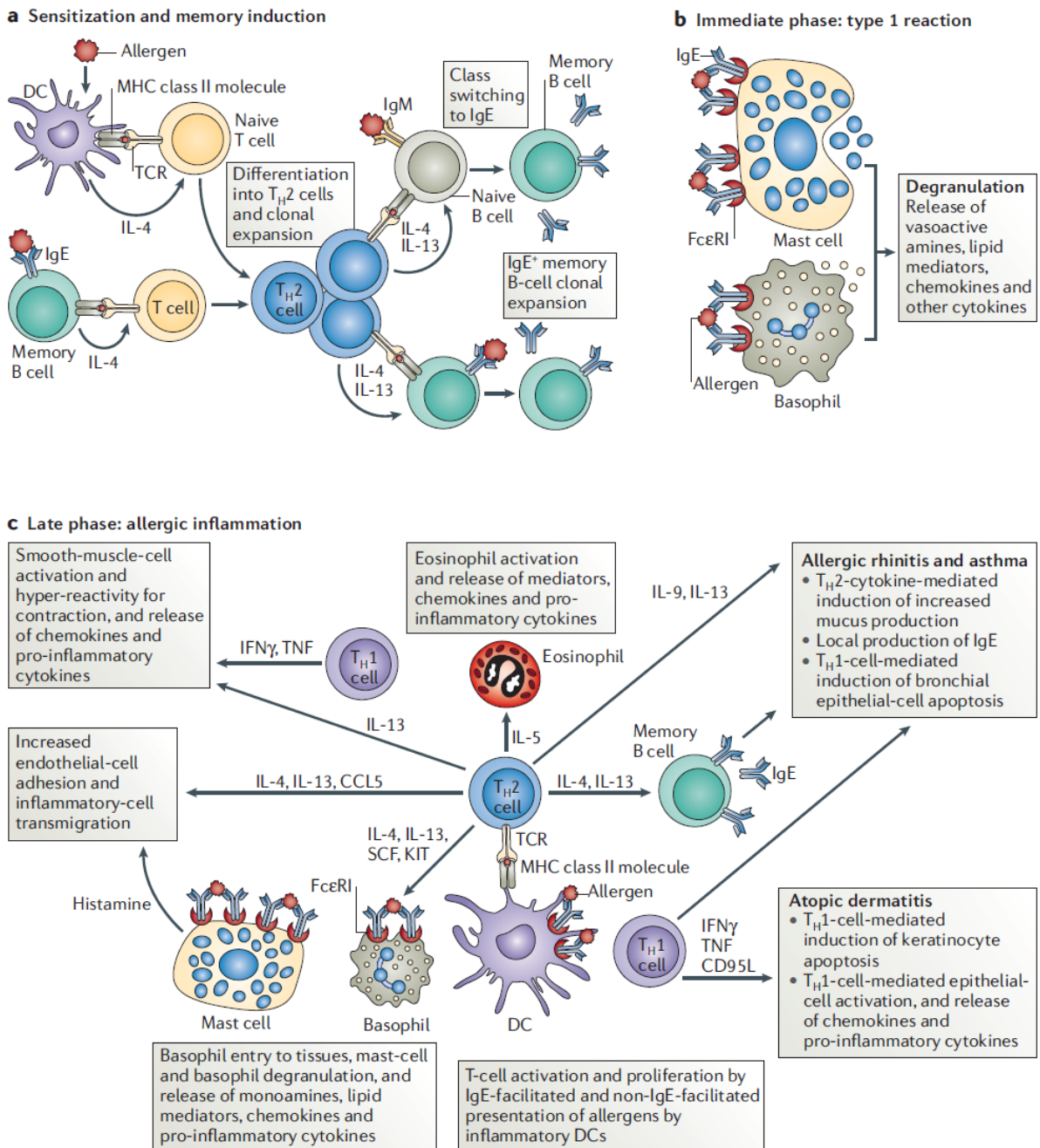
Figure 1: Mechanisms of allergic reactions [19].
a: Sensitization phase: Upon the first encounter with the allergen, differentiation and clonal expansion lead to the production of cytokines, which induce immunoglobulin class switching to allergen-specific IgE. **b:** Immediate phase: Cross-linking of mast cell and basophil surface FcεRI (high-affinity receptor for IgE)-bound IgE by allergens leading to degranulation, the release of inflammatory mediators, and to immediate symptoms. **c:** Late phase: Migration and expansion of allergen-specific T cells reactivate the allergic reaction cycle leading to allergic inflammation.

The resulting allergic reaction can be classified into two different temporal phases. The early or immediate phase reaction occurs within seconds to minutes after allergen contact and includes vasodilation, contraction of the bronchial smooth muscle and increased secretion of mucus varying according to the site of the

reaction [1]. Also, nociceptors of sensory nerves in the nose, skin and airway leading to sneezing, itching or coughing can be stimulated by these mediators [1,20-22]. Furthermore, direct introduction of the allergen into the bloodstream (e.g. bee or wasp stings) or rapid absorption of the allergen from the gut into the bloodstream immediately activate blood vessels throughout the body resulting in the widespread release of inflammatory mediators that cause anaphylaxis [13]. The late phase reaction occurs 2 to 6 hours and often peaks after 6 to 9 hours after allergen exposure and is characterized by an excessive inflammation of local tissue induced by continued synthesis and release of mediators secreted from inflammatory cells, like mast cells, basophils, DCs, neutrophils, eosinophils, T cells and macrophages (Fig. 1c) [1,23]. Type II allergic reactions are characterised by cytotoxic antibodies of the IgG and IgM isotype directed against antigens of the individuals own cells. Successive cell damage results from two different mechanisms. On the one hand, it is induced by the direct action of macrophages, neutrophils and eosinophils that are linked to immunoglobulin-coated target cells through the Fc receptor of the antibody. On the other hand, antibody-mediated activation of the complement system results in lysis of the target cell.[24]

Tissue damage caused by the accumulation of immune complexes is characteristic for type III hypersensitivity reactions. This response occurs when the antigen reacts in the tissue spaces with potentially precipitating antibodies (mainly IgM), forming micro-precipitates in and around small vessels, causing secondary damage to cells. If the antigen is present in excess, soluble immune complexes are formed and further deposited in the endothelial lining of blood vessel walls, fixing complement and causing local inflammation in the lung, joints, kidneys and the skin. Recruited immune cells such as macrophages and neutrophils further contribute to the tissue damage.[24]

Type IV hypersensitivity reactions are mediated by T cells instead of antibodies. The reaction is triggered by recognition of the antigen presented by APCs through T lymphocytes causing lymphocyte stimulation and cytokine release. Symptoms such as skin eruption (contact dermatitis) in response to drugs, cosmetics and environmental chemicals usually occur within 2 to 14 days after exposure to the allergen. Therefore, type IV is also known as the delayed type hypersensitivity reaction.[13,24]

Conventional diagnostics of type I allergic reactions are based on detecting the specific IgE antibodies in the blood or skin using their reactivity to allergen extracts obtained from various sources such as pollen grains, house dust mite, or cat dander [25]. In general, the diagnosis of a patient with suspected IgE-mediated reactions follows a diagnostic algorithm including clinical evaluation and examination followed by skin prick tests and *in vitro* analysis of allergen-specific IgE [25]. Limitations of the diagnostic approach are false positive test results, e.g. distinction between different Hymenoptera venoms. The positive results may either reflect true double or multiple sensitization to the venoms, homologous peptide sequences in proteins present in the venoms or may be caused by IgE antibodies directed against cross-reactive carbohydrate determinants (CCDs) [26]. Instead of extracts containing glycosylated and unglycosylated proteins, lipids, etc. of which the majority are irrelevant for the allergic reaction and diagnostics, the use of specific allergenic molecules has introduced a new area of component-resolved diagnostics and changed the understanding of sensitization profiles and cross-reactivity [25,27].

1.2 Immunoglobulin E and its receptors

Antibodies are glycoproteins of the immunoglobulin (Ig) superfamily secreted by differentiated B cells and key player in the adaptive immune response. There are five different classes of immunoglobulins in mammals – IgA, IgD, IgE, IgG and IgM – which can be distinguished by their constant region. The heterotetrameric molecules are composed of two identical heavy and two identical light chains, which are linked by disulphide bridges resulting in a roughly Y-shaped structure.[13]

In humans, the antibody class representing 75% of serum antibodies is IgG with a concentration of 10 mg/mL, responsible for antibody-dependent cellular cytotoxicity, phagocytosis and complement-dependent cytolysis [28,29]. In contrast, immunoglobulin E represents the latest discovered (in 1968 by JOHANSSON *et al.*) and least abundant serum antibody isotype with healthy human serum concentrations being approx. 50 ng/mL [30,31]. Elevated IgE titers are an indicator for severe diseases observed in individuals with parasitic or viral infections (e.g. schistosomiasis, Epstein-Barr virus or human immunodeficiency virus), inflammatory diseases (e.g. Kimura disease or Kawasaki's disease), hematologic malignancies (e.g. Hodgkin's lymphoma, IgE myeloma), cutaneous diseases (e.g. Netherton's syndrome, bullous pemphigoid), cystic fibrosis, nephrotic syndrome, and primary immunodeficiency diseases [17].

Regarding evolution, the dominant role of IgE was to protect the host from parasitic infections, especially helminth infections [32]. Nowadays, elevated IgE titers in atopic individuals most likely reflect the development of an allergic disease, as more than 25% of the population are affected [1,17,32]. In healthy individuals, the role of IgE is the first line defence against endoparasites and toxins [33,34].

Structurally, IgE shares the same basic molecular architecture as antibodies of other classes, but the heavy ε-chain contains four domains compared to three domains for the heavy γ-chain. The Cε3 and Cε4 domains have a sequence homology of 32% and similar quaternary structure as the Cγ2 and Cγ3 domains of IgG, but as a substitute for the flexible hinge region of IgG, the IgE has an additional Cε2 domain located at the same position [35]. As evident from the crystal structure of the IgE Fc Cε2-Cε4 shown in Fig. 2A, the Cε2 domain is folded back and has extensive contact with the Cε3 and even the Cε4 domain resulting in a compact, bent conformation [36]. Additionally, the Cε2 domain flips from one side of the IgE Fc Cε3-Cε4 to the other

and transiently adopts an extended conformation, as demonstrated in molecular dynamic simulations and biophysical studies in solution [37]. Furthermore, the Cε3 and Cε4 domain adopt different conformational states ranging from a closed to an open conformation (Fig. 2B+C), which is a key feature of the interaction with the high- and low-affinity receptor [38].
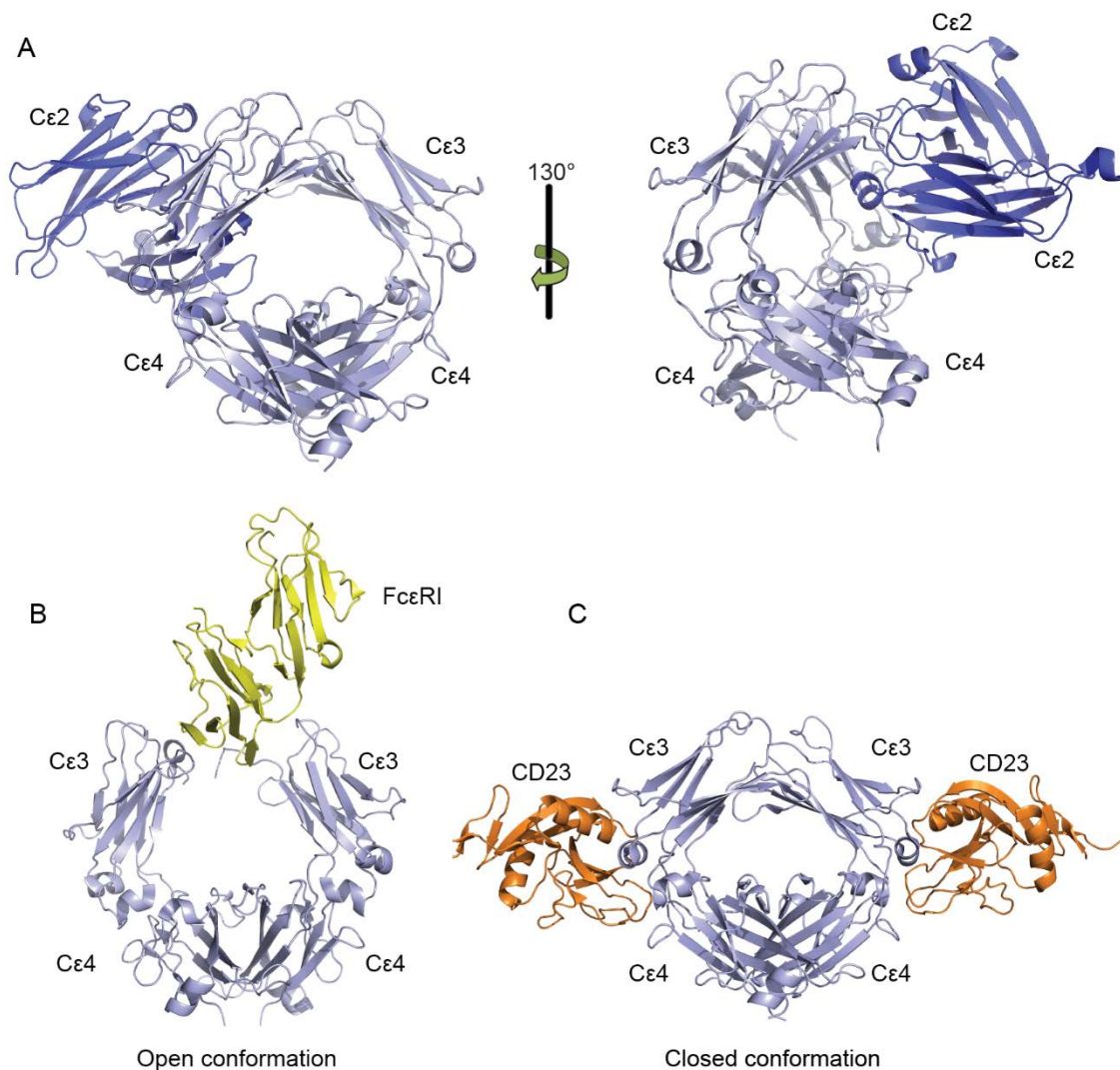
Figure 2: Cartoon representation of IgE Fc and the Fc receptors in complex with IgE Fc.
A: Front and side representation of the compact, bent conformation of IgE Fc with the Cε2 (dark blue) folded back and in contact with the Cε3 and Cε4 domains (light blue). [PDB: 2WQR] **B:** IgE Fc Cε3-Cε4 (light blue) in complex with the high-affinity receptor (FcεRI; yellow) adopting the open conformation. [PDB: 1F6A] **C:** IgE Fc Cε3-Cε4 (light blue) in complex with the low-affinity receptor (CD23, orange) binding in a 1:2 stoichiometry and adopting the closed conformation. [PDB: 4GKO]

Structural studies unravelled the highly ordered and specific interaction of IgE with its receptors. The high-affinity receptor (FcεRI) binding site is primarily located on the Cε3 domain, whereas the low-affinity receptor (FcεRII or CD23) mainly binds to the

Cε3 and Cε4 domains illustrated in Fig. 3a [39,40]. Mechanistically, the FcεRI binds asymmetrically to the open conformation of the IgE Fc Cε3-Cε4, and CD23 to the closed conformation in a 2:1 stoichiometry making binding of both receptors mutually exclusive and preventing overlap of the two pathways (Fig. 2B+C and Fig. 3b) [41].

Figure 3: Schematic representation of organisation and conformational rearrangements of the IgE Fc [42]. a: Relative locations of the FcεRI- (purple) and CD23- (orange) binding sites on IgE. **b:** Open and closed conformations of the IgE Fc Cε3-Cε4 domains (including G335C mutant locked in a closed conformation), and reciprocal allosteric inhibition by FcεRIα (purple) and CD23 (orange).

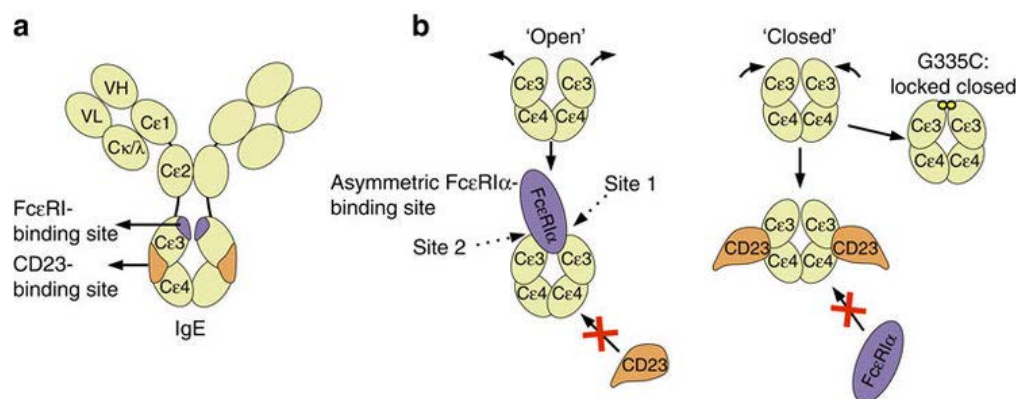The high-affinity receptor is expressed as a tetramer ($\alpha\beta\gamma_2$) on mast cells and basophils responsible for immediate hypersensitivity reactions, and as a trimer ($\alpha\gamma_2$) on human antigen-presenting cells, monocytes, eosinophils, platelets and smooth-muscle cells [43]. The α-chain (sFcεRIα) is highly glycosylated and contains the IgE binding function on the two extracellular domains, which interact with the Cε3 domain of the IgE [44]. The extensive hydrophobic buried surface explains the high affinity of $K_d \approx 10^{-10}$ M, which, at physiologic concentrations of IgE, results in fully saturated receptors [31,45]. Furthermore, the high affinity allows IgE to persist for several weeks to months when bound to FcεRI [31].

As described above, cross-linking of allergen-specific IgE bound to the FcεRI leads to the aggregation of surface FcεRI, activation and degranulation of mast cells and basophils followed by the secretion of inflammatory mediators [46]. The exocytosis of mediators is induced by the immunoreceptor tyrosine-based activation motifs (ITAMs) on FcεRIβ and FcεRIγ, which stimulate a phosphorylation cascade [46].

The low-affinity receptor FcεRII (also named CD23) belongs to the C-type (calcium-dependent) lectin superfamily and is a type-II transmembrane protein that is

expressed on several hematopoietic cell types including antigen-presenting cells [38]. In the membrane-bound form of CD23, the C-terminal head domain consisting of three lectin domains is spaced from the membrane by the triple α-helical coiled-coil stalk region [38,47]. The stalk region is mainly susceptible to proteolysis by the endogenous protease ADAM10 (a disintegrin and metalloproteinase 10), leading to the release of soluble CD23 fragments (sCD23) from the cell [48]. The ability of sCD23 to diminish or enhance IgE synthesis in stimulated B cells is linked to its oligomerization state [49]. The sCD23 fragments containing stalk sequences form trimers, which display a biphasic interaction with IgE Fc fragments and enhance IgE synthesis by activated B cells [49].

In general, the *N*-terminal intracellular sequence of CD23 exists in two different isoforms, that differ in their first seven (CD23a) or six (CD23b) amino acid residues and are expressed by various cell types [47]. CD23a is constitutively expressed in B cells, while IL-4 stimulation induces expression of CD23b in B cells or monocytes [38,47]. The IgE binding activity of CD23 is contained within the head domain, where the affinity of a single head for IgE Fc is low ($K_d \approx 10^{-6}$ - 10^{-7} M), giving CD23 its name low-affinity receptor [50]. Interestingly, the avidity effect of the trimer leads to an overall affinity of $K_d \approx 10^{-8}$ - 10^{-9} M approaching the high affinity of FcεRI [38].

Despite being a C-type lectin, the IgE binding ability of CD23 is carbohydrate-independent [51]. However, in addition to IgE, CD21 binds in a carbohydrate-dependent manner to CD23 and is expressed by B cells, follicular dendritic cells, activated T cells and basophils, linking IgE and the complement system with consequences for IgE regulation and also allergic reactions [38].

In general, IgE is the most densely glycosylated immunoglobulin with seven possible *N*-glycosylation sites and an attribution of oligosaccharides of roughly 12% of the molecular mass of IgE [52]. PLOMP *et al.* determined the typical *N*-glycans of human IgE by mass spectrometry. The study confirmed the presence of complex-type glycans at position Asn21, Asn49, Asn99, Asn146 and Asn252, whereas oligomannosidic glycan structures were present at position Asn275, suggesting six out of seven *N*-glycosylation sites were occupied or partially occupied (Asn99, Asn252, Asn275), as illustrated in Fig. 4 [52]. Recently, the importance of the highly conserved *N*-linked site Asn275, occupied by oligomannose glycans, in the binding of IgE to the FcεRI on mast cells was demonstrated [53]. The selective removal of the

glycan led to changes in the conformation of IgE resulting in the inhibition of the interaction with the high-affinity receptor [53]. This verifies that the glycosylation at position Asn275 of IgE is an absolute requirement for the initiation of the allergic reaction. Thus, the IgE oligomannose may be a potential therapeutic target for both cell-bound and circulating IgE [53].
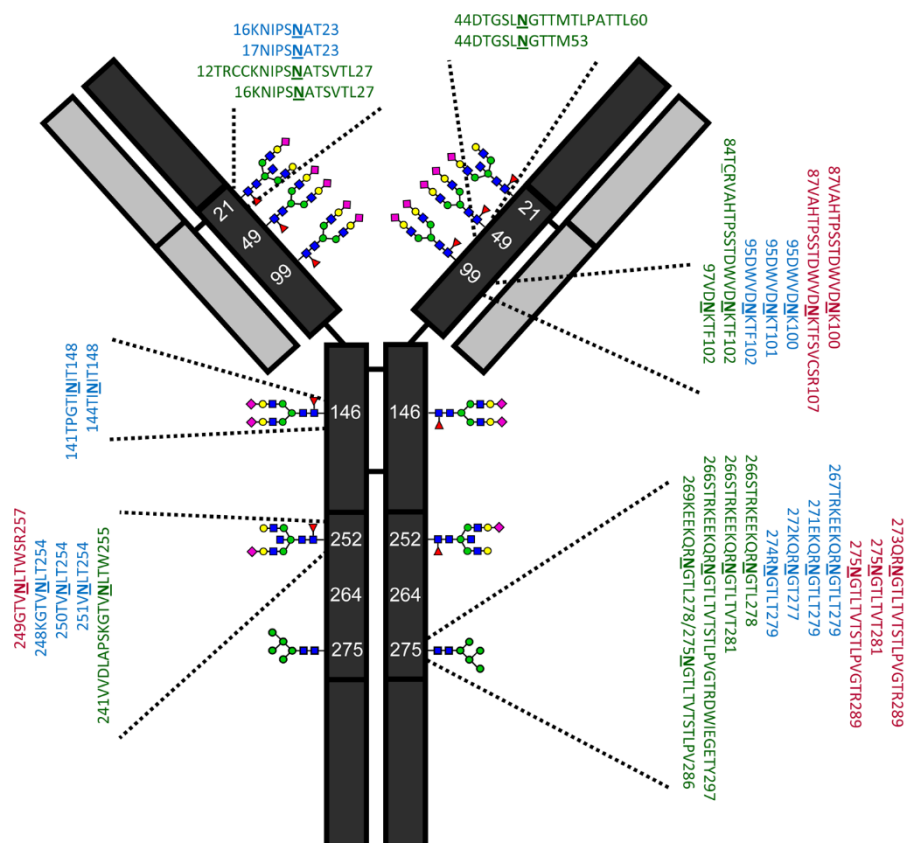
Figure 4: A model of the heavily glycosylated IgE [52].
The seven potential *N*-glycosylation sites are indicated by their amino acid residue number on the heavy chain, and the most common glycan structure (green circle: mannose, blue square: *N*-acetylglucosamine, yellow circle: galactose, red triangle: fucose and pink square: *N*-acetylneuaminic acid) present at each site in IgE from healthy donors. Several peptide sequences are shown for each occupied *N*-glycosylation site, that were observed during digestion with trypsin (red), proteinase K (blue), or chymotrypsin (green).

1.3 Cross-reactive carbohydrate determinants (CCDs)

Glycosylation is the most common and complex posttranslational modification of proteins, which can be found in the entire phylogenetic spectrum ranging from archaea and eubacteria to eukaryotes [54,55]. Protein glycosylation is differentiated between *O-* and *N*-glycosylation. *O*-glycosylation, in which monosaccharides are successively assembled, is catalysed by different glycosyltransferases starting with the glycosylation of hydroxyl groups of amino acids like serine, threonine and tyrosine [54,56]. In contrast, biosynthesis of *N*-linked oligosaccharides begins with the *en bloc* transfer of 14 monosaccharides ($Glc_3Man_9GlcNAc_2$) onto asparagine residues of polypeptides entering the endoplasmic reticulum (ER) [55-57]. The glycosylation is subsequently modified and completed by different enzymes in the Golgi complex [56]. Only asparagine residues in the tripeptide sequence Asn-X-Ser and Asn-X-Thr (where X is any amino acid except proline) are potential *N*-glycosylation sites [56]. Furthermore, α-mannose can be linked to the C2 position of tryptophan via a C-C bond (C-mannosylation) [58]. Glycosylation plays an important role in many aspects, for example, protein folding, cell-cell contact, developmental processes and in many diseases [59-61]. In allergy, glycosylation affects the immune cell recognition and the uptake of allergens, but more interestingly carbohydrates are the most frequently encountered individual epitope structure for IgE antibodies [62]. In 1981 Aalberse *et al.* described the cross-reactivity of IgE from patients' sera with extracts from various allergenic food as well as insect venoms. Treatment of the extracts with periodate abolished the reaction, which was explained by antibodies specific for cross-reactive carbohydrates [63]. The structural basis for the cross-reactivity became evident by discovering the presence of α-1,3-core-fucosylation in insects and plants and the β-1,2-xylosylation also in plants. Both modifications were also identified in helminths [62,64]. Figure 5 illustrates different immunogenic *N*-glycan motifs from various sources. The α-1,3-core-fucosylation and β-1,2-xylosylation, as well as the "premature" termination of the antennae with mannose, *N*-acetyl-glucosamine or galactose residues instead of sialic acid are characteristic for plant *N*-glycan structures [62]. In insect glycoproteins, the α-1,3-core-fucosylation is regularly found accompanied by a second α-1,6-linked fucose, whereas the α-1,3-core-fucosylation does not occur in mammals and exhibits pronounced immunogenicity [62,65].
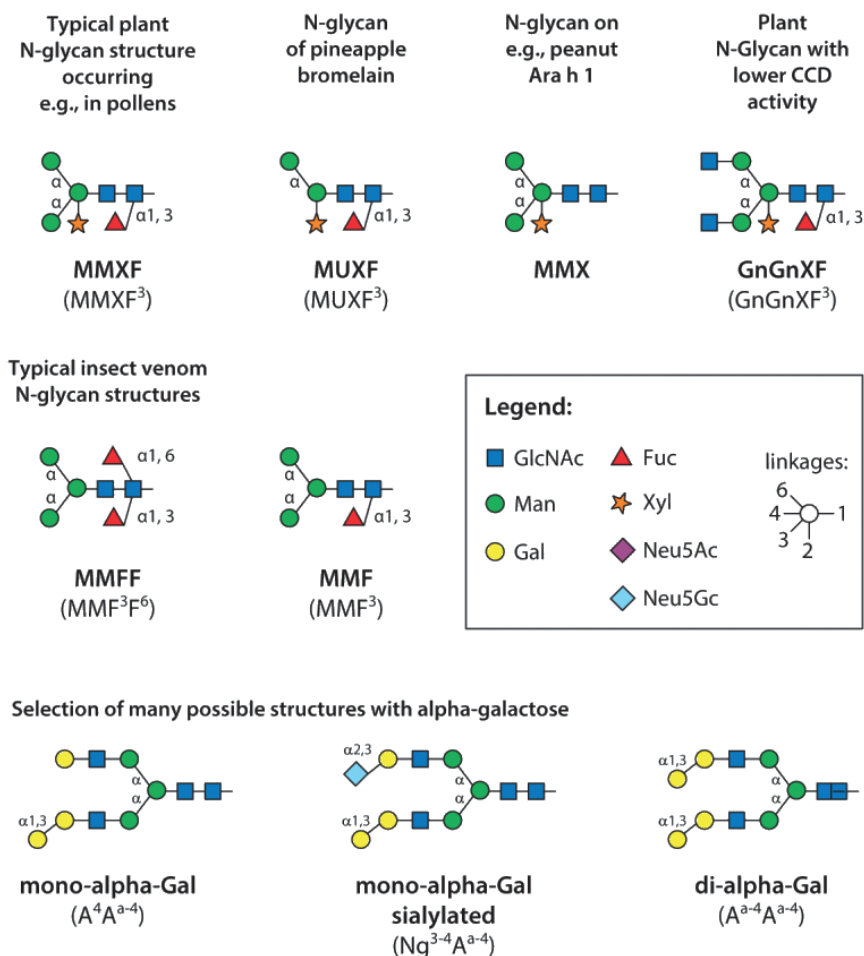
Figure 5: Schematic representation of cross-reactive carbohydrate determinants [66].
Typical plant *N*-glycan structures, containing β-1,2-xylosylation and α-1,3-core-fucosylation represented on top. In the middle, the α-1,3- and α-1,6-core-fucosylation of insect glycoproteins is shown. At the bottom, a selection of different alpha-Gal modifications is represented. (GlcNAc = *N*-acetylglucosamine, Fuc = fucose, Man = mannose, Gal = galactose, Xyl = xylose, Neu5Ac = *N*-acetylneuraminic acid, Neu5Gc = *N*-glycolyl-neuraminic acid).

As mentioned before, CCDs are often responsible for false positive test results in extract-based sIgE determination. Two studies by JAPPE *et al.* revealed the prevalence of up to 72% anti-CCD-IgE positive patients with insect venom allergy and between 10 - 50% anti-CCD-IgE positive food allergic patients [67,68]. HOLZWEBER *et al.* showed the incidence of anti-CCD-IgE to be 22% among 6,220 sera from allergic patients [69]. While the diagnostic importance of the CCDs is evident, the clinical relevance is generally considered low, because the CCDs seem to be unable to induce severe clinical symptoms [65]. JIN *et al.* hypothesised that the limitation of clinical relevance is not due to the low binding affinity of anti-CCD IgE ($K_d = 10^{-10}$ M) but to the high affinity of IgG antibodies that act as blocking antibodies and inhibit the clinical activity of anti-CCD-IgE [70].

12

Another hypothesis is the developing tolerance towards CCDs, which was observed in investigations of serum samples from beekeepers [71]. Nevertheless, CCDs are able to induce histamine release or activate basophils *in vitro*, however, these results are considered clinically irrelevant [72].

1.4 The alpha-Gal epitope

Another cross-reactive carbohydrate determinant with significant clinical relevance is the alpha-Gal epitope. The disaccharide galactose-α-1,3-galactose (alpha-Gal), depicted in Fig. 5, is a ubiquitous carbohydrate in cells and tissues of most non-primate mammals and New World monkeys, however, not in Old World monkeys, apes, and human beings [5]. Therefore, the primary source of CCD allergen is mammalian meat (red meat), not fish or poultry [65]. Roughly 28 million years ago the evolutionary loss of the gene coding for α-1,3-galactosyltransferase in humans and other members of the catarrhine group of primates led to a lack of the synthetic machinery to generate alpha-Gal [6,7]. Hence, alpha-Gal is an immunogenic glycan structure in these species. Naturally, IgM and IgG antibodies directed against alpha-Gal are produced and are responsible for the hyperacute rejection response in xenogenic transplantations from pigs to primates [5,73]. In the last decade, the importance of alpha-Gal in IgE-mediated drug and food allergies was realized. In 2008, investigations of patients with colon carcinoma in the Southeastern U.S., who were suffering from immediate hypersensitivity reactions during the first infusion of the monoclonal antibody cetuximab, led to alpha-Gal as the relevant epitope [74]. Structural studies revealed the presence of alpha-Gal modified glycans at position Asn88 in the Fab portion of cetuximab produced in the SP2/0 murine myeloma cell line [75,76]. At the same time, screening of patients with atopic histories including asthma, chronic urticaria, atopic dermatitis, and anaphylaxis resulted in a strong correlation between the IgE level to alpha-Gal and the individuals who described a history of delayed urticaria or anaphylaxis to red meat [77]. Open food challenges with red meat showed a delayed hypersensitivity reaction of at least two hours which is unusual in traditional IgE-mediated food allergies [77]. The delayed reaction remains enigmatic, but the prevailing hypothesis is that the digestion, absorption, and transit of glycoproteins and/or glycolipids are important [7]. Not every exposure leads to a clinical reaction, which suggests that allergen dose and other modifying factors are relevant, for example, concomitant alcohol consumption appears to be a significant co-factor [7,65]. Besides the USA, alpha-Gal related reactions have also been described in Australia, Europe (e.g. Germany), Japan, South Korea, and Central America and the number of case reports increased since 2008 [78-83].

The putative sensitization mechanism for alpha-Gal-mediated red meat allergy is depicted in Fig. 6. Hard ticks, like *Amblyomma americanum* or *Ixodes ricinus*, are associated with the alpha-Gal IgE sensitization and recent studies identified alpha-Gal glycan modifications in the midgut and saliva of these species [84,85]. Injection of tick saliva was sufficient to induce alpha-Gal-specific IgE production in an alpha-Gal knockout mouse model [85]. Therefore, tick bites seem to promote the sensitization mechanism. Alpha-Gal in the form of glycoproteins or glycolipids was present at the site of the tick lesion and cytokines like IL-25, IL-33, and TSLP are released from epithelial cells [86]. Also, prostaglandins, lipocalins, phospholipases, and adenosine present in the tick saliva can act on epithelial or subepithelial immune cells and favour T_H2 response [87-89]. Mast cells, ILC2, and dendritic cells promote the differentiation of T_H2 cells and T follicular helper 2 cells (Tfh2) leading to IgE production.

Furthermore, alpha-Gal itself may be recognised as a pathogen-associated molecular pattern (PAMP) by carbohydrate-binding lectin receptors and stimulate IgE production directly [7].
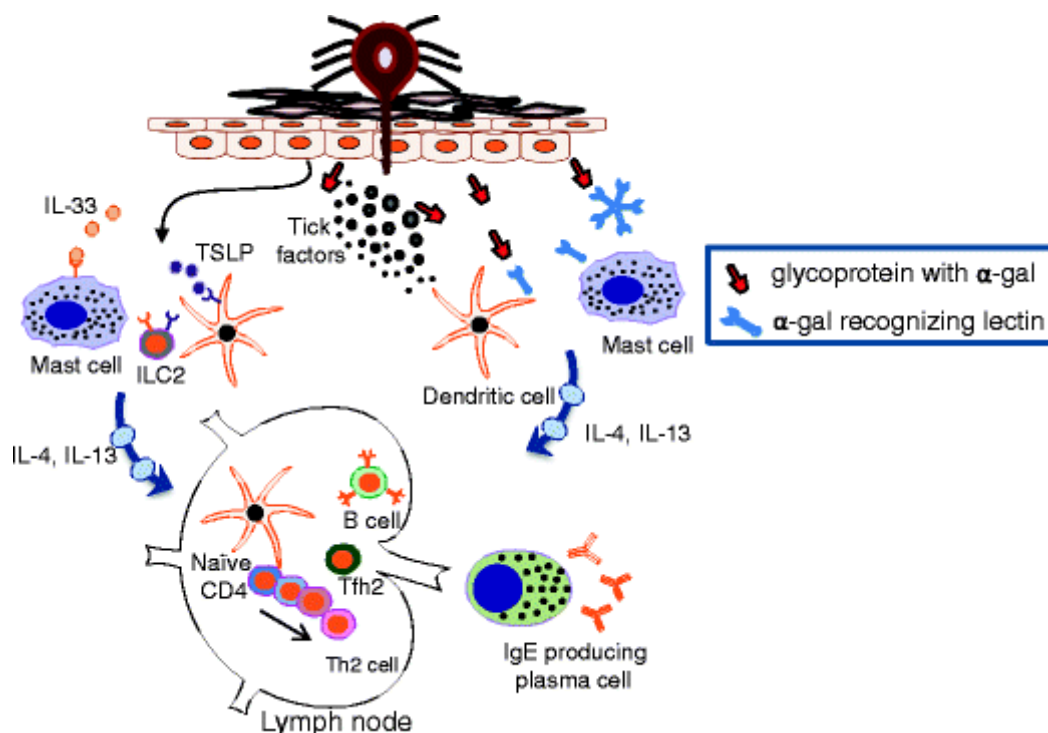
Figure 6: Putative alpha-Gal sensitization mechanism [7].
Hard ticks can promote alpha-Gal sensitization by injection of alpha-Gal present in the form of glycoprotein or glycolipid at the site of tick lesion. Cytokines (IL-25, IL-33, and TSLP) are released, and differentiation of T_H2 cells and/or T follicular helper 2 cells promoted by immune cells (mast cells, ILC2, and dendritic cells) lead to B cell class switch to IgE. Furthermore, alpha-Gal itself may be recognised as a pathogen-associated molecular pattern (PAMP) by carbohydrate-binding lectin receptors and directly stimulate IgE production.

15

Nevertheless, the sensitization mechanism is not entirely understood, and different questions remain open. For instance, why ticks of the species *A. americanum*, *I. ricinus*, *I. holocyclus*, and members of *A. cajennense* lead to clinically relevant sensitization while other ticks do not. Moreover, the involvement of T cell help in IgE-specific alpha-Gal class switch and the IgE-mediated delayed reaction raises questions. Therefore, alpha-Gal induced red meat allergy represents an interesting research field for the discovery of mediators and pathways.[7]

1.5 Anti-IgE therapy

The identification of IgE antibodies as a therapeutical target in allergic diseases has been known for many years, but the difficulty has been to discover immunological drugs that are able to block its effect [2]. Thus far, therapy for allergic diseases has mostly been limited to blocking the effects of specific mediators (e.g. leukotriene modifiers and anti-histamines) or the use of corticosteroids to reduce the consequences of mediator release in the inflammatory cascade [90]. The breakthrough occurred in 1989, when it became evident that the Cε3 domain of the IgE Fc selectively binds to a particular component of the α-chain of the tetrameric FcεRI [91]. In 1995, initial clinical results for the first therapeutic anti-IgE antibody named omalizumab (Xolair®) were published [92].

1.5.1 Omalizumab

Omalizumab was developed by hybridoma techniques resulting in a recombinant humanised monoclonal anti-IgE antibody targeting the Cε3 domain of the IgE Fc [93]. Recently, the crystal structure of omalizumab Fab binding IgE Fc Cε3-Cε4 was solved and confirmed the proposed binding site in the Cε3 domain [42]. Due to steric overlaps with the FcεRI and the CD23, omalizumab efficiently blocks binding of both receptors to free IgE, illustrated in Fig. 7.
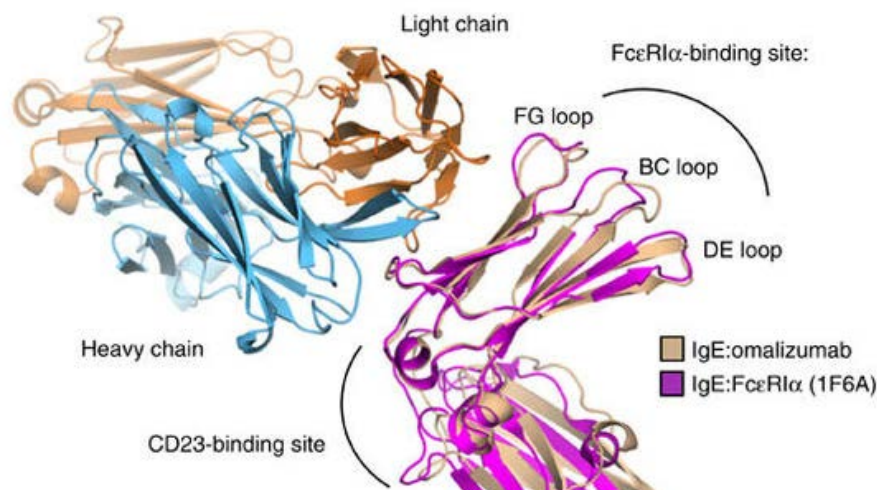

Figure 7: Cartoon representation of omalizumab Fab:IgE Fc complex [42].
Omalizumab Fab (light chain: orange, heavy chain: turquoise) binds within the Cε3 domain of IgE Fc between the CD23- and FcεRI-binding site sterically inhibiting both. Alignment of the complex with the IgE:FcεRIα complex suggests an open conformation of the IgE Fc.

Ex vivo and *in vivo* experiments showed the ability of omalizumab to reduce receptor-bound IgE from human basophils [94]. This indicates that the reported downregulation of FcεRI density on allergic effector cells in patients receiving anti-IgE treatment within the first week of omalizumab application might not only be due to depletion of free IgE but also could result from omalizumab-induced accelerated dissociation of IgE from FcεRI [94]. The FDA approved omalizumab in 2003 in the United States and 2009 in the European Union. To date, it is the only anti-IgE antibody approved for treatment of moderate to severe asthma and also chronic idiopathic urticaria in patients symptomatic despite anti-histamine treatment [95,96]. Alongside the improvement of the patient's life quality and the reduction of asthma exacerbations, the long-term effects of omalizumab include a reduced airway wall area, reduced sputum eosinophilia, increased baseline lung function, and reduced epithelial reticular basement membrane thickening [90,97]. Omalizumab has proven to be a generally well-tolerated medication, but several side effects were reported. Frequent adverse events, besides a local reaction at the injection site, in patients treated with omalizumab were viral infections (23%), sinusitis (16%), headaches (15%) and pharyngitis (11%) [96]. The development of cancer was also reported in two different studies with 4127 and 3726 patients receiving treatment with omalizumab. 20 (0.5%) and 13 (0.35%) patients developed solid tumours after treatment, consequently, the package insert for omalizumab includes malignancy as a potential risk [90,96]. The clinical study Evaluating Clinical Effectiveness and Long-term Safety in Patients with Moderate-to-Severe Asthma (EXCELS) assessed the long-term safety of omalizumab in a clinical practice setting as part of a phase IV US Food and Drug Administration postmarketing commitment. Results from the EXCELS study suggested that an omalizumab therapy is not associated with an increased risk of malignancy [98]. Furthermore, anaphylaxis associated with omalizumab treatment was reported in 41 out of 39,510 (0.09%) patients. Unfortunately, not all asthma patients receiving omalizumab benefit from the treatment [99]. Failure may be caused by pharmacologically active, stable omalizumab:IgE complexes that hamper the correct dosing of omalizumab [99,100]. Therefore, serological measurement of free IgE, not in complex with omalizumab, needs to be addressed [99]. The reported non-responder rate of patients that received omalizumab treatment is 39% [101]. Hence, there remains a need for optimised anti-IgE treatments that may overcome these disadvantages.

Aptamers, phage display-selected peptides, and anti-FcεRI antibodies have been identified as potential high-affinity inhibitors of IgE-receptor binding. However, second-generation anti-IgE molecules such as designed ankyrin repeat protein E2_79 (DARPin), MEDI4212, IgE026, and ligelizumab were developed, and few exhibited the potential to outperform omalizumab in clinical trials.

1.5.2 Designed ankyrin repeat protein (DARPin) E2_79

E2_79 was selected from a DARPin library, which includes alternative binding scaffolds based on a consensus sequence derived from natural ankyrin repeat proteins [102,103]. It prevents binding of free IgE to FcεRI and disrupts preformed IgE:FcεRIα complexes through a facilitated dissociation mechanism [104].

Furthermore, *ex vivo* and *in vivo* experiments showed the accelerated dissociation of IgE from the surface of allergic effector cells, not dependent on the affinity of the inhibitor (K_D = 6.29 nM) but rather on its epitope specificity [94,103].

As mentioned, omalizumab is also able to accelerate the dissociation of preformed IgE:FcεRI complexes on the surface of allergic effector cells at high concentrations, but E2_79 is 300x more efficient [94]. This increased efficacy of E2_79-induced IgE dissociation is due to the partial steric overlap between E2_79 and FcεRI at the second binding site [94]. Parts of the epitope become exposed during partial IgE:FcεRI complex dissociation and can be engaged by the competitor E2_79 [94].

1.5.3 MEDI4212

MEDI4212 is a monoclonal human IgG1λ antibody selected by phage display technology and optimised with combinatorial mutagenesis strategies. It selectively binds human IgE with an affinity of 1.95 pM, more than 100-fold higher than the affinity of omalizumab [105]. In clinical phase I trials (NCT01544348), MEDI4212 showed a rapid reduction of free serum IgE to a greater extent than omalizumab in individuals with diagnostic IgE ≥ 30 IU/mL, which may be of clinical interest for patients with high allergen-specific IgE in which a near-complete IgE suppression is required for clinical response [106]. Nevertheless, the pharmacokinetic analysis demonstrated a rapid clearance of MEDI4212 accompanied by a rapid recovery of free IgE, which provides no benefit to the current therapy using omalizumab regarding dosing intervals [106].

1.5.4 Ligelizumab (QGE031)

Another anti-IgE drug currently in clinical trials is the monoclonal human IgG1 antibody ligelizumab (QGE031) [4]. Ligelizumab was selected against recombinant human IgE from a Fab library generated from the humanised murine antibody TES-C21 [107]. Three clones with a higher affinity compared to the parental antibody were further characterised and one of them was ligelizumab (CL-2C). Hence, this antibody was designed to obtain greater suppression of free IgE and IgE bound to mast cells and basophils compared to omalizumab, which might overcome some limitations of omalizumab and lead to better clinical outcomes. *In vitro* experiments showed a 50-fold higher affinity compared to omalizumab (139 pM vs 6.98 nM) translated into six- to nine-fold greater potency *in vivo* [108,109]. Phase I studies showed a greater and longer suppression of free IgE and surface IgE of basophils, as well as superior suppression of skin prick test responses to allergen. Even in individuals with high baseline IgE, these effects were apparent suggesting that ligelizumab may be more potent than omalizumab in allergy treatment [108,109]. However, most of the clinical trials in asthma and bullous pemphigoid were terminated [4]. The only promising phase II trial to evaluate the efficacy and safety of chronic spontaneous urticaria was completed in June 2017 [4], but the results are not available yet. An initial study assumed that the binding site of ligelizumab may be comparable to the binding site of omalizumab at the Cε3 domain of IgE [108], but structural data are also not available.

1.5.5 Single domain antibody (Nanobody)

Most therapeutic antibodies were developed as monoclonal humanised IgG1 antibodies, and monoclonal antibodies were optimized to reduce the immunogenicity and to increase the clinical efficacy since years [110]. However, the size of the whole antibodies leads to practical drawbacks, e.g. slow production at high costs, weak tissue penetration, or prolonged serum half-life [110,111]. Consequently, the demand for a cheap and renewable source of antibodies is continuously increasing. Hence, the isolation of high-affinity variable heavy chain domains from V_H domain libraries in 1990 paved the way for new molecular engineering approaches [110]. Nowadays, the heavy chain antibodies (HCAbs) are isolated from immunized species from the family of *Camelidae*, including Old World camelids (*Camelus dromedaries* and *C. bactrianus*) and New World camelids (*Lama glama*, *L. pacos*, *L. guanicoe*, and *L. vicugna*) [112]. HCAbs can also be found in sharks and in sera of patients with the pathological disorder known as heavy chain disease [113,114]. The latter HCAbs are not functional in antigen binding since the V_L and part of the V_H domain are missing in contrast to the HCAbs in *Camelidae* and sharks. Structurally, the variable heavy chain domain of HCAbs is joined directly to the hinge region, illustrated in Fig. 8. It is the smallest intact antigen-binding fragment derived from a functional immunoglobulin with a molecular weight of 15 kDa and a size of 4 nm by 2.5 nm in diameter, and therefore also called nanobody [117].
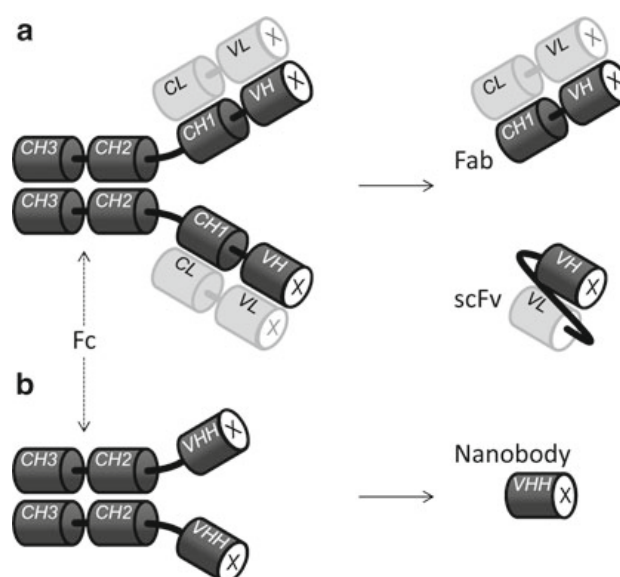

Figure 8: Schematic representation of a conventional (a) and a camelid heavy chain (b) IgG antibody [117]. The antigen-binding fragments for both antibody types - Fab or scFv for classical antibodies and V_{HH} or nanobody for heavy chain antibodies - are depicted, and the antigen-binding site is denoted by a cross.

Recombinant nanobodies are preferentially expressed in *Escherichia coli*, but also in yeast systems with higher production rates and even the expression in tobacco plants is possible demonstrating the feasibility of economic sources [115,116]. Besides the high production rates in simple expression systems, nanobodies have peculiar biochemical features which render them multifunctional molecules. Nanobodies have an extraordinary stability with a shelf life ranging from several weeks at 37 °C until months at 4 °C and even longer at -20 °C while maintaining full antigen-binding capacity [117]. Moreover, they resist chemical and thermal denaturation due to the hydrophilic content and the CDR3 loop folding. Thermal unfolding between 67 - 78 °C was often shown to be entirely reversible and functional activity could be retained up to 90 °C [117]. The introduction of an additional disulphide bond at position 54 and 78 leads to even more stabilised nanobodies highly resistant to pepsin or chymotrypsin degradation suggesting oral administration routes [117]. The small size allows a rapid blood clearance and a fast tissue penetration, which permits the delivery of cargoes to tissues that are difficult to access, even crossing of the blood-brain-barrier is possible [110,117]. These features can be used for diagnostic approaches like tumour targeting or *in vivo* imaging but might limit the efficacy of therapeutic applications. Therefore, bispecific nanobodies have been targeted to albumin, immunoglobulins or polyethylene glycol (PEG) which increased the serum half-life [117]. Sharing a high degree of sequence identity with human V_H, nanobodies are considered to induce no immune response in humans, which allows the use of nanobodies as therapeutic tools for example in oral immunotherapy or toxin and virus neutralisation [117].

The structure of nanobodies adopts a regular immunoglobulin fold consisting of nine β-strands spread over two β-sheets and linked with a conserved disulphide bond (Fig. 9). The antigen-binding capability is favoured by significant differences from V_Hs in the hypervariable regions. CDR1 (in light blue, Fig. 9) is extended towards the *N*-terminal end, and CDR2 loop structures (in green, Fig. 9) differ from the canonical loop structures that are defined for V_Hs, even though the key residues are conserved. Importantly, the CDR3 loop (in red, Fig. 9) has an average length of 18 amino acids compared to 14 and 11 residues in human and mouse V_Hs, respectively. It is folded back to cover the former V_L interface and together with the other CDR loops an increased antigen-binding surface area of 600 - 800 $Å^2$ can be covered.[110,117]
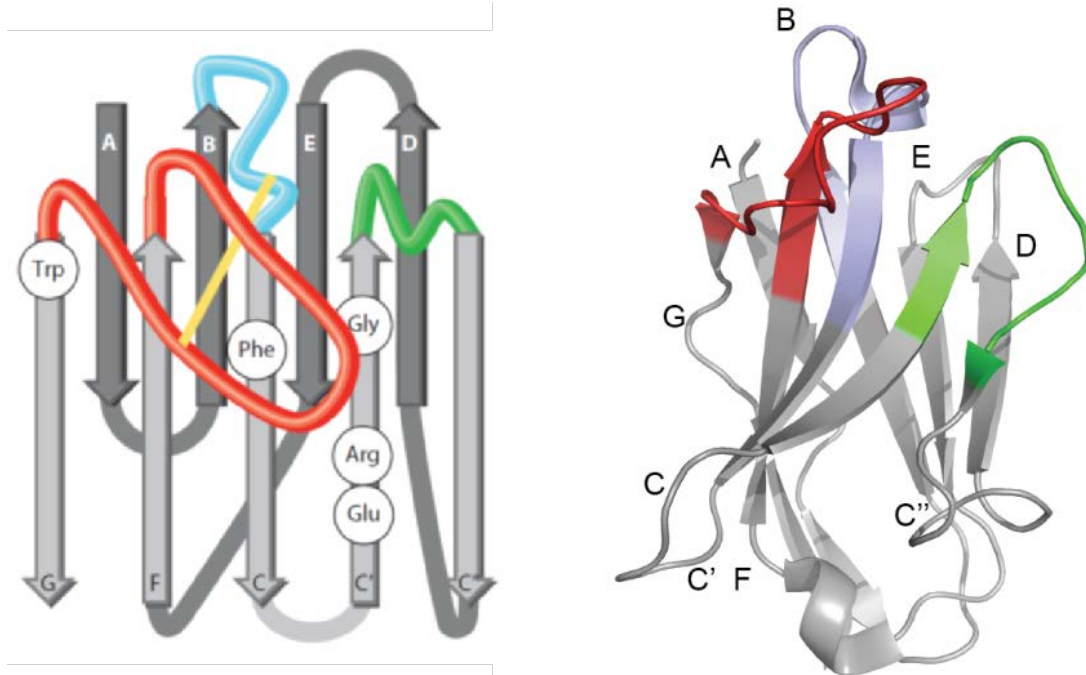
Figure 9: Schematic representation of a folded V_HH and cartoon representation of a nanobody [117]. The A, B, E and D β-strands in the back sheet and the G, F, C, C' and C'' strand in the front sheet are shown in both representations, as well as the color coded CDR regions (CDR 1: blue, CDR 2: green, and CDR 3: red). [PDB: 2X1O]

1.5.6 IgE026

Nanobodies with its beneficial biochemical features suggest a promising tool in therapeutic applications. Therefore, an anti-IgE single domain antibody was developed as a therapeutic drug in allergic reactions. Nanobodies were isolated from a llama library where the IgE-specific nanobody 38D11 was the most potent one [118]. Sequence optimisation, affinity maturation, and mutagenesis resulted in seven different variants in which IgE026 was the most promising nanobody. Affinity measurements showed an affinity to human IgE of 19 pM, which is higher than omalizumab and even ligelizumab [118]. Furthermore, the IC_{50} values for blocking IgE-mediated degranulation of RBL-FcεRI were determined for the anti-IgE variants compared to omalizumab. The nanobody with the lowest IC_{50} was IgE026 with 0.2480 nM compared to omalizumab IC_{50} = 0.8179 nM [118].

So far, structural data and the mode of action of the anti-IgE nanobody are not available, which could offer new strategies for future development of therapeutics for the treatment of allergic diseases.

1.6 Objectives

In this thesis, the structural and molecular basis of IgE antibodies should be investigated in the context of allergic reactions, particularly red meat allergy. The sensitization mechanism and the extraordinary characteristics of IgE antibodies, specifically in the delayed allergic reaction directed against the disaccharide galactose-α-1,3-galactose (alpha-Gal) present on mammalian proteins, remain enigmatic [7]. Therefore, the IgE reactivity profile of a broad panel of different red meat allergic patients should be analysed to get more profound insights into the sensitization profile and the fine specificity of individual red meat allergic patients. Moreover, the structural basis of carbohydrate-specific antigen binding of IgE should be analysed.

Furthermore, the identification of IgE antibodies as a therapeutical target in allergic diseases has been known for many years, but the difficulty has been to discover novel immunological drugs that are able to block its effect [2]. Hence, the interaction of human IgE in complex with different anti-IgE antibodies should be analysed by biophysical methods exploring the conformational states of IgE with respect to future anti-IgE drug development.

2. Materials

2.1 Enzymes and ladders

The following enzymes and ladders were purchased from:

Thermo Fisher Scientific (Waltham, MA, USA):
- Restriction enzymes
- DreamTaq™ DNA Polymerase
- Phusion High-Fidelity DNA Polymerase
- FastAP™ Thermosensitive Alkaline Phosphatase
- T4-DNA-Ligase
- Page Ruler Plus Prestained Protein Ladder
- Gene Ruler 1 kb DNA Ladder
- Gene Ruler 100 bp DNA Ladder
- FastRuler Middle Range DNA Ladder

2.2 Antibodies

The following antibodies were used as primary antibodies, conjugated antibodies or secondary antibodies:

BD Biosciences (Heidelberg, Germany):
- Anti-human-IgE-biotin, monoclonal, mouse
- Anti-human-IgE-AP, monoclonal, mouse

BIOZOL Diagnostica Vertrieb GmbH (Eiching, Germany):
- Anti-human-IgE-AP, polyclonal, goat

DAKO (Glostrup, Denmark):
- Anti-human-IgE, polyclonal, rabbit

QIAGEN GmbH (Hilden, Germany):
- Anti-Penta His, monoclonal, mouse

Sigma (Taufkirchen, Germany):
- Anti-human IgG (*γ-chain specific*)-AP, polyclonal, goat
- Anti-human κ-*light chain*-AP, polyclonal, goat
- Anti-mouse IgG (whole molecule)-AP, polyclonal, goat
- ExtrAvidin®-AP

2.3 Chemicals

Standard chemicals were purchased from:

Bio-Rad Laboratories (Munich, Germany), Merck (Darmstadt, Germany), Sigma (Taufkirchen, Germany), Roth (Karlsruhe, Germany), AppliChem (Darmstadt, Germany), Calbiochem (Schwalbach, Germany) or Stratagene Europe (Amsterdam, Netherlands).

2.4 Chromatography columns

GE Healthcare (Chicago, IL, USA):

HiLoad 16/600 Superdex 75 pg

HisTrap excel (1 mL/5 mL)

HiTrap *KappaSelect* (1 mL/5 mL)

MonoS 5/50 GL

Resource Q (6 mL)

Superdex 75 10/300 GL

Superdex 200 10/300 GL

Source 15 PHE (1 mL)

2.5 Strains of bacteria

The following *E. coli* strains were used for cloning: XL10-Gold, XL1-Blue, DH10bac and TOP10.

2.6 Cell lines and cell culture

Human embryonic kidney 293 cells (HEK293, ATCC® CRL-1573™) and the insect cell line *Sf*9 (Invitrogen *life technologies*, Karlsruhe, Germany) were used for recombinant expression. RBL-2H3-SX38 cells, kindly provided by Prof. J.-P. Kinet (Harvard University, Boston, MA, USA), were used for the degranulation assay.

Cell culture media, additives and tissue culture flasks were purchased from:

Biochrom AG (Berlin, Germany):

Fetal calf serum (FCS)

GE Healthcare (Chicago, IL, USA):

HyClone™ SFX-Insect™ Media

Greiner Bio-One GmbH (Frickenhausen, Germany)
and Sarstedt (Nümbrecht, Germany):

Tissue culture flasks

Thermo Fisher Scientific (Waltham, MA, USA):   Dulbecco's Modified Eagle Media (DMEM), Minimum Essential Media (MEM), RPMI, Trypsin-EDTA, Penicillin G, Streptomycin, Gentamicin, G418, Zeocin

2.7 Cloning vectors

The M86huIgE antibody, ligelizumab Fab and M86 Fab were cloned into pFastBac Dual (Thermo Fisher Scientific, Waltham, MA, USA).

IgE026wt and the IgE026 mutants were cloned into pET22b(+) (Merck, Darmstadt, Germany).

The human IgE Fc was cloned into pcDNA3.1/Zeo (Thermo Fisher Scientific, Waltham, MA, USA).

PCR products were subcloned for sequencing using the TOPO® TA cloning® kit with pCR®2.1-TOPO® vector (Thermo Fisher Scientific (Waltham, MA, USA)).

2.8 Oligonucleotides

All used oligonucleotides were synthesised by *metabion* Gesellschaft für angewandte Biotechnologie GmbH (Planegg-Martinsried, Germany) or Sigma (Taufkirchen, Germany). The sequence data are listed in the appendix.

2.9 Buffer and solutions

The composition of the used buffers and solutions is listed below. All buffer solutions were autoclaved or filtered through a 0.22 µm filter before use.

Ampicillin stock solution: 20 mg/mL ampicillin in 70% EtOH,
filtered sterile
Storage at -20 °C

AP detection buffer:
0.1 M   TRIS-HCl, pH 9.5
0.1 M $MgCl_2$
0.1 M   NaCl

27

AP detection solution: 5 mg/mL p-nitrophenyl phosphate in AP detection buffer

APS stock solution: 10% (w/v) ammonium persulfate in ddH$_2$O, Storage at 4 °C

BCIP stock solution: 0.5% (w/v) 5-bromo-4-chloro-3-indolyl phosphate in water, Storage at -20 °C

Carbonate buffer (0.1 M, pH 10):

60 mL	0.1 M Na$_2$CO$_3$
40 mL	0.1 M NaHCO$_3$

Citrate buffer (0.1 M, pH 4.5):

49.5 mL	0.1 M citric acid monohydrate
50.5 mL	0.1 M monosodium citrate

Coomassie staining solution:

0.1% (w/v)	coomassie brilliant blue R-250
1% (v/v)	acetic acid
40% (v/v)	ethanol

Coomassie destaining solution:

45% (v/v)	ethanol
45% (v/v)	ddH$_2$O
10% (v/v)	acetic acid

DNA loading dye (6x):

0.09% (w/v)	bromophenol blue
0.09% (w/v)	xylen cyanol FF
60% (w/v)	glycerol
60 mM	EDTA

Glucose stock solution: 20% (w/v) glucose, filtered sterile

HRP detection buffer:

15 mL	50 mM citrate buffer, pH 4.0
3.3 mg	ABTS
0.2% (v/v)	H$_2$O$_2$

Kanamycin stock solution: 20 mg/mL   kanamycin in ddH$_2$O,
filtered sterile
Storage at -20 °C

NBT stock solution: 0.1% (w/v)   NBT in 0.1 M TRIS-HCl pH 9.5,
Storage at -20 °C

PAGE collection buffer (4x):   0.5 M   TRIS-HCl pH 6.8
0.4% (w/v)   SDS
Storage at 4 °C

PAGE running buffer (5x):   0.125 M   TRIS-HCl pH 8.3
0.96 M   glycine
0.5% (w/v)   SDS

PAGE sample buffer (4x):   50 mM   TRIS-HCl pH 6.8
40% (v/v)   glycerol
8% (w/v)   SDS
0.004% (w/v)   bromophenol blue

    reducing: add 100 mM   DTT

PAGE separation buffer (4x):   1.5 M   TRIS-HCl pH 8.8
0.4% (w/v)   SDS
Storage at 4 °C

pNAG (8 mM):   2.74 mg/mL in citrate buffer
Storage at -20 °C

PBS: 100 mM   NaCl
40 mM   Na$_2$HPO$_4$ anhydrous
10 mM   NaH$_2$PO$_4$-monohydrate
pH 7.4, filtered through 0.45 µm

SDS stock solution: 10% (w/v)   sodium dodecyl sulphate in ddH$_2$O

| TE buffer: | 10 mM | TRIS-HCl pH 8.0 |
| | 1 mM | EDTA |

TPBS:	0.1% (v/v)	Tween 20 in PBS
Transfer buffer:	25 mM	TRIS
	19.2 mM	glycine
	20%	isopropanol
	pH 8.3	

| TRIS buffer: | 1 M | TRIS-HCl, pH 7.5 or 9.0 |

Tyrode's incomplete:	130 mM	NaCl
	5 mM	KCl
	10 mM	HEPES
	1.4 mM	$CaCl_2$ dihydrate
	1 mM	$MgCl_2$ hexahydrate
	pH 7.4, autoclaved	

Tyrode's complete:	additional:	
	5.6 mM	glucose
	0.1% (w/v)	BSA

| X-Gal stock solution: | 20 mg/mL X-Gal in DMF | |

2.10 Culture media

Media were autoclaved before use. Antibiotics or additives were added after cooling down to 60 °C.

| Cell freezing medium for HEK293: | 90% (v/v) | FCS |
| | 10% (v/v) | DMSO (for cell culture) |

LB medium:	10 g/L	tryptone
	10 g/L	NaCl
	5 g/L	yeast extract

30

SOB medium:	20 g/L	tryptone
	0.5 g/L	NaCl
	5 g/L	yeast extract
	2.5 mM	KCl
	ad 950 mL	ddH$_2$O
	pH 7.5	
	ad 1000 mL	ddH$_2$O
	10 mL	1 M MgCl$_2$ (filtered sterile)
SOC medium:	1 L	SOB medium
	7.2 mL	50% glucose (filtered sterile)
	Storage in 2 mL aliquots at -20 °C	
TYE agar:	10 g/L	tryptone
	8 g/L	NaCl
	5 g/L	yeast extract
	15 g/L	agar
2YT medium:	16 g/L	tryptone
	5 g/L	NaCl
	10 g/L	yeast extract

2.11 Commercial kits

The commercial kits used were purchased from:

Bethyl (Montgomery, USA):	Human IgE ELISA QuantitationSet
MACHEREY-NAGEL GmbH & Co. KG (Düren, Germany):	NucleoBond® Xtra Midi
	NucleoSpin® Gel and PCR Clean-up
	NucleoSpin® Plasmid EasyPure
Thermo Fisher Scientific (Waltham, MA, USA):	GeneJET™ Plasmid Miniprep Kit
	GeneJET™ Gel Extraction Kit
	SilverQuest™ Silver Staining Kit

2.12 General consumable supplies

The general consumable supplies including plastic ware were purchased from Sarstedt AG & Co. (Nümbrecht, Germany), Perbio *Science* Germany GmbH (Bonn, Germany), Greiner Bio-One GmbH (Frickenhausen, Germany), Eppendorf AG (Hamburg, Germany), Renner GmbH (Dannstadt, Germany), Millipore GmbH (Bad Schwalbach, Germany), Heiland MED Vertriebsgesellschaft mbH (Hamburg, Germany), Carl Roth GmbH & Co. KG (Karlsruhe, Germany) and Amersham *Biosciences Europe* GmbH (Freiburg, Germany).

2.13 Equipment

The following equipment was used:

Amersham Biosciences Europe GmbH: (Freiburg, Germany)	Electrophoresis power supply EPS 3500XL
Bibby Scientific (Staffordshire, UK):	Stuart™ Hotplate Stirrer CB 162 Stuart™ Roller Mixer SRT6
Bio-Rad Laboratories GmbH: (Munich, Germany)	Trans-Blot Semi-Dry Transfer Cell Gel Doc XR system Criterion™ Vertical Electrophoresis Cell S1000™ Thermal Cycler
Bruker (Billerica MA, USA):	ESI-Q-TOF (maXis 4G)
Carl Zeiss Microscopy GmbH: (Göttingen, Germany)	Primovert microscope
Eppendorf AG (Hamburg, Germany):	BioPhotometer ThermoMixer C MiniSpin™ centrifuge Centrifuge 5417 C Centrifuge 5417 R Mastercycler gradient

GE Healthcare (Chalfont St Giles, UK):   Pharmacia LKB GPS 200/400 Power Supply

ÄKTA™ Start

ÄKTA™ PURE 25

Xampler Ultrafiltration Cartridge MWCO 10,000

Typhoon Trio Plus laser scanner

Hirschmann Laborgeräte:

(Eberstadt, Germany)   Pipetus™ Standard pipetting aid

Hoefer Scientific Instruments: SE260 Mighty Small II Deluxe Mini

(San Francisco, CA, USA)   Vertical Electrophoresis Unit

IKA Labortechnik (Staufen, Germany):   MS1 Minishaker

KS 200 basic shaker

Integra Bioscience AG (Zizers, Switzerland):   CELLROLL roller unit

VACUSAFE

Martin Christ Gefriertrocknungsanlagen GmbH: Alpha 1-2 LDplus

(Osterode am Harz, Germany)

Memmert GmbH (Schwabach, Germany):   Waterbath WNB 7

CO_2 incubator INCO 153med

New Brunswick Scientific GmbH: Innova™ 44 incubator shaker

(Nürtingen, Germany)   Innova™44 refrigerated incubator shaker

Pall ForteBio (Portsmouth, UK):   Octet® RED96

peqLab Biotechnologie GmbH: Horizontal gelelectrophorese system

(Erlangen, Germany)   Microcentrifuge PerfectSpin24

NanoDrop ND-1000

Phenomenex (Torrance CA, USA):	Aeris Peptide 1.7u XB-C18
	Aeris Widepore 3.6u XB-C8
Sartorius (Göttingen, Germany):	Arium pro water purification system
SCIE-PLAS (Cambridge, UK):	V20 Semi-Dry blotter
TECAN Germany GmbH:	Infinite M200Pro Multi-Detection Reader
(Crailsheim, Germany)	
Thermo Fischer Scientific:	Holten horizontal laminar airflow
(Waltham MA, USA)	clean bench
	Megafuge 40R
	Owl™ A2 horizontal gel system
	Ultimate 3000 HPLC
VWR (Darmstadt, Germany):	Power Source 250 V + 300 V
	INCU-Line IL 53
	MicroStar 17R centrifuge
	SympHony SB70P Digital, pH-Meter
	VACUBOY

3. Methods

3.1 Molecular biological methods

Molecular biological standard procedures such as polymerase chain reaction (PCR), DNA restriction, ligation, transformation, and plasmid isolation were performed according to established protocols [119].

All buffers, solutions, and media were prepared with ultrapure water. Solutions and working equipment were autoclaved or sterilised with ethanol. The experiments were carried out in a biosafety level 1 laboratory according to the GenTG.

3.1.1 Preparation of chemically competent *E. coli* cells

The chemically competent *E. coli* cells were prepared according to INOUE *et al.* [120]. An o/n culture with 10 mL 2YT medium was inoculated with XL1-Blue cells. The next day three 1 L flasks with 200 mL SOB medium were inoculated with 1 mL, 2 mL, and 5 mL of the o/n culture and incubated at 18 °C and 220 rpm until OD_{600} of 0.6. The culture was incubated on ice for 10 minutes and then centrifuged at 2500 x g at 4 °C for 30 minutes. The medium was discarded, the cells were resuspended in 80 mL ice cold Inoue buffer and centrifuged at 2500 x g at 4 °C for 30 minutes. The cells were resuspended in 20 mL Inoue buffer, 1.5 mL DMSO was added, and the bacterial suspension was incubated on ice for 10 minutes. The cells were dispensed in 100 µL aliquots in 1.5 mL tubes, snap-frozen in liquid nitrogen, and stored at -80 °C.

3.1.2 PCR product clean-up prior to sequencing

The PCR clean-up reaction removes unincorporated primers and degrades unincorporated nucleotides. The PCR product can be directly used for sequencing without additional purification. Therefore, 5 µL of the PCR reaction, 0.5 µL (10 u) Exonuclease I and 1 µL (1 u) FastAP™ were incubated at 37 °C for 15 minutes. The reaction was stopped by heating the mixture to 85 °C for 15 min.

3.1.3 Sequencing

The sequencing of plasmid DNA or PCR fragments was performed with the cycle sequencing technology (dideoxy chain termination sequencing) by Eurofins Genomics (Ebersberg, Germany).

3.1.4 Cloning and isolation of recombinant bacmid DNA

The gene of interest was cloned into the donor plasmid pFastBac Dual (Thermo Fisher Scientific). This plasmid has a polyhedrin promoter for the expression of the heavy chain, a p10 promoter for the expression of the light chain and an ampicillin selection marker.

A 3 mL culture with 50 µg/mL kanamycin, tetracycline and gentamicin was inoculated with the specific *E. coli* clone and incubated at 37 °C and 180 rpm overnight. The cells were centrifuged at 4000 x g for 10 minutes at 4 °C, the supernatant discarded and the cells resuspended in 250 µL resuspension buffer (NucleoSpin® Plasmid EasyPure kit). 250 µL lysis buffer were added, the reaction tube inverted and incubated for 5 minutes at rt. The reaction was neutralised with 350 µL neutralising buffer, incubated for 10 minutes at 4 °C, and centrifuged for 10 minutes at 11,000 x g. The DNA was precipitated with 750 µL isopropanol, incubated for 10 minutes at 4 °C, and centrifuged for 30 minutes at 11,000 x g. The pellet was washed with 500 µL 70% ethanol and centrifuged for 5 minutes at 11,000 x g. The supernatant was discarded, the pellet was dried at rt and then resuspended in 50 µL ddH$_2$O.

3.2 Cell biological methods

3.2.1 Expression of proteins in *E. coli*

Antibody fragments, e.g. nanobodies or single-chain variable fragments, can be easily expressed in *Escherichia coli*. Therefore, the gene of interest was cloned in pET22b(+) expression vector and transformed into BL21 (DE3) chemically competent cells. A single colony was grown in 5 mL 2YT medium containing 100 µg/mL ampicillin overnight at 37 °C and 180 rpm. The next day, 200 mL 2YT medium containing 100 µg/mL ampicillin was inoculated with 200 µL of the overnight culture and grown until OD$_{600}$ of 0.6. Protein expression was induced using 1 mM IPTG and the culture was incubated overnight at 30 °C and 180 rpm.

3.2.2 Cultivation and expression of proteins in *Sf*9 cells

Baculovirus-mediated expression in *Sf*9 insect cells permits proper folding and post-translational modifications which are important tools for the expression of eukaryotic proteins. *Sf*9 insect cells were grown in HyClone^{TM} SFX-Insect^{TM} Media (GE Healthcare) containing 10 µg/mL gentamicin at 27 °C. Transfection of the cells was performed with the Bac-to-Bac system according to established protocols [121]. In test expression verified and titered cell stocks were used for expression in 500 mL *Sf*9 cells (1 · 10^6 cells/mL) containing 10 µg/mL gentamicin. The culture was incubated for 5 days at 27 °C and 100 rpm.

3.2.3 Cultivation and expression of proteins in HEK293 cells

The human IgE Fc Cε2-4 was expressed in human embryonic kidney 293 (HEK293) cells in order to exhibit natural post-translational modifications. The cells were grown in DMEM medium containing 10% FCS, 100 µg/mL penicillin, 100 µg/mL streptomycin and 2 mM L-glutamine at 37 °C, 95% humidity and 5% CO_2 fumigation. Transfection of the cells was carried out using Nanofectin (GE Healthcare) according to the recommendations of the distributor. Stably transfected cells were selected by addition of zeocin (1:1000). HEK cells at 90% confluence were used for expression. Therefore, the medium was removed, the cells detached with 2 mL trypsin/EDTA and the cell suspension transferred into 500 mL DMEM medium containing 10% FCS, 2 mM L-glutamine, 100 µg/mL penicillin, 100 µg/mL streptomycin and 9 mL Pluronic F86 in a roller bottle (Greiner CELLMASTER^{TM}). The cells were incubated 14 days at 37 °C, 95% humidity and 5% CO_2 fumigation on an incubator cell roll system (Thermo Fisher Scientific).

3.2.4 Cultivation of RBL-SX38 cells

RBL-SX38 cells were grown in MEM medium containing 15% heat-inactivated FCS, 2 mM L-glutamine, 1 mM sodium pyruvate, 10 µg/mL penicillin, 10 µg/mL streptomycin and 1 mg/mL G418 at 37 °C, 95% humidity and 5% CO_2 fumigation. At 90% confluence, the medium was removed, the cells were washed with PBS and detached with 3 mL trypsin/EDTA. Afterwards, 7 mL fresh medium was added and passaged 1:5. After 3-4 subcultures the cells were used in mediator release assays.

3.3 Protein methods

Protein standard procedures such as SDS-PAGE, Western blotting, and ELISA were performed according to established protocols [119].

3.3.1 Affinity chromatography with kappaSelect matrix

The kappaSelect matrix (GE Healthcare) is based on a highly rigid agarose matrix which features a ligand that binds to the constant region of the kappa chain. Therefore, human kappa-specific antibodies can be purified with high purity and yield.

The purification of human Fab fragments and human IgE antibodies was done using the HiTrap kappaSelect (1 mL or 5 mL/GE Healthcare) and the FPLC system ÄKTA-Start™ (GE Healthcare). The cell culture supernatant was centrifuged for one hour at 4000 x g and 4 °C, filtered through a 0.22 µm filter and applied to the previously with PBS equilibrated column with a flow rate of 0.5 mL/min (1 mL/min). The column was washed with 10 CV of PBS to remove unbound proteins. The protein of interest was eluted with 30 mL of 0.1 M glycine buffer pH 2 with a gradient from 0 - 100%. The 1 mL fractions were directly neutralised with 500 µL 1 M TRIS pH 7.5.

3.3.2 Affinity chromatography with IgE026 matrix

The anti-IgE single domain antibody IgE026 was coupled to an affinity matrix in order to purify IgE antibodies from human serum. All steps were performed in the cold room at 4 °C. Therefore, 2 mL Affi-Gel 15 (BioRad) were washed with 10 mL ddH$_2$O for 5 min on a roller unit and then centrifuged at 4000 x g for 2 min. This step was repeated three times. 28.5 mg IgE026 were coupled to the gel for 4 h, and the reaction was stopped by addition of 100 µL 1 M ethanolamine to the matrix for 1 h. Thereafter, the matrix was transferred into an empty column and equilibrated with 60 mL PBS. The human serum was applied to the column. To remove unspecific proteins the column was washed with 50 mL PBS, and the human IgE antibodies were eluted with 10 mL 0.1 M glycine pH 2. The elution fractions were directly neutralised with 500 µL 1 M TRIS pH 7.5.

3.3.2 Immobilised metal ion affinity chromatography (IMAC)

The initial purification of proteins from cell culture supernatant was done using IMAC and the FPLC system ÄKTA-Start^{TM} (GE Healthcare). The pH of the supernatant was adjusted to 7.4, centrifuged for one hour at 4000 x g and 4 °C, and filtered through a 0.22 µm filter. The supernatant was applied to a, with PBS equilibrated, 1 mL (5 mL) HisTrap excel column (GE Healthcare) with a flow rate of 1 mL/min (5 mL/min). Unspecific bound proteins were removed with 10 CV 5% 300 mM imidazole in PBS. The protein of interest was eluted in 1.5 mL fractions with a gradient of 5 - 100% 300 mM imidazole in PBS.

3.3.3 Ion exchange chromatography (IEX)

In the next purification step, the proteins for crystallography or SAXS were separated based on their net surface charge. Proteins bind to moieties which are oppositely charged by forming ionic bonds to the insoluble polymer matrix. The functional groups are positively charged in anion exchange chromatography (AIEX) and negatively charged in cation exchange chromatography (CIEX). To ensure a sufficient de- or protonation, the pH of the buffer solution has to be adjusted to 1 - 1.5 units over or under the isoelectric point of the protein of interest. Therefore, the protein was dialysed against the running buffer to ensure a low salt concentration and applied to the equilibrated column. The unbound proteins were removed in a washing step with the running buffer, and the protein of interest was eluted with a high salt buffer.

3.3.4 Hydrophobic interaction chromatography (HIC)

Separation using HIC is based on the reversible interaction between a protein and the hydrophobic ligand bound to the chromatography matrix. Hydrophobic amino acids are usually exposed from the protein surface to allow the interaction with the hydrophobic ligands on the matrix under high salt concentrations.

The sample was dialysed against the running buffer (1.6 M $(NH_4)_2SO_4$, 20 mM HEPES, pH 7.2) overnight at 4 °C to ensure a high salt concentration and applied to the previously in running buffer equilibrated 1 mL Source 15PHE column (GE Healthcare). After washing with 5 CV of running buffer, the protein was eluted with a 15 CV gradient from 0 - 100% elution buffer (50 mM NaCl, 20 mM HEPES, pH 7.2).

3.3.5 Size-exclusion chromatography (SEC)

In the last purification step, the proteins were separated based on their Stokes radii, which are proportional to the molecular weight for globular proteins.

The protein solution was concentrated to a volume of 0.5 to 6 mL, dependent on the column size, with a VivaSpin protein concentrator (GE Healthcare). The solution was applied to the previously in running buffer (20 mM HEPES, 50 mM NaCl, pH 7.2) equilibrated column and the protein of interest was isocratically eluted with 1.3 CV.

3.3.6 Enzyme-linked immunosorbent facilitated antigen binding (ELIFAB)

The ELIFAB is an ELISA-based method for analysing the allergen-IgE-complex interactions with the low-affinity receptor CD23 developed by SHAMJI et al. [122]. It is a modification of the B cell-based IgE-FAB assay (IgE-Facilitated Antigen Binding) and uses instead of B cells the monomeric human recombinant sCD23 (soluble CD23) fragments. The ELIFAB assay is a research tool to assess the success of a specific immunotherapy (SIT), in which the allergen-specific IgG_4 titer increases in a patient and competes with the allergen-specific IgE for the allergen binding.

The ELIFAB assay of IgE026 was performed by DR. C. MÖBS and PROF. DR. MED. W. PFÜTZNER at the Institute of Clinical and Experimental Allergology at the Philipps University Marburg according to the protocol of SHAMJI et al. [122].

20 µL of patient serum (>100 kUA/L) were preincubated with 30 µL of the respective allergen at 37 °C for 1 hour to allow complex formation in the presence of different concentrations of IgE026. 50 µL/well sCD23 (12.5 µg/mL) (R&D Systems®) were coated to a Nunc MediSorp flat-bottom 96 well plate (Nunc®) overnight at rt. The wells were washed twice with 200 µL T-PBS and blocked with 200 µL 1% BSA in PBS for 1 hour at 37 °C. The wells were washed three times with 200 µL T-PBS and then the preincubated IgE:allergen complexes were transferred to the plate and incubated for 1 hour at rt. 100 µL (1:1000) biotin-conjugated anti-human IgE antibody (BD Biosciences®) in 1% BSA/PBS were applied to the wells after four times washing with 200 µL T-PBS and incubated 1 hour at rt. After an additional washing step (five times) 100 µL (1:1000) streptavidin-peroxidase (Sigma-Aldrich®) in 1% BSA/PBS were added to the wells and incubated 30 minutes at rt. The ELIFAB was developed, after six times washing, with 100 µL TMB substrate solution (Calbiochem, Merck Millipore), which was incubated 10 minutes under light

exclosure. The reaction was stopped by addition of 50 µL 1.8 M sulphuric acid. Detection was done at 405 nm, and all samples were analysed in duplicates.

3.3.7 Cellular mediator release assay with humanised RBL-SX38 cells

200 µL of $5 \cdot 10^5$ cells/mL were incubated in a sterile 96-well plate overnight at 37 °C, 95% humidity, and 5% fumigation. The next day, the medium was removed from the cells, the recombinant IgE or IgE Fc was diluted in RBL cell medium, and 100 µL were added to the cells for 120 min at the conditions described above. The antibody solution was removed, and the cells were washed 4 times with tyrode's buffer. Cross-linking was achieved by the addition of 100 µL goat anti-human IgE for 60 min. 60 µL of the supernatant were transferred to another 96-well plate, 25 µL pNAG substrate solution were incubated with 60 µL cell supernatant for 60 min at 37 °C (supernatant 1). Cells were washed 2 times and lysed with 100 µL tyrode's complete buffer with 0.1% Triton-X for 60 min at 37 °C. In addition, 60 µL lysed cell supernatant were transferred to a 2nd 96 well plate and incubated with 25 µL pNAG substrate solution for 60 min at 37 °C (supernatant 2). The reaction of the substrate and the released β-hexosaminidase was quenched with 100 µL carbonate buffer, and the absorbance was measured at 405 nm.

3.3.8 Basophil activation test (BAT)

The BAT of IgE026 and omalizumab was performed by DR. C. MÖBS and PROF. DR. MED. W. PFÜTZNER at the Institute of Clinical and Experimental Allergology at the Philipps University Marburg according to the manufacturer's instructions.

Peripheral blood from sensitized donors was drawn in ethylenediaminetetraacetic acid (EDTA)-containing collection tubes. Blood was preincubated with IgE026 or omalizumab in different concentrations in IL 3-containing stimulation buffer or stimulation buffer alone (Bühlmann) for 15 min on a shaker. To activate basophils, recombinant Bet v 1 (100 ng/mL; Biomay) diluted in stimulation buffer was added to the test samples. One sample was left unstimulated to exclude background activation. All samples were incubated with 15 µL of staining reagent (Bühlmann) consisting of anti-CCR3-PE and anti-CD63-FITC in a 37 °C water bath for 15 min. Erythrocytes were lysed for 7 min followed by centrifugation at 500 x g for 5 min. Cell pellets were resuspended in 100 µL washing buffer, and basophil activation was measured by flow cytometry (FACS Calibur, BD Biosciences). In order to address

41

the allergen-independent activation of basophils, EDTA blood samples were treated as above-mentioned but incubated with polyclonal anti-IgE (5 µg/mL; KPL, SeraCare) ± 15 µM IgE026. Subsequently, cells were stained with anti-CCR3-PE and anti-IgE-APC (BioLegend) for 20 min at 4 °C. The mean fluorescence intensity (MFI) of IgE on CCR3$^+$SSC^{low} basophils was measured by flow cytometry. Results were analysed using FlowJo software (FlowJo LLC). Basophils were identified as CCR3$^+$SSC^{low} cells, and CD63$^+$ basophils were considered as activated. CDsens analyses were performed as basophil allergen threshold stimulation as previously described in detail [123]. The higher the CDsens, the higher is the basophil allergen sensitivity. Percentage of CD63 upregulation after stimulation with the allergen was taken as a measure of basophil reactivity.

3.3.9 Glycan array

The glycan array with alpha-Gal positive sera was performed according to the manufacturer's instructions (RayBiotech). The dried glass slide was blocked with 400 µL sample diluent solution for 30 min at rt. 400 µL of the diluted and centrifuged sample were applied to each well and incubated overnight at 4 °C. The next day, the wells were washed 5 times with 800 µL wash buffer I and 2 times with 800 µL wash buffer II for 5 min each at rt. Bound IgE was detected with 400 µL monoclonal biotinylated anti-human IgE (1:5000, BD Pharmingen) incubated overnight at 4 °C. Again, the wells were washed as described above and 400 µL Cy3-conjugated streptavidin were added to the wells and incubated for 1 hour under light exclosure. After a final washing step, the glass slide was dried at rt, and the fluorescence was measured using a Typhoon Trio Plus laser scanner (GE Healthcare) with a wavelength of 532 nm.

3.3.10 Sample preparation of proteins for mass spectrometry

For the tryptic digestion of the IgE Fc for mass spectrometry, 10 µg IgE Fc were concentrated under vacuum and resuspended in 10 µL 6 M urea with 0.1 M DTT and incubated for 30 min at 60 °C. The denatured IgE Fc was diluted with 90 µL 0.1 M sodium hydrogen carbonate (pH 8.3) and incubated with 1 u Trypsin Gold (Promega) for 24 h at 37 °C. The chromatographic separation of peptides and glycopeptides from the tryptic digestion was performed with an ultra-high performance liquid chromatography (UHPLC) using an Aeris Peptide XB-C18 column. 100 µL (10 µg) sample solution were separated with a flow rate of 0.250 mL/min for 90 min at 55 °C.

The proteins were eluted with 0.1% formic acid in water (pH 3) as buffer A and 0.1% formic acid in acetonitrile (pH 3) as buffer B. The gradient elution program was: 0 min: 2% B, 5 min: 2% B, 72 min: 50% B, 74 min: 90% B, 82 min: 90% B, 85 min: 2% B, 90 min: 2% B.

The denatured IgE Fc was applied to an Aeris Widepore XB-C8 column. 50 µL (10 µg) sample solution was separated with a flow rate of 0.250 mL/min for 90 min at 60 °C. The proteins were eluted with 0.1% formic acid in water (pH 3) as buffer A and 0.1% formic acid in acetonitrile (pH 3) as buffer B. The gradient elution program was: 0 min: 5% B, 5 min: 5% B, 45 min: 60% B, 47 min: 95% B, 54 min: 95% B, 55 min: 5% B, 60 min: 5% B.

3.4 Biophysical methods

3.4.1 Protein crystallisation

Protein crystallisation is the most widely used technique for resolving protein structures to an atomic level. The crystallisation process is governed by thermodynamic and kinetic factors, by which the molecules arrange themselves in a natural manner to form a repetitive three-dimensional structure. Crystallisation proceeds in two inseparable steps: Nucleation and crystal growth. Nucleation represents a first-order phase transition by which molecules gather into clusters, which become stable nuclei when they reach a critical size under the current operating condition. The stable nucleus will grow until the system regains equilibrium. The nucleation, as well as the crystal growth, depends on the supersaturation. The supersaturated state is a nonequilibrium condition in which the dissolved protein reaches concentrations beyond the solubility limit of the solvent, for example by changing the ionic strength or precipitants. The equilibrium is reestablished by the formation and development of a solid state, such as crystals or precipitate, as the saturation limit is reached.[124]

In this thesis, the protein crystallisation, data collection and analyses were performed with the help of PROF. G. R. ANDERSEN, DR. N. S. LAURSEN and R. K. JENSEN, M.SC. from the Department of Molecular Biology and Genetics at Aarhus University, Denmark.

For the crystallisation of the proteins commercial screens (Molecular Dimensions Limited and Hampton Research) and sitting drop vapour diffusion were used for

initial screening. 400 nL drops (200 nL protein and 200 nL reservoir solution) were set up in MRC 2 Lens crystallisation microplates (SWISSCI AG) with the help of the mosquito® Crystal dispenser (TTP Labtech Ltd). All reservoirs contained 60 μL of crystallisation reagents. Initial crystals were optimised with grid screens, streak seeding or hanging drops (500 μL reservoir solution and 4 μL drops in different protein:reservoir solution ratios). Crystals were cryoprotected in liquid nitrogen. Data were collected at Diamond Light Source (Oxfordshire, UK), Deutsches Elektronen-Synchrotron (Hamburg, Germany) or European Synchrotron Radiation Facility (Grenoble, France) and processed with XDS[125]. The structure was determined by molecular replacement with PHASER[126] using a suitable search model. The model was rebuild in Coot[127] and refined with Phenix.refine[128] and iMDFF[129]. Figures were prepared with the PyMOL Molecular Graphics System (Schrödinger LLC).

3.4.2 Small angle X-ray scattering (SAXS)

SAXS is a method used in structural biology to determine biological molecules in solution. In SAXS experiments, the sample is exposed to X-rays of a specific wavelength, which scatter elastically between 0 - 5 degrees to produce a spatially averaged intensity distribution. This distribution results in low-resolution imaging because the structural information is reduced to one or two dimensions. Therefore, the extraction of three-dimensional information may be difficult, compared to high-resolution techniques, such as X-ray crystallography, nuclear magnetic resonance (NMR) spectroscopy, or even electron microscopy (EM). Even though the images are in a low resolution, SAXS allows the determination of pore size, specific inner surface, surface to volume ratio, solution structure factor, and lattice type. Additionally, reaction kinetics or time-resolved SAXS allow for the study of conformational changes of a protein under physiological conditions.[130]

In this thesis, the SAXS data collection and evaluation were performed by Rasmus K. Jensen from the Department of Molecular Biology and Genetics at Aarhus University, Denmark.

The SAXS data of the IgE Fc and IgE Fc:IgE026 were collected in batch mode at the ESRF BM29 beamline (Grenoble, France) using a PILATUS 1M pixel detector and a wavelength λ of 0.992 Å in a temperature controlled capillary at 4 °C. The sample-to-detector distance was 2.872 m, covering a range of momentum transfer

$0.04 < q < 5$ nm^{-1} with $q = (4 \times \pi \times \sin \theta) \div \lambda$, where 2θ is the scattering angle. Samples were investigated in the concentration ranges 0.5 - 1.7 mg/mL and 2.2 - 9.0 mg/mL in 20 mM HEPES, 50 mM NaCl, pH 7.2 for the IgE Fc:IgE026 complex and IgE Fc, respectively. Data were collected with ten exposures of two seconds. Radial averaging, buffer subtraction and concentration scaling were performed using the beamline pipeline [131]. For the IgE Fc:IgE026 complex a concentration of 1.7 mg/mL was used for further modelling. For IgE Fc the data points at 2.2 and 9.0 mg/mL were merged using ALMERGE[132]. The pair distribution function was calculated by indirect Fourier Transform using GNOM[133]. Rigid body refinements were performed using a momentum transfer range of $q < 3.0$ nm^{-1} with CORAL[134]. IgE026 and IgE Fc Cε3 and Cε4 domains were used as a single rigid body taken directly from the crystal structure. The two Cε2 domains from the PDB entry 2WQR were grouped into a single rigid body, and the C-terminal of both of the Cε2 domains were linked to the *N*-terminal residue of their corresponding Cε3 domain with a distance restraint of 25 Å. Calculation of theoretical scattering profiles of atomic structures and their fits to the experimental data (as measured by the χ^2-value) were done using CRYSOL3[135]. Calculation of the angle of rotation between the SAXS models and the extended (PDB: 4J4P) and bent (PDB: 2WQR) conformation of IgE Fc was performed using DynDom[136].

3.4.3 Mass spectrometry

The mass spectrometry of the IgE Fc was performed by M. BÄRENFÄNGER, M.Sc. from the Department of Organic Chemistry at Hamburg University, Germany.

The MS and MS/MS data for the peptides and glycopeptides were acquired in positive ion mode on an ESI-quadrupole/time-of-flight mass spectrometer (MaXis 4G, Bruker). The ion source was set at a nebulizer pressure of 4.0 bar, a dry gas flow rate of 10 L/min, and a dry temperature of 200 °C. The spectra rate was 1 Hz for MS and MS/MS with a spectral width of 150 - 2,700 m/z. As collision gas, nitrogen was used, and the fragmentation energy was between 30 and 50 eV depending on the m/z. The three most abundant ions in the preceding MS spectrum were automatically fragmented. For the denatured IgE Fc, the fragmentor voltage was set to 60 eV. The ion source was set at a nebulizer pressure of 4.0 bar, a dry gas flow rate of 9 L/min, and a dry temperature of 200 °C. The spectra rate was 0.5 Hz for MS with a spectral width of 600 - 4,500 m/z.

The data were calibrated using a lock mass calibration and a pre-run calibration utilizing a phosphazine mix (Agilent, Tab. 1)

Table 1: ESI-TOF Tuning Mix.

Phosphazene	Mass [Da]
$C_6H_{19}N_3O_6P_3$	322.05
$C_{12}H_{19}F_{12}N_3O_6P_3$	622.03
$C_{18}H_{19}F_{24}N_3O_6P_3$	922.01
$C_{24}H_{19}F_{36}N_3O_6P_3$	1221.99
$C_{30}H_{19}F_{48}N_3O_6P_3$	1521.97
$C_{36}H_{19}F_{60}N_3O_6P_3$	1821.95
$C_{42}H_{19}F_{72}N_3O_6P_3$	2121.93
$C_{48}H_{19}F_{84}N_3O_6P_3$	2421.91

The IgE Fc spectra were summed up over 30 s to improve the signal-to-noise ratio. The resulting spectrum was deconvoluted with maximum entropy deconvolution (Compass DataAnalysis, Bruker). For the denatured IgE Fc, a spectral width of 0.5 - 50 kDa was used. Theoretical spectra of glycans were adjusted, and data were analysed in Matlab 2017a (Math Works) and GlycoWorkbench 2.0 (A. Ceroni, K. Maass, D. Damerell).

4. Results

The results presented in this thesis were obtained in collaboration with different research groups as evident from the published and submitted manuscripts listed in the publication list.

4.1 Structural and functional analysis of the sdab IgE026

The only anti-IgE antibody approved for treatment of moderate to severe persistent asthma and chronic spontaneous urticaria is the humanised IgG1 antibody omalizumab. Other anti-IgE molecules are currently under investigation, but initial results suggest limited improvement. The basic structural and functional aspects of anti-IgE remain unclear. Therefore, the mode of action of the single domain antibody IgE026 should be investigated by biophysical and functional assays in this thesis.

4.1.1 Cloning, expression and purification of IgE026

The DNA sequence of the single domain antibody IgE026 accessible in the patent WO2012/175740A1[118] was used as a template for gene synthesis directly introducing the restriction sites NotI/NcoI. The synthetic gene was digested with NotI and NcoI as well as the bacterial expression vector pET22b(+) providing a pelB signal sequence and C-terminal His-tag. After ligation, the positive clones were transformed in BL21-Gold(DE3) cells, which induce protein expression under the T7 promoter. A 1 L expression culture was inoculated with 100 µL of the overnight culture and cultured until cells reached the logarithmic phase at 37 °C. Protein expression was induced with IPTG and incubated at 30 °C overnight.
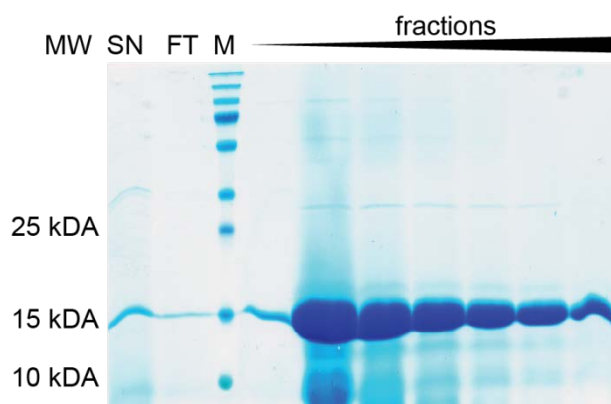
Figure 10: SDS-PAGE analysis of recombinant IgE026 purified with IMAC.
IgE026 was expressed in 1 L *E. coli*, purified with 5 mL HisTrap excel column (GE Healthcare), and supernatant (SN), flow-through (FT) and elution fractions were analysed on 15% TRIS-glycine gel, which was stained with Coomassie brilliant blue. 2 µL marker (M) and 20 µL non-reduced samples were used.

The supernatant was purified with 5 mL HisTrap excel column using the ÄKTA Start system, and purification fractions were analysed on a SDS-PAGE gel stained with Coomassie. In Fig. 10 the IMAC of IgE026 is depicted, where the major band at approx. 15 kDa represents the IgE026 single domain antibody, which has a theoretical molecular weight of 14.7 kDa. The flow-through still contained IgE026, probably due to the high expression level of max. 80 mg/L and an overload of the column, hence an additional purification round was performed using the flow-through. Furthermore, high molecular weight contaminants and degradation products around 10 kDa were detected in the Coomassie-stained gel.

The elution fractions containing IgE026 were pooled and dialysed against 20 mM TRIS, 50 mM NaCl, pH 8.5. IgE026 was further purified by anion exchange chromatography using a 6 mL Resource Q column and eluted with a 0 - 50% gradient of 20 mM TRIS, 1 M NaCl, pH 8.5. The elution fractions were analysed on a Coomassie-stained polyacrylamide gel.
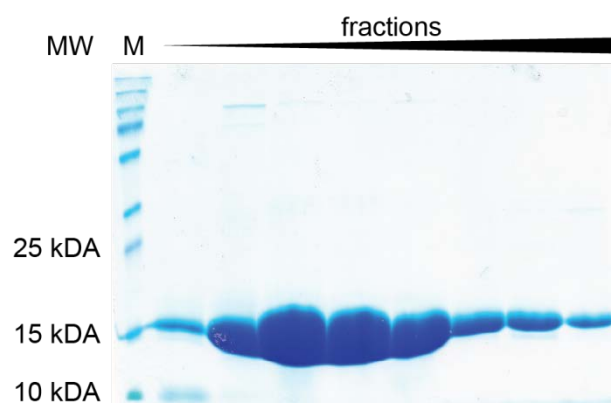
Figure 11: SDS-PAGE analysis of recombinant IgE026 purified by anion exchange chromatography.
IgE026 was purified with 6 mL Resource Q column (GE Healthcare), and the elution fractions were analysed on 15% TRIS-glycine gel, which was stained with Coomassie brilliant blue. 2 µL marker (M) and 20 µL non-reduced samples were used.

Minor contaminations at approx. 100 kDa were identified in the Coomassie gel in Fig. 11, but nevertheless, IgE026 obtained from anion exchange chromatography was assessed pure enough for complex formation with human IgE Fc.

4.1.2 Expression and purification of human IgE Fc

The heavy chain constant region Cε2-4 was introduced into pcDNA3.1/Zeo expression vector providing a human immunoglobulin signal sequence and a C-terminal His-tag [137].

Stably transfected HEK293 cells were cultured in 500 mL medium and the supernatant was collected and purified with a 5 mL HisTrap excel column using the ÄKTA Start system. The purification fractions were analysed by SDS-PAGE.
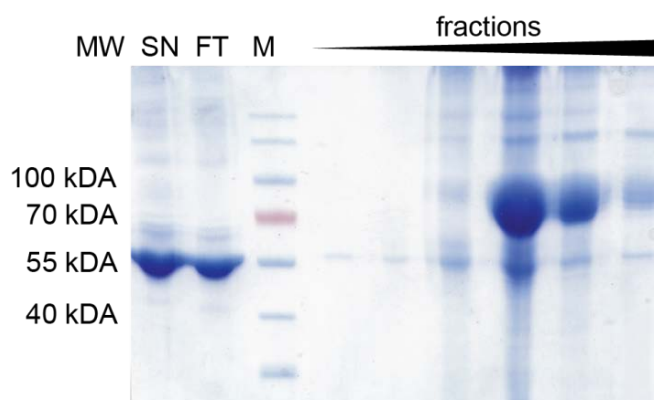
Figure 12: SDS-PAGE analysis of recombinant human IgE Fc purified with IMAC.
Human IgE Fc was expressed in 500 mL HEK293 cells, purified with 5 mL HisTrap excel column (GE Healthcare), and supernatant (SN), flow-through (FT) and elution fractions were analysed on 10% TRIS-glycine gel, which was stained with Coomassie brilliant blue. 2 µL marker (M) and 20 µL non-reduced samples were used.

The IgE Fc Cε2-4 has a theoretical molecular weight of 72.8 kDa. The purified fractions showed a distinct band between 70 and 100 kDa in the SDS-PAGE gel due to glycosylations (Fig. 12). The pronounced bands in the supernatant and the flow-through at approx. 55 kDa were albumins from the foetal calf serum supplemented in the HEK cell medium, which were removed by washing with 5% imidazole prior to the elution. Furthermore, a degradation product of the IgE Fc Cε2-4 was identified at 55 kDa. Fractions containing the IgE Fc were pooled, dialysed against 20 mM NaOAc, 50 mM NaCl, pH 6.5, and subsequently applied to a 1 mL MonoS 5/50 cation exchange column. IgE Fc was eluted with a 0 - 50% gradient of 20 mM NaOAc, 1 M NaCl, pH 6.5 and the elution fractions were analysed on a polyacrylamide gel stained with Coomassie.
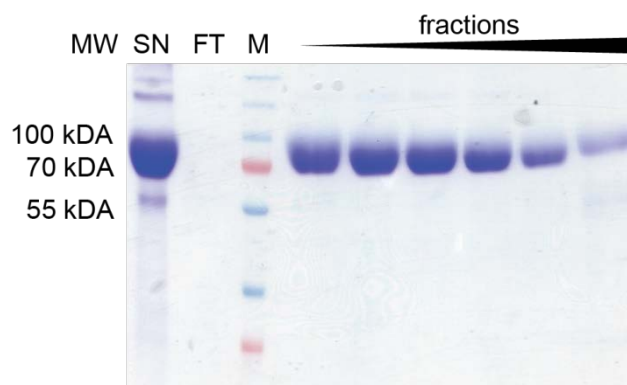
Figure 13: SDS-PAGE analysis of recombinant human IgE Fc purified by ion exchange chromatography.
Recombinant human IgE Fc was purified with 1 mL MonoS 5/50 GL column (GE Healthcare) and supernatant (SN), flow-through (FT) and elution fractions were analysed on 10% TRIS-glycine gel, which was stained with Coomassie brilliant blue. 2 µL marker (M) and 20 µL non-reduced samples were used.

The major contaminants were removed using cation exchange chromatography, depicted in Fig. 13. Faint bands were still detectable at approx. 55 kDa, which represent the degradation of IgE Fc Cε2-4. Because of the structural similarity, it was accepted as pure enough for complex formation.
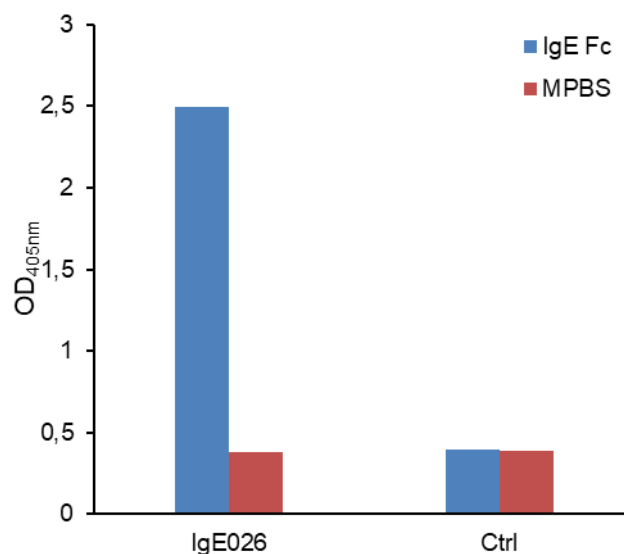
Figure 14: Immunoreactivity of IgE026 to IgE Fc in ELISA.
25 µL (100 ng/µL) IgE026 were coated overnight. The wells were blocked with 4% MPBS for 30 min at rt. After the wells had been washed with TPBS and PBS, 50 µL (100 ng/µL) IgE Fc were incubated for 2 hours at rt. For detection 100 µL anti-human IgE (1:30,000) conjugated with alkaline phosphatase were used. The development was performed with pNPP and detected at 405 nm.

The reactivity of the purified IgE026 and IgE Fc was verified by ELISA shown in Fig. 14. IgE Fc bound to IgE026 was detected with anti-human IgE-AP and showed pronounced reactivity.

4.1.3 Crystallisation of recombinant IgE026 in complex with human IgE Fc

The complex was formed with a molar ratio of 1:4 in which 2 mg IgE Fc were incubated with 1.6 mg of IgE026 overnight at 4 °C. In order to analyse complex formation and separate the unbound molecules from the complex a gel filtration was performed. Therefore, the complex mixture was concentrated, applied to a Superdex 200 10/300 GL gel filtration column and eluted isocratically with 20 mM HEPES, 50 mM NaCl, pH 7.2. In Fig. 15, the chromatogram of the size exclusion chromatography of IgE026:IgE Fc is illustrated compared to the elution profile of IgE Fc alone. The shift to an earlier retention volume indicates the formation of the complex. The peak between 17 and 20 mL represents the excess IgE026.
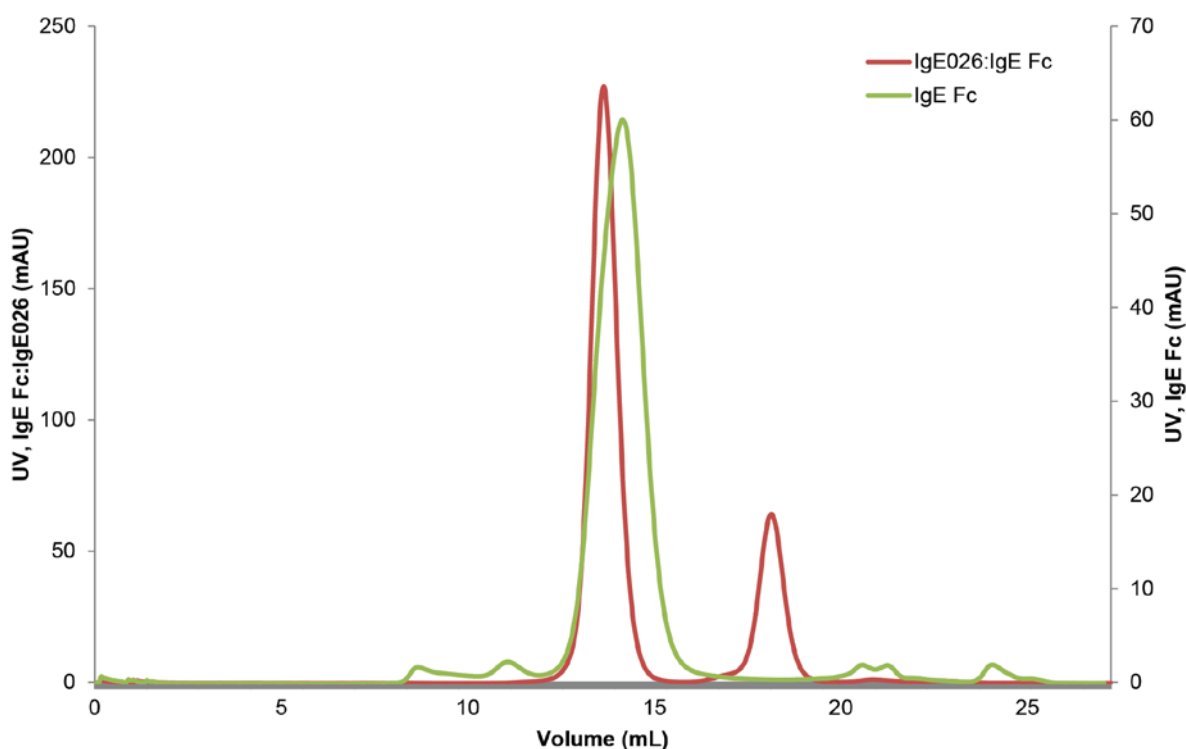
Figure 15: Purification of the IgE026:IgE Fc complex for crystallisation with gel filtration.
The IgE026:IgE Fc complex (red) was formed with a 4:1 ratio overnight and purified with Superdex 200 10/300 GL column (GE Healthcare) compared to IgE Fc alone (green) demonstrating the formation of the complex.

The elution fractions of the IgE026:IgE Fc complex were pooled, concentrated to 5 mg/mL and analysed on a polyacrylamide gel stained with Coomassie. The SDS-PAGE gel in Fig. 16 shows the successful formation of the IgE026:IgE Fc complex with IgE Fc Cε2-4 between 70 and 100 kDa and IgE026 at approx. 15 kDa.

51

Notably, a minor degradation product between 33 and 55 kDa was still present in the sample, which based on its size is the IgE Fc Cε3-4.
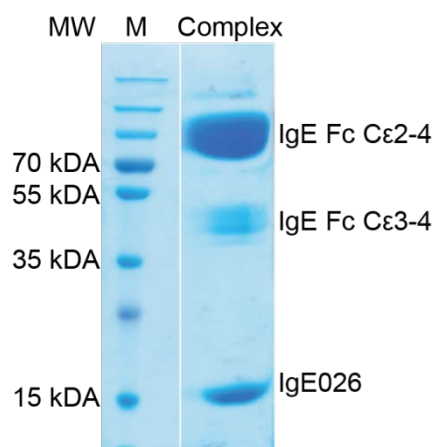
Figure 16: SDS-PAGE analysis of IgE026:IgE Fc purified by gel filtration.
The complex IgE026:IgE Fc was formed with a 4:1 ratio overnight and purified with Superdex 200 10/300 GL column (GE Healthcare). The elution fractions were concentrated, and the complex was analysed on 15% TRIS-glycine gel, which was stained with Coomassie brilliant blue. 2 µL marker (M) and 20 µL non-reduced sample were used.

The IgE026:IgE Fc complex was crystallised by vapour diffusion in sitting drops formed by mixing protein and reservoir solution in the ratio 1:1. Initial commercial crystallisation trays (PEGRx and SaltRx) were set up with 200 nL protein solution and 200 nL reservoir solution at 4 °C and 19 °C using the mosquito® Crystal dispenser. After three days crystals were obtained in 0.1 M imidazole pH 7, 12% w/v PEG 20,000 at 4 °C (Fig. 17).

Figure 17: Microscopic image of the IgE026:IgE Fc crystals (8x magnification).
IgE026:IgE Fc complex was concentrated to 5 mg/mL in 20 mM HEPES, 50 mM NaCl, pH 7.2, and crystallised by vapour diffusion in sitting drops formed by mixing 200 nL protein and 200 nL reservoir solution containing 0.1 M imidazole pH 7.0 and 12% w/v PEG 20,000.

The crystallisation conditions were optimised with grid screens resulting in additional crystals and crystalline material. Suitable crystals were cryoprotected in 0.1 M imidazole pH 7.0, 12% w/v PEG 20,000 and 30% glycerol, mounted and cryo-cooled in liquid nitrogen. The data were collected at the Diamond I24 beamline at Diamond Light Source (Oxfordshire, UK), and processed with XDS[125]. The structure was determined by molecular replacement with PHASER[126] using the PDB entry 2WQR as search model. The model was rebuilt in Coot[127] and refined with Phenix.refine[128] as well as iMDFF[129].

The refinement parameters, listed in the appendix, were used for the evaluation of the final model. The complex diffracted in X-rays to 3.4 Å in the tetragonal space group $P4_12_12$. Iterative rebuilding and refinement resulted in a final structure with R_{work}/R_{free} values of 0.212/0.241. Clear electron density present for the majority of residues and a complete data set (99%) allowed tracing of the amino acids with confidence.

4.1.4 Structure of the IgE Fc bound by two IgE026 single domain antibodies

The structure modelling revealed the symmetrical binding of two single domain antibodies in green to IgE Fc in blue, illustrated in Fig. 18 in the side and bottom view. During structure refinement, it became apparent that the crystal contained the IgE Fc Cε3-4 fragment and not Cε2-4 as expected. In detail, the IgE026 is positioned between Cε3 and Cε4 of two different ε-chains of the IgE Fc dimer.
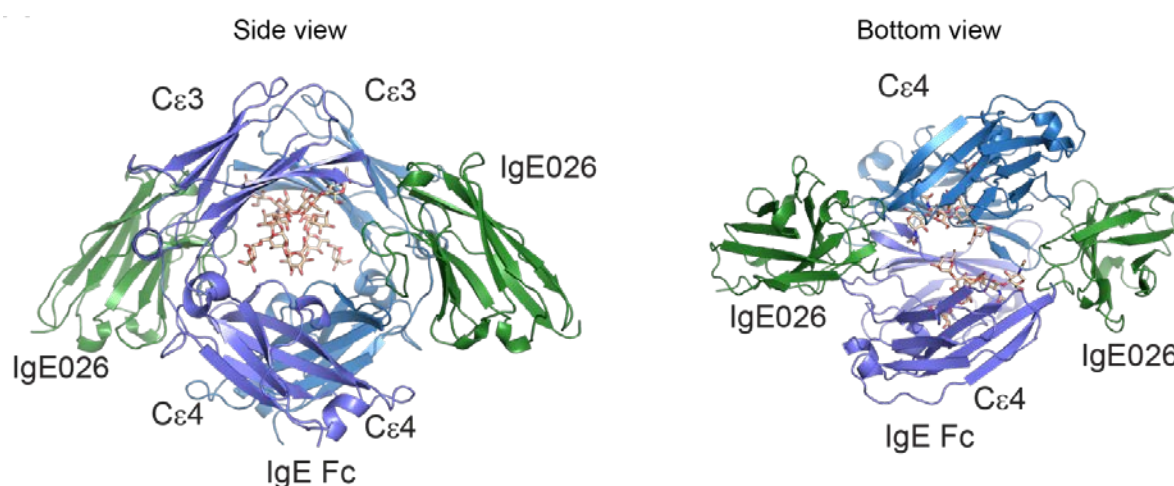
Figure 18: Cartoon representation of IgE026:IgE Fc Cε3-4 complex.
The cartoon representation showing IgE Fc Cε3-4 and two IgE026 sdab molecules binding symmetric sites (green: IgE026, blue: IgE Fc heavy chain 1, violet: IgE Fc heavy chain 2). The side view shows the IgE026 approaching perpendicularly relative to the Cε3-4 domain. An oligomannosidic glycan at position Asn394 is visible in the core of the IgE Fc Cε3-4. The bottom view reveals the two symmetric IgE026 epitopes on the Cε3 and Cε4 domains.

Each IgE026 molecule has a total buried surface area of ~800 Å^2 on the IgE Fc, where Cε3 and Cε4 contribute with 30% and 70%, respectively, which was calculated in PISA[138] (Fig. 19A). Furthermore, the quality of the electron density map (Fig. 71 in the appendix) allowed suggesting putative intermolecular hydrogen bonds and salt bridges. The large CDR3 region of the single domain antibody is mainly involved in binding and contacts several residues in the D-E loop of Cε4. Residues D99 and D110 in the single domain antibody possibly take part in electrostatic interactions with the side chain of IgE Fc K497, and E108 appears to form hydrogen bonds to IgE Fc residues T498-S501 (Fig. 19B). Residue R393 in the IgE Fc C-D loop binds several residues in CDR1 and CDR3 of the single domain antibody, e.g. D33 and E100, through hydrogen bonds and salt bridges (Fig. 19C). Apart from the CDR1 and CDR3 regions of the single domain antibody, the residue Q39 in the FR2 region forms two hydrogen bonds with R440 of the IgE Fc, and R44 is in position to form hydrogen bonds to A442 and N468 (Fig. 19D).
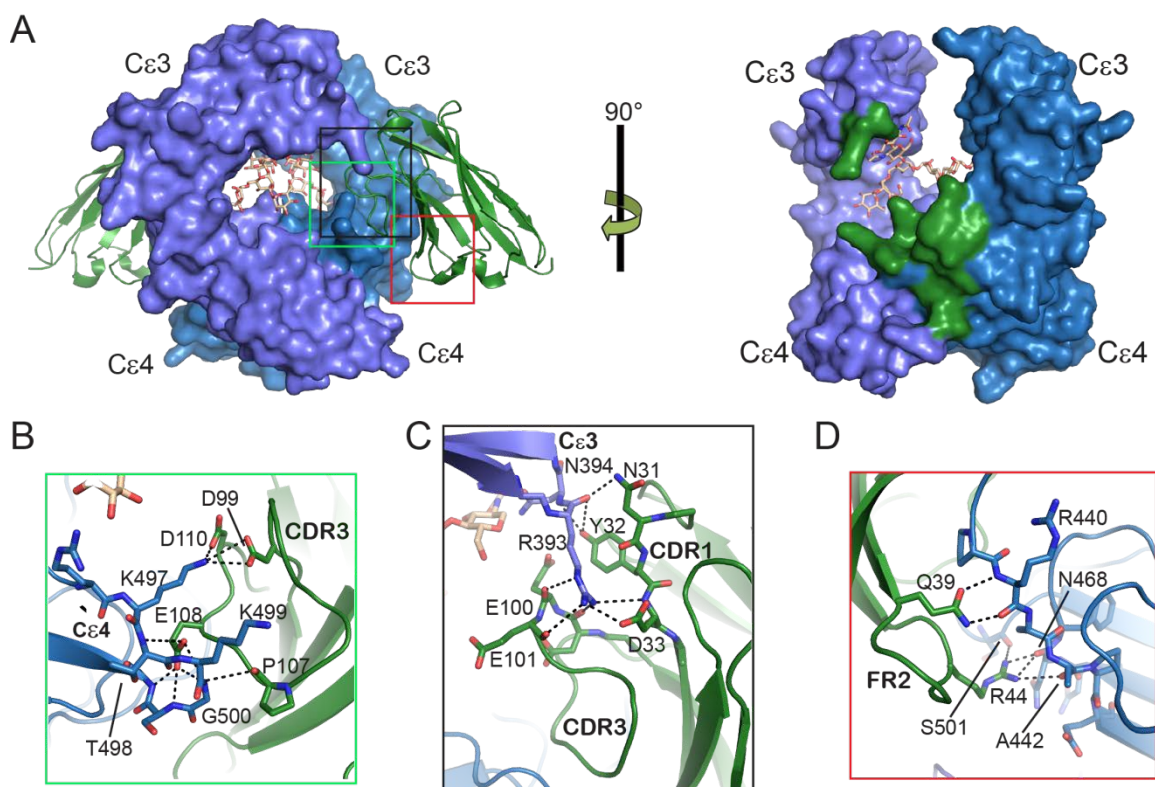
Figure 19: Close-up of the IgE026 binding epitope.
A: Side view of the IgE Fc Cε3-4 with IgE026 (left) and without (right) showing the binding epitope of IgE026 (green). **B-D:** The detailed view of the IgE026:IgE Fc interface reveals the residues involved in the binding of IgE026. Putative hydrogen bonds and salt bridges are shown as dotted lines.

Crucial residues in the single domain antibody responsible for binding the IgE Fc were calculated in PISA and mutated to analyse the impact of the residues in binding the IgE Fc. Five different residues were mutated in the pET22b(+)-IgE026wt plasmid by site-directed mutagenesis.

As visualised in Fig. 20, one residue in the CDR1 (D33), one in the FR2 region (R44), and three residues in the CDR3 region (E108, D110, Y112) were mutated.
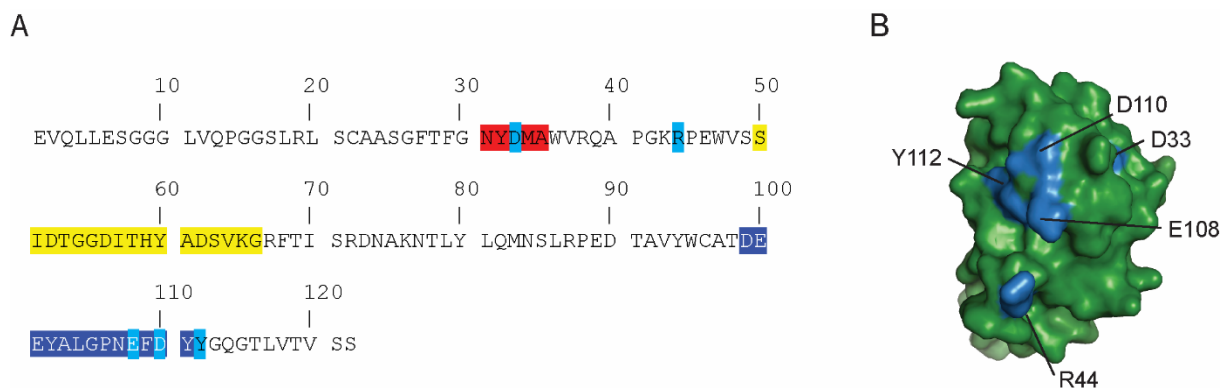
Figure 20: Location of the mutated residues.
A: Sequence of IgE026 with CDR1 in red, CDR2 in yellow, and CDR3 in blue. Mutations are indicated in light blue, **B:** Surface representation of IgE026 with the introduced mutations in blue. All mutations are present on the interface of IgE026 and IgE Fc.

The IgE026 mutants were expressed in 50 mL *E. coli* culture and manually purified with Ni-NTA resin. The expression level of each mutant was analysed on a Coomassie-stained polyacrylamide gel.
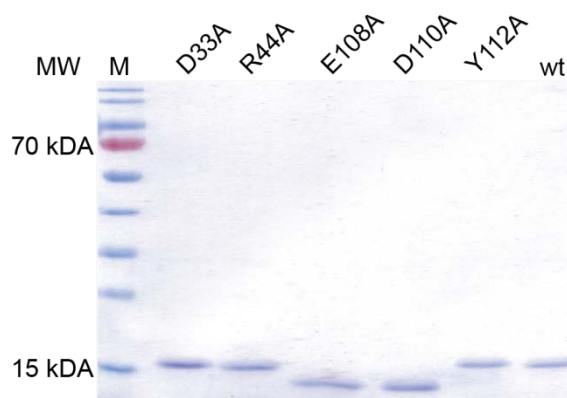
Figure 21: SDS-PAGE analysis of IgE026 mutants purified with Ni-NTA resin.
IgE026 wt and mutations were expressed in 50 mL *E. coli*, purified with 1 mL Ni-NTA resin and analysed on a 15% TRIS-glycine gel, which was stained with Coomassie brilliant blue. 2 µL marker (M) and 20 µL non-reduced samples were used.

The SDS-PAGE gel in Fig. 21 shows the successful expression of all mutants compared to the wild type. All single domain antibodies had a comparable expression level and purity. Interestingly, the mutants E108A and D110A showed different migration behaviour in the SDS-PAGE gel compared to the wild type and the other mutations. The immunoreactivity of the five mutants and the wild type of IgE Fc was assessed by ELISA (Fig. 22).
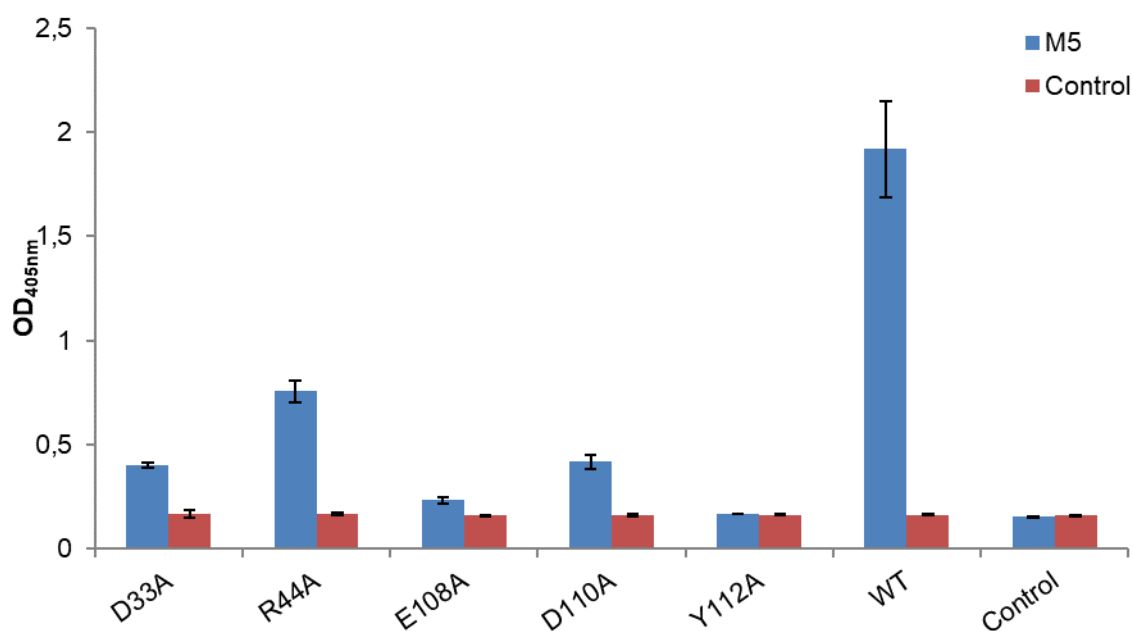
Figure 22: Immunoreactivity of IgE026 mutants and wt in ELISA in triplicates.
50 µL (50 ng/µL) of the IgE026 mutants and wt were coated overnight. The wells were blocked with 4% BSA for 30 min at rt. After the wells had been washed with TPBS and PBS, 100 µL of recombinant M5huIgE (10 µg/mL) were added and incubated for 3 h. For detection 100 µL anti-human IgE (1:30,000) conjugated with alkaline phosphatase were used. The development was performed with pNPP and detected at 405 nm.

The five mutations showed a significant reduction of the reactivity, suggesting a critical role in the interaction with the IgE Fc. Furthermore, the CDR1 (D33A) and CDR3 regions (E108A, D110A and Y112A) seem to have an essential function in the binding of IgE Fc. The ELISA data support that the mutated residues are involved in the IgE Fc binding.

Despite the overall resolution of 3.4 Å, the complex structure is well resolved in the core of IgE Fc, which allowed identifying an oligomannosidic heptasaccharide at position N394 (Fig. 23). Although the proximity of the single domain antibody epitope to the glycan might suggest an architectural relevance, apparently there is no direct contact visible at this resolution. Putative hydrogen bonds between a terminal mannose residue and R496 are shown in black dotted lines in Fig. 23 calculated with PISA and suggesting limited flexibility of the IgE Fc glycan.
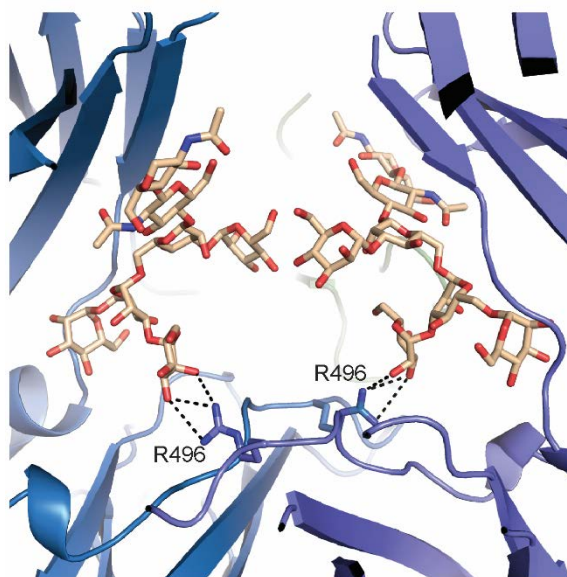
Figure 23: Structure of the heptasaccharide at position N394 of the IgE Fc.
The IgE Fc is shown in blue and the oligomannosidic glycan in stick representation at position N394. Putative hydrogen bonds between R496 and a mannose residue are shown as black dotted lines.

4.1.5 Glycoproteomic analysis of IgE Fc

For deeper insights into the glycosylation pattern of IgE Fc at this position, glycoproteomic analysis was performed. After digestion of 10 µg IgE Fc with trypsin, the sample was purified by ultra-high performance liquid chromatography using an Aeris Peptide XB-C18 column. The elution fractions were analysed on an ESI-quadrupole/time-of-flight mass spectrometer, and the resulting spectrum is illustrated in Fig. 24.
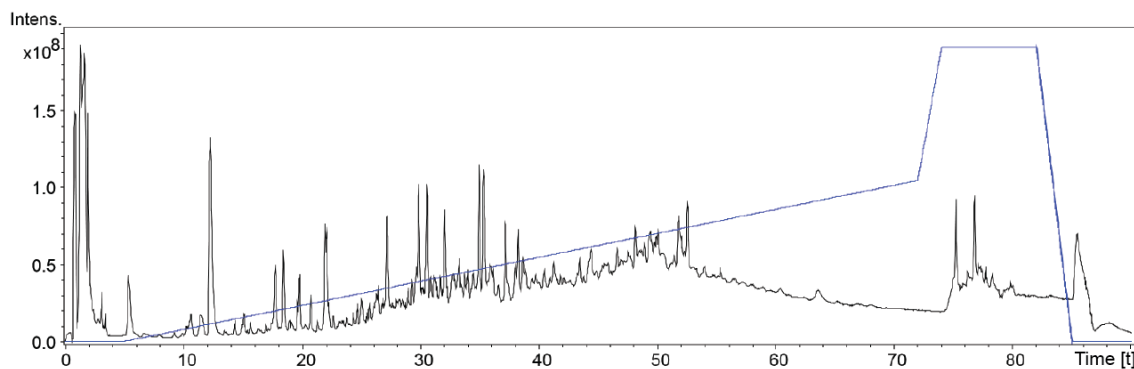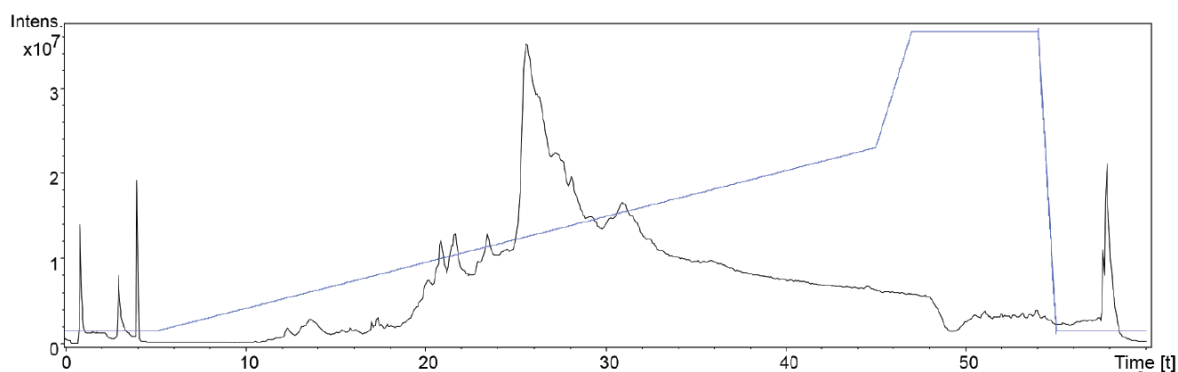
Figure 24: Total ion chromatogram of the tryptic digestion of the IgE Fc (black).
The gradient of the elution buffer (acetonitrile + 0.1% formic acid) is illustrated in blue.

The total ion chromatogram was summed up over 30 s to improve the signal-to-noise ratio (Fig. 25). Data were analysed in Matlab 2017a (Math Works), and GlycoWorkbench 2.0 (A. Ceroni, K. Maass, D. Damerell) and the glycopeptide with the sequence [394]NGTLTVTSTLPVGTR[408] was identified.
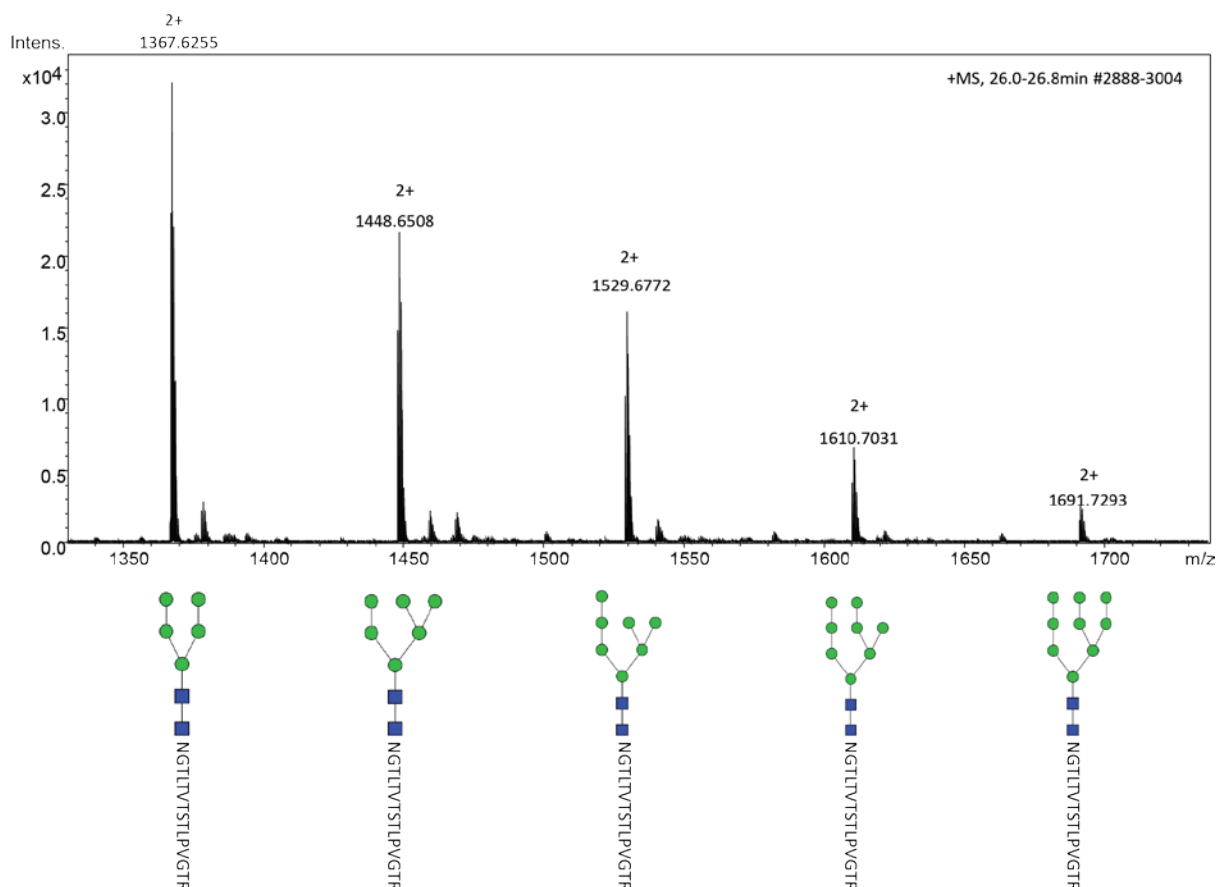
Figure 25: Sum spectrum of proteolytic digestion of IgE Fc.
The sum spectrum shows the most abundant mass over a period of 26.0 - 26.6 min. The corresponding (estimated) glycan compositions are illustrated below the peaks.

Five different glycan compositions (HexNAc$_2$Hex$_{5-9}$) were identified at this position, which are listed in Tab. 2. Only one peptide was identified by mass spectrometry suggesting the occupancy of just one glycosylation site out of three on the IgE Fc.

Table 2: Identified glycopeptides after tryptic digestion.

Measured m/z (monoisotopic)	Calculated m/z	RT [min]	Peptide sequence	Glycan
1367.1239 (z=2)	1367.1321	26.5	[394]NGTLTVTSTLPVGTR[408]	HexNAc$_2$Hex$_5$
1448.1489 (z=2)	1448.1585	26.3	[394]NGTLTVTSTLPVGTR[408]	HexNAc$_2$Hex$_6$
1529.1754 (z=2)	1529.1849	26.2	[394]NGTLTVTSTLPVGTR[408]	HexNAc$_2$Hex$_7$
1610.2015 (z=2)	1610.2113	26.1	[394]NGTLTVTSTLPVGTR[408]	HexNAc$_2$Hex$_8$
1691.2281 (z=2)	1691.2377	26.0	[394]NGTLTVTSTLPVGTR[408]	HexNAc$_2$Hex$_9$

In addition, the denatured IgE Fc was analysed on an ESI-quadrupole/time-of-flight mass spectrometer to verify the occupancy of just one glycosylation site. The resulting spectrum is illustrated in Fig. 26.

Figure 26: Total ion chromatogram of the denatured IgE Fc (black).
The gradient of the elution buffer (acetonitrile + 0.1% formic acid) is illustrated in blue.

The total ion chromatogram was summed up from 25.4 - 26.0 min and subsequently deconvoluted with a maximum entropy algorithm. The resulting spectrum was overlaid with the theoretically calculated spectrum, which is illustrated in Fig. 27.
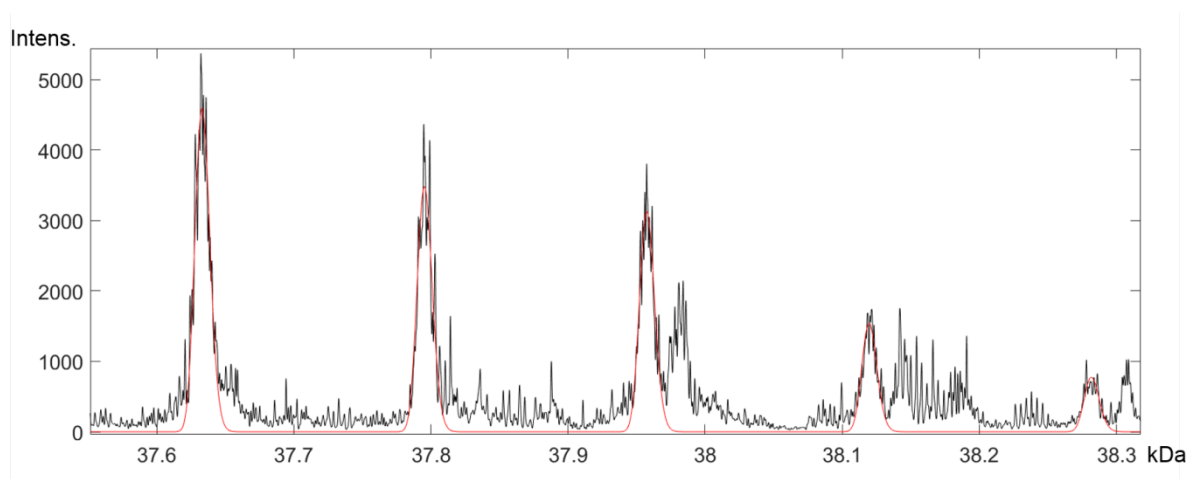
Figure 27: Sum spectrum of denatured IgE Fc (black) overlaid with a theoretical spectrum (red).

The ratio of glycans present on the denatured IgE Fc was calculated with the theoretical spectrum (Tab. 3). The calculation revealed several glycan structures at position N394 of the IgE Fc with the majority of 83% being hepta-, octa- and nonasaccharides ($HexNAc_2Hex_{5-7}$). Decasaccharides ($HexNAc_2Hex_8$) and undecasaccharides ($HexNAc_2Hex_9$) were also present at this position but in a very low ratio of 11% and 6%, respectively.

The most abundant glycan at this biologically important position is the heptasaccharide with 34%, confirming the glycan structure resolved in the crystal structure.

Table 3: Ratio of glycan structures present on the denatured IgE Fc.

Measured mass (average in Da)	Peptide molecular formula	Glycan	Ratio in %
37647	$C_{1596}H_{2502}N_{463}O_{493}S_{11}$	$HexNAc_2Hex_5$	34
37808	$C_{1596}H_{2502}N_{463}O_{493}S_{11}$	$HexNAc_2Hex_6$	26
37970	$C_{1596}H_{2502}N_{463}O_{493}S_{11}$	$HexNAc_2Hex_7$	23
38134	$C_{1596}H_{2502}N_{463}O_{493}S_{11}$	$HexNAc_2Hex_8$	11
38294	$C_{1596}H_{2502}N_{463}O_{493}S_{11}$	$HexNAc_2Hex_9$	6

4.1.6 Structural basis for the inhibitory activity of the single domain antibody

In general, anti-IgE therapeutics aim for the direct inhibition of the FcεRI-binding in the Cε3 domain, but the single domain antibody IgE026 mainly binds to the Cε4 domain. Therefore, direct inhibition of the FcεRI-binding must be negligible as the overlapping epitope between the FcεRI and IgE026 includes only four residues (Q392 - G395), and no steric inhibition can be observed. In contrast, there is a significant overlap between IgE026 and the CD23 epitopes (Fig. 28). In particular, IgE Fc residues S437 - A442 interact with IgE026 and provide an essential part of the CD23 epitope. Besides the overlapping epitopes, IgE026 also collides sterically with CD23 supporting the inhibitory effect.
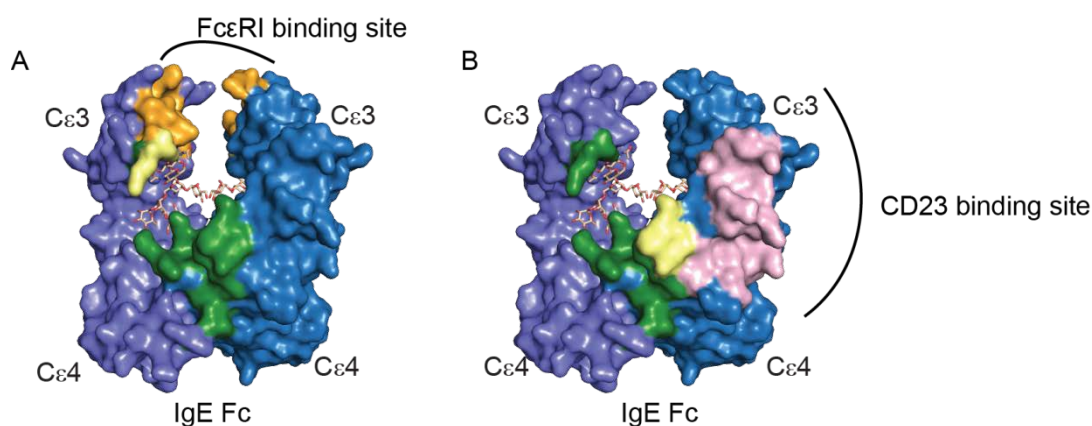
Figure 28: Overview of epitopes on the IgE Fc.
Surface representation of IgE Fc Cε3-4 (blue) with binding epitopes of IgE026 (green), FcεRI (orange) and CD23 (pink). **A:** Minor overlap of the epitopes (yellow) of IgE026 and FcεRI. **B:** Significant overlap of the epitopes (yellow) of IgE026 and CD23.

Binding to FcεRI and CD23 stabilizes different conformations of the IgE Cε3-4 domains, the open and closed state, respectively. As evident from the comparison of the IgE Fc distances (between the Cα atom of residue 394 and the Cα of residue 497 in the opposing chain) and the superimposed structures of the IgE026:IgE Fc, the CD23:IgE Fc, and the FcεRI:IgE Fc complex, illustrated in Fig. 29 and 30, IgE026 induces a conformational state of the IgE Fc in a closed conformation similar to the conformation adopted while CD23 binding.
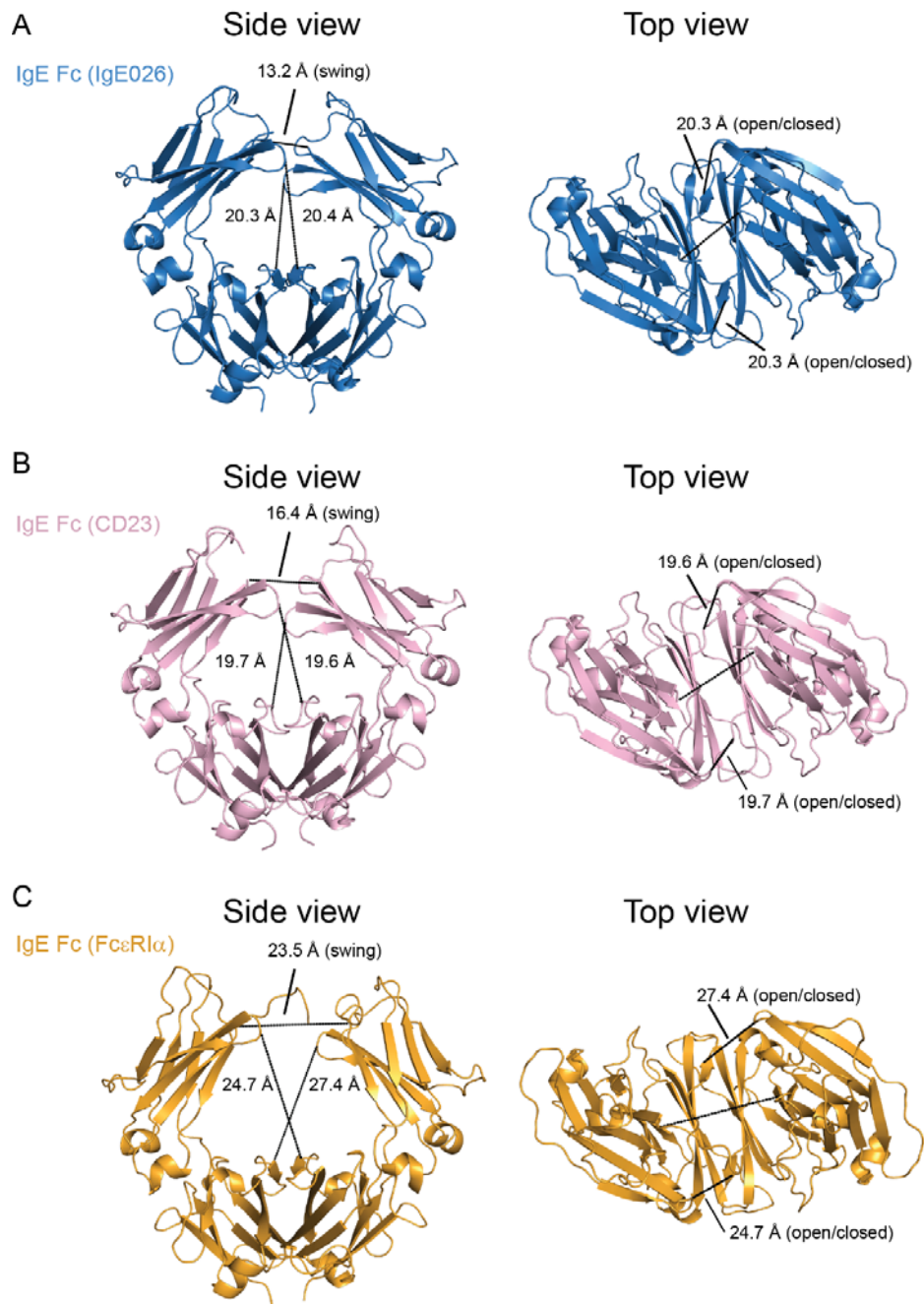
Figure 29: IgE026 is bound to a closed conformation of IgE Fc.
Structures of IgE Fc in complex with IgE026, CD23 and FcεRI with distances (black lines) defining their "open/closed" properties. Open/closed is defined by the distance between Cα atom of residue 394 and the Cα of residue 497 in the opposing chain [139]. **A:** The IgE Fc in complex with IgE026 shown in top and side views. **B+C:** As in panel A, but displaying the IgE Fc:CD23 (panel B) and IgE Fc:FcεRI complex (panel C).

The IgE026 mediated stabilization of the closed conformation provides an assumption for the inhibitory mechanism of the single domain antibody with respect to IgE-FcεRI interaction, whereas CD23 binding to IgE is directly prevented by steric hindrance.
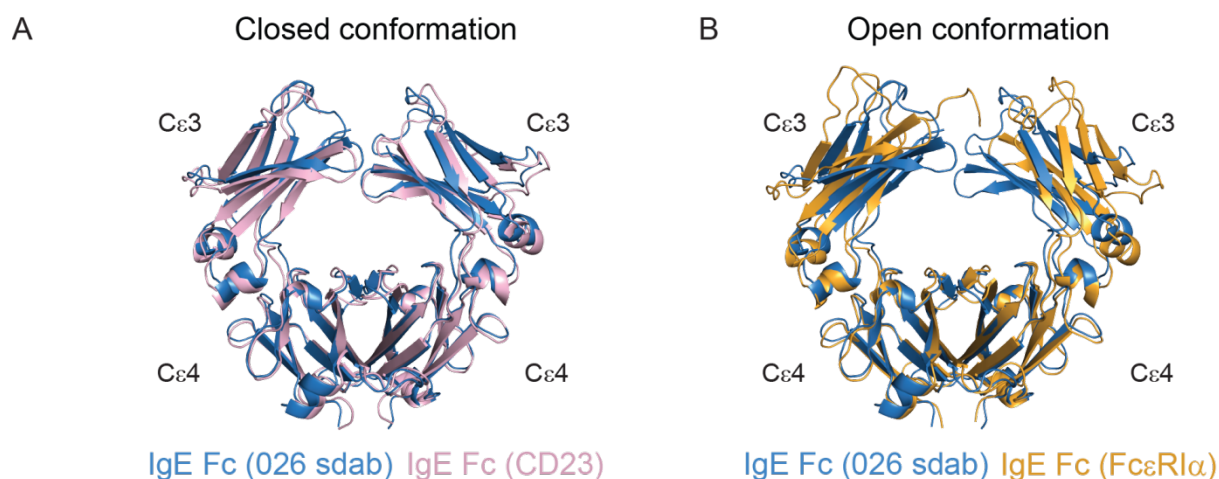
Figure 30: Comparison of IgE026 and CD23 epitopes and IgE Fc conformation.
Superposition of the IgE Fc domains reveals the similarity of the IgE Cε3-4 closed conformations in the complex with IgE026 in blue and CD23 in magenta (**A**) in contrast to the open conformation in the complex with FcεRI in yellow (**B**).

4.1.7 Effect of IgE026 on FcεRI and CD23 binding

From the structural data, it is evident that the binding sites of CD23 and IgE026 are overlapping whereas the binding sites of FcεRI and IgE026 are without significant overlap that could explain the inhibitory activity of IgE026 by competition. Therefore, the inhibitory effect of IgE026 on IgE bound to both IgE receptors was assessed in different biological assays.

To validate the observed sterical clash and overlap between IgE026 and CD23 epitopes the capability of IgE026 to interfere with CD23 binding of IgE was assessed in ELIFAB assays. ELIFAB assays are able to detect the binding of preformed oligovalent IgE:allergen complexes to CD23 [122]. Sera of patients with an elevated level of specific IgE (>100 kUA/L) against the honeybee venom allergen Api m 1, the birch pollen allergen Bet v 1 and the yellow jacket venom allergen Ves v 5 were incubated with the respective allergen and the IgE:allergen complexes applied to CD23. First, IgE026 was preincubated with different concentrations with the IgE:allergen complexes and then added to CD23. CD23 binding of the IgE:allergen complex rapidly decreased with increasing IgE026 concentrations. The inflexion point of IgE026 concentrations is allergen dependent and between 8 - 12 µg/mL (Fig. 31A). Hence, IgE026 efficiently prevented binding of the IgE:allergen complexes to CD23.
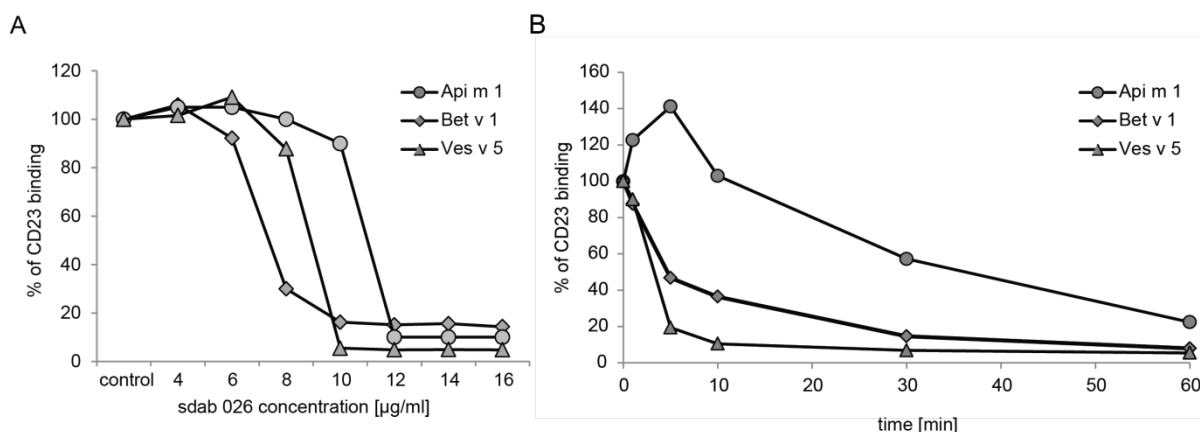
Figure 31: Inhibitory activity of IgE026 in ELIFAB.
A: Inhibition of IgE binding to CD23 by IgE026 analysed by ELIFAB. The binding of allergen:IgE complexes to surface-bound CD23 was detected by anti-IgE antibodies. Complexes were formed using sera of allergic patients having highly elevated specific IgE to Api m 1, Bet v 1 and Ves v 5 (>100 kUA/L), respectively.
B: The displacement of preformed IgE:allergen complexes from CD23 using sera as in A by the sdab was analysed by detecting remaining binding of IgE:allergen complexes after incubation with IgE026.

Furthermore, the IgE:allergen complexes were incubated with CD23 to allow binding. Thereafter, IgE026 was added to the CD23:IgE:allergen complex in order to analyse the disruptive effect. Within ten minutes the CD23 binding was significantly decreased, and after 60 min almost no binding was detected suggesting an efficient displacement of IgE:allergen complexes from CD23 (Fig. 31B).

Developed to interfere with the FcεRI binding, the impact of IgE026 in basophil activation was analysed with a panel of six birch pollen allergic patients. Basophils in the peripheral EDTA blood from the six donors were preincubated with and without IgE026 followed by adding the allergen Bet v 1. Upon cross-linking the FcεRI, sensitized basophils degranulate and express the cell surface marker CD63. CD63+ basophils were detected by flow cytometry and compared to the total amount of basophils, which was determined by the constitutively expressed basophil marker CCR3.

In order to compare the different basophil activation tests, the changes in basophil allergen threshold sensitivity (CDsens) to the birch pollen allergen Bet v 1 were investigated. CDsens is a well-established measure to quantify effector cell sensitivity to an allergen and reflects the amount of allergen needed for efficient activation.
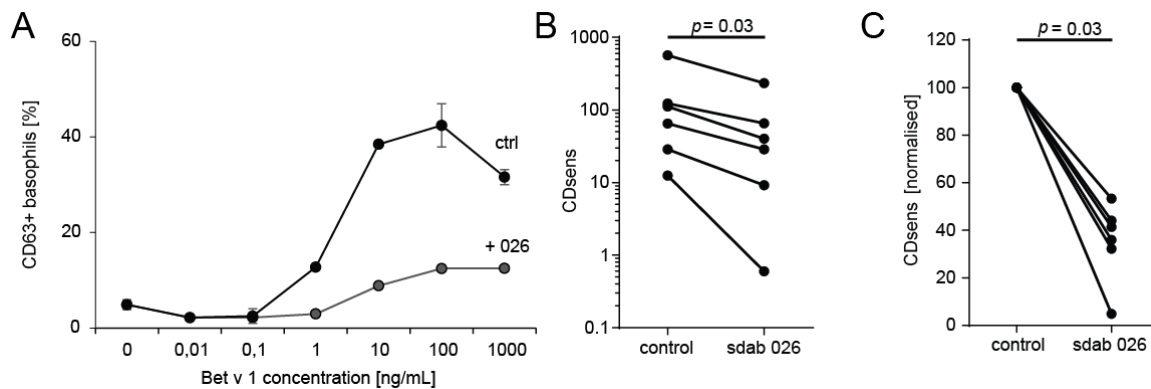
Figure 32: Inhibition of mediator release from basophils by IgE026.
A: The capability to reduce basophil sensitivity by displacement of IgE from the high-affinity receptor was analysed by basophil activation test (BAT). Basophils were incubated with IgE026 followed by incubation with the respective allergen. Activation was assessed by detecting CD63+ basophils in flow cytometry (Example of BAT of one donor analysed in B). **B:** Six birch pollen-sensitized patients were analysed as described in A. Reduction of effector cell sensitivity was evaluated by CDsens analysis. Samples with and without IgE026 treatment were compared using Wilcoxon signed-rank test. Differences considered statistically significant at p-values < 0.05. **C:** CDsens values normalised to 100 without IgE026 treatment.

In Fig. 32, the significant reduction between 50 - 95% of CDsens for patients' basophils treated with IgE026 is represented. Furthermore, comparison of the levels of sIgE to Bet v 1 and total IgE in the serum of patients suggest that a smaller ratio of sIgE to tIgE translates into a more pronounced reduction of CDsens suggesting a more effective treatment with IgE026, as depicted in Fig. 33.
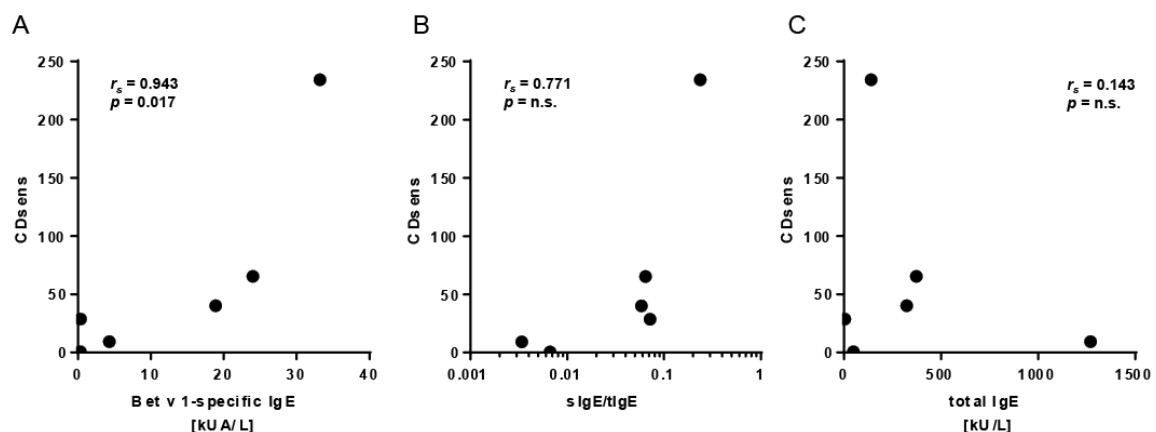
Figure 33: Correlation of CDsens and the IgE level of sensitized patients.
Correlation of CDsens with allergen-specific IgE (**A**), the ratio of sIgE and total IgE (**B**), and tIgE serum concentrations alone (**C**) for six birch pollen-sensitized patients. The correlation analyses were performed by using two-tailed Spearman's rank correlation coefficient. Differences were considered statistically significant at p-values < 0.05.

Moreover, the disruptive effect of IgE026 was investigated by flow cytometry analysis of surface IgE on human basophils obtained from three allergic patients sensitized to inhalative (birch pollen) and injected (Hymenoptera venom) allergens (Fig. 34).

IgE bound to the FcεRI on the surface of basophils was treated with IgE026 for 15 min and then stained with anti-IgE-FITC.
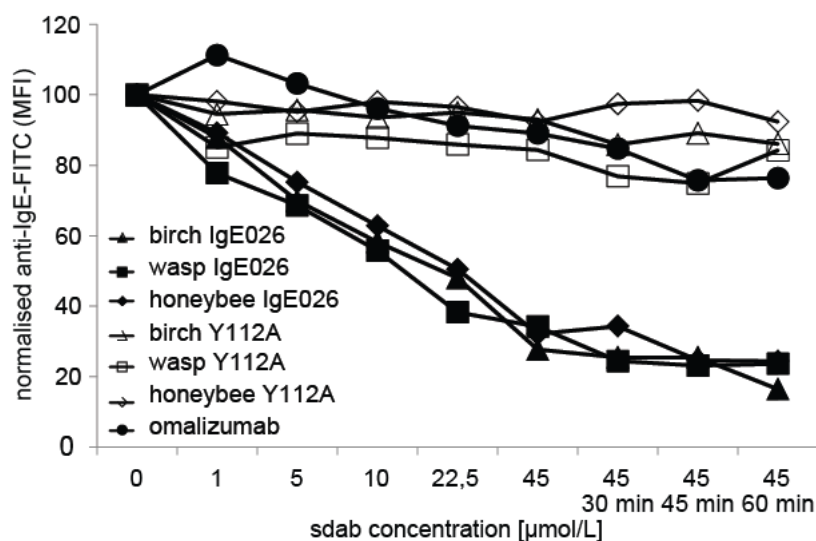

Figure 34: Flow cytometry analysis of surface IgE on human basophils.
Removal of IgE from the surface of basophils by IgE026, the inactive mutant Y112A and omalizumab were analysed by surface staining of IgE in flow cytometry. Basophils of patients with three different allergies were used.

The analysis showed the reduction of the amount of surface IgE to approx. 30%, depicted in Fig. 34. Prolonging the incubation time further reduced surface IgE to approx. 20%, which proves the disruptive effect of IgE026. Neither the inactive sdab mutant Y112A nor omalizumab exhibited comparable reduction, whereas high concentrations of omalizumab showed a slightly disruptive effect in accordance to the literature [94]. The biological data support the structural basis for the inhibitory effect of IgE026, and furthermore, indicate a disruptive effect of the IgE026 for the high- and low-affinity receptor.

4.1.8 SAXS analysis of IgE026 in complex with human IgE Fc

The crystal structure revealed the binding of the single domain antibody to the IgE Fc Cε3-4, but not the influence of the Cε2 domain. Therefore, the binding of IgE026 to IgE Fc Cε2-4 was analysed with small angle X-ray scattering. The contaminating IgE Fc Cε3-4 was removed by hydrophobic interaction chromatography. The IgE Fc was dialysed against 1.6 M $(NH_4)_2SO_4$, 20 mM HEPES, pH 7.2 and applied to a 1 mL Source 15PHE column. The protein was eluted with a 0 - 100% gradient of 50 mM NaCl, 20 mM HEPES, pH 7.2 and the elution fractions were analysed on a Coomassie-stained polyacrylamide gel.
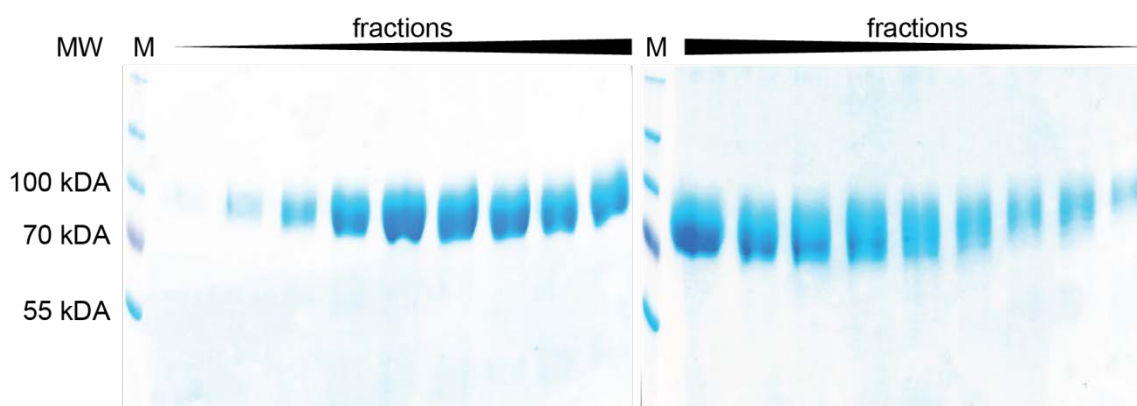
Figure 35: SDS-PAGE analysis of recombinant IgE Fc purified with HIC.
Recombinant human IgE Fc was purified with 1 mL Source 15PHE column (GE Healthcare), and elution fractions were analysed on 10% TRIS-glycine gel, which was stained with Coomassie brilliant blue. 2 µL marker (M) and 20 µL non-reduced samples were used.

IgE Fc Cε2-4 was detectable without contaminating IgE Fc Cε3-4 between 70 kDa and 100 kDa (Fig. 35). The fractions were pooled, and the complex with IgE026 was formed as described in chapter 4.1.3. Subsequently, the complex was concentrated, applied to a Superdex 200 10/300 GL gel filtration column and eluted isocratically with 20 mM HEPES, 50 mM NaCl, pH 7.2. In Fig. 36, the chromatogram of the size exclusion chromatography of IgE026:IgE Fc compared to the elution profile of IgE Fc alone is illustrated. The shift to an earlier retention volume indicates the formation of the complex. The peak between 17 and 20 mL represents the excess IgE026.
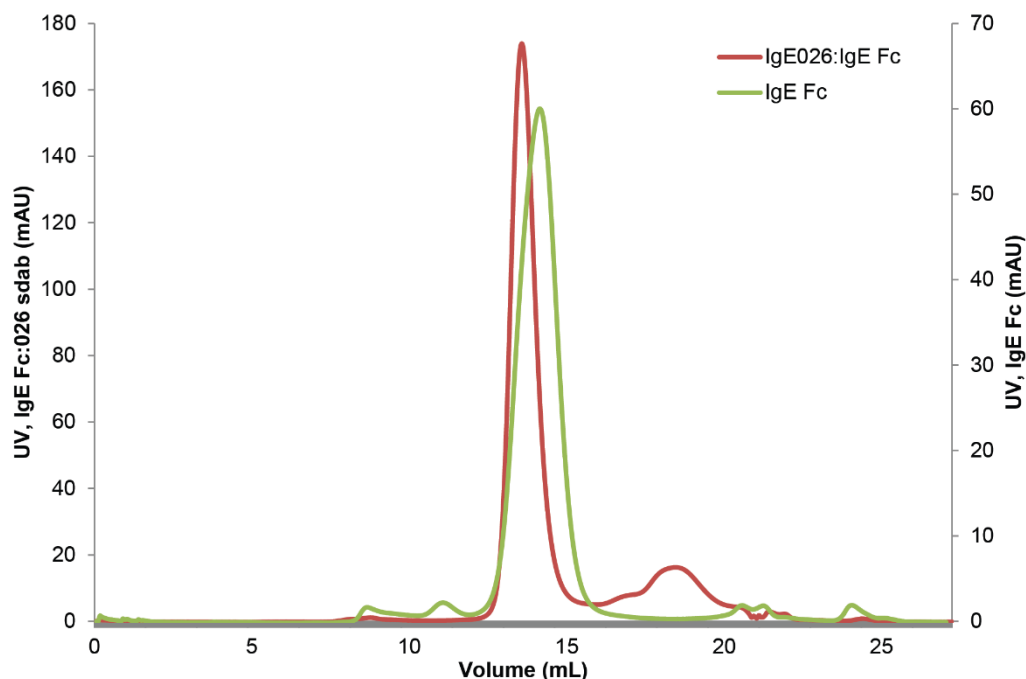
Figure 36: Chromatogram of the purification of the IgE026:IgE Fc complex for SAXS with gel filtration.
The IgE026:IgE Fc complex (red) was formed with a 4:1 ratio overnight and purified with Superdex 200 10/300 GL column (GE Healthcare) compared to IgE Fc alone (green) demonstrating the formation of the complex.

The elution fractions of the IgE026:IgE Fc complex were pooled and analysed on a polyacrylamide gel stained with Coomassie. The SDS-PAGE gel in Fig. 37 shows the successful formation of the IgE026:IgE Fc complex with IgE Fc Cε2-4 between 70 kDa and 100 kDa and IgE026 at approx. 15 kDa. Notably, the IgE Fc Cε3-4 was separated completely.
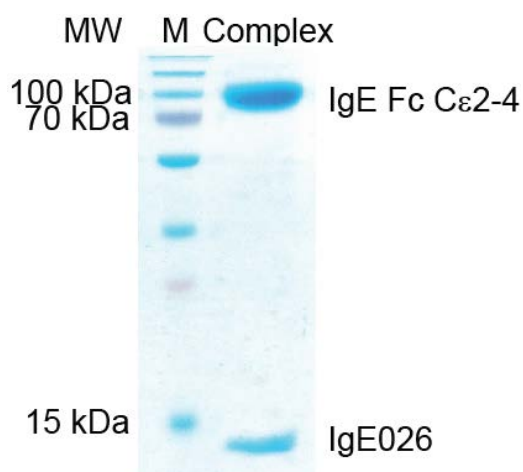
Figure 37: SDS-PAGE analysis of IgE026:IgE Fc purified with gel filtration.
The complex IgE026:IgE Fc was formed with a 4:1 ratio overnight and purified with Superdex 200 10/300 GL column (GE Healthcare). The elution fractions were concentrated, and the complex was analysed on 15% TRIS-glycine gel, which was stained with Coomassie brilliant blue. 2 µL marker (M) and 20 µL non-reduced sample were used.

The SAXS data of IgE Fc alone and in complex with IgE026 were collected in batch mode at the ESRF BM29 (Grenoble, France) beamline. The samples were investigated in concentration ranges of 0.5 - 1.7 mg/mL and 2.2 - 9.0 mg/mL for the IgE026:IgE Fc complex and IgE Fc, respectively. In order to evaluate the presence of sample aggregation or concentration-dependent scattering, the collected data were diagrammed in a Guinier plot. The linear fit, illustrated in Fig. 38A+B, suggests no signs of interparticle effects for the IgE Fc and the IgE026:IgE Fc complex. Furthermore, the radius of gyration was calculated for both proteins from the gradient of the linear fit resulting in a radius of 3.3 nm for the IgE Fc and 3.6 nm for the complex, which is similar to values previously observed for IgE Fc [140]. The flexibility of the structure was analysed in the Kratky plot, which is depicted in Fig. 38C. Here, the shape of the curve helps to identify the conformation of the molecule. A distinct peak is an indicator for a compact or folded conformation, whereas a rise to a plateau indicates an unfolded protein. The IgE Fc, as well as, the IgE026:IgE Fc complex show a distinct peak followed by a plateau tend to approach zero suggesting well-folded proteins with limited flexibility.
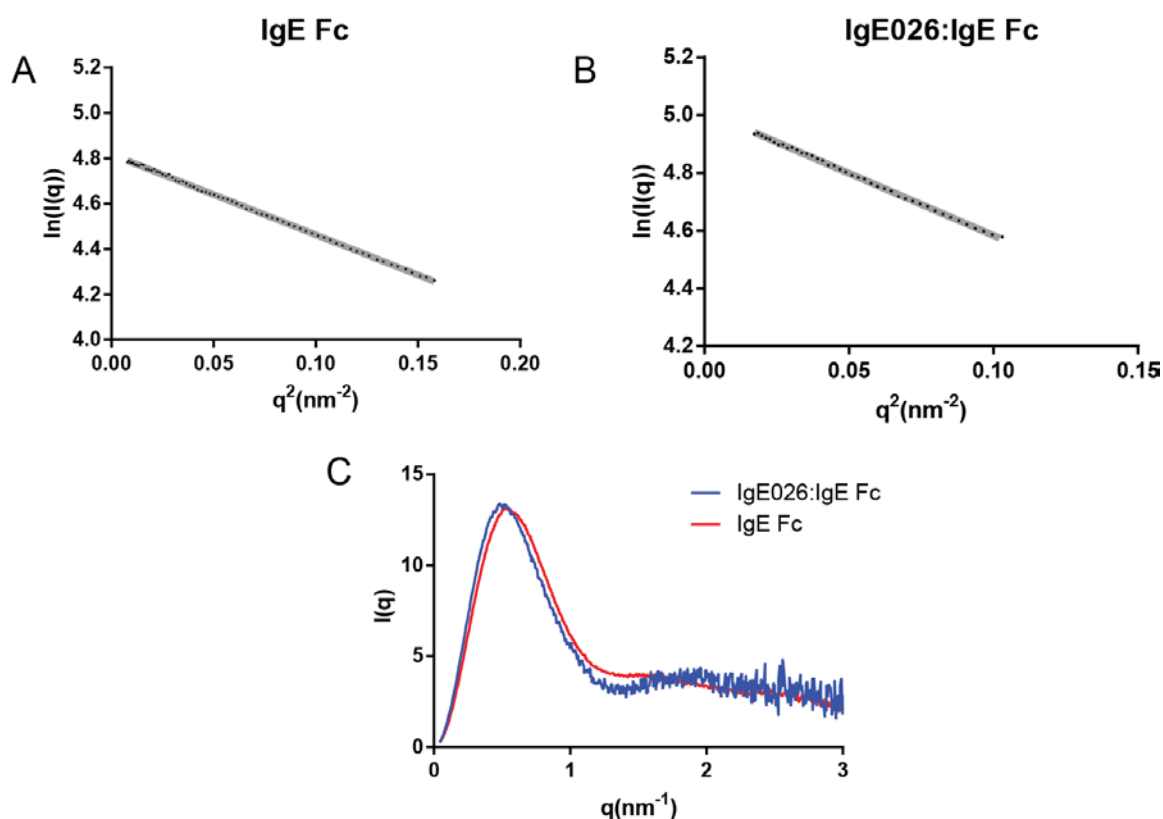

Figure 38: Solution scattering analysis of IgE Fc and its complex with IgE026.
A+B: The Guinier plot for IgE Fc and IgE026:IgE Fc (black dots) and the linear fit (gray line). No sign of interparticle effects are present and the plot suggests a radius of gyration of 3.3 nm for IgE Fc and 3.6 nm for the complex calculated with the gradient of the linear fit. **C:** The Kratky plot of IgE Fc (red) and IgE026:IgE Fc (blue) shows that both proteins are well folded and have limited flexibility.

Overall, the observed results in the Guinier and the Kratky plot suggest a good data quality for the structure modelling. The modelling of the SAXS structures was done as described in chapter 3.4.2 and resulted in a tightly clustered ensemble of solutions for the IgE026:IgE Fc complex fitting the SAXS curve well with an average $\chi^2 = 1.063 \pm 0.019$ (Fig. 39).
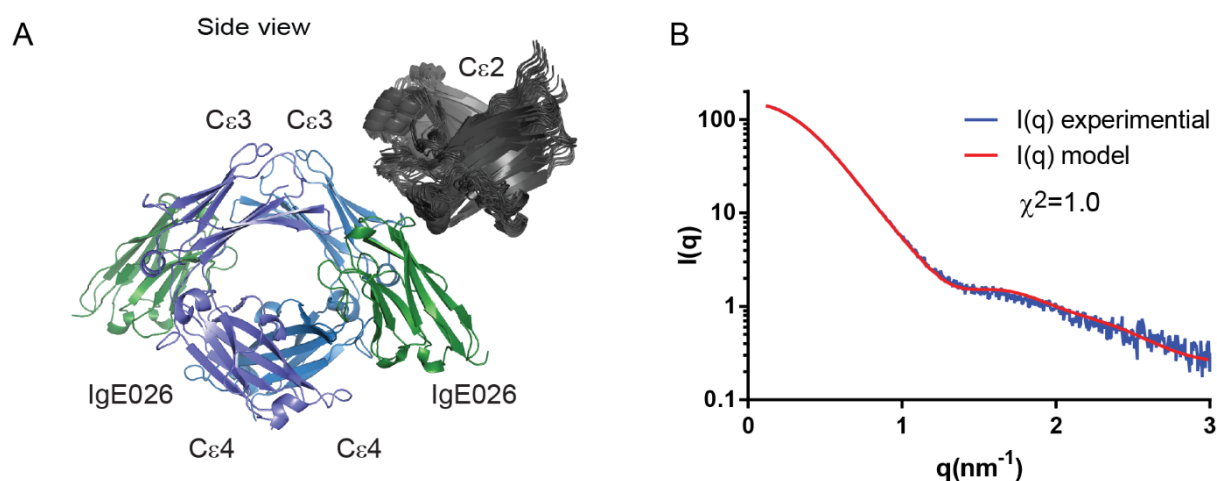

Figure 39: SAXS analysis of the IgE026:IgE Fc complex.
A: Side view of 20 superimposed rigid body models obtained with IgE026 (green), IgE Fc Cε3-4 (blue), and Cε2 domain (grey). **B:** Fit of the scattering curve calculated from a representative rigid body model to the experimental curve.

Rigid body modelling strongly suggested a bent conformation of the free IgE Fc Cε2-4 with the Cε2 domain oriented towards the Cε3 domain in accordance with published bent solution structures of IgE Fc[140] and free rat IgE[141] (Fig. 40A). Compared to the experimental data of unbound IgE Fc in either closed or open conformation, the model resulted in a less tightly clustered set of solutions having χ^2 values in the range of 1.91 - 2.50 during refinements reflecting the dynamic behaviour of the Cε2 domain (Fig. 40B). However, qualitatively all output models assumed the bent conformation with the Cε2 domains located towards the Cε3 domains.
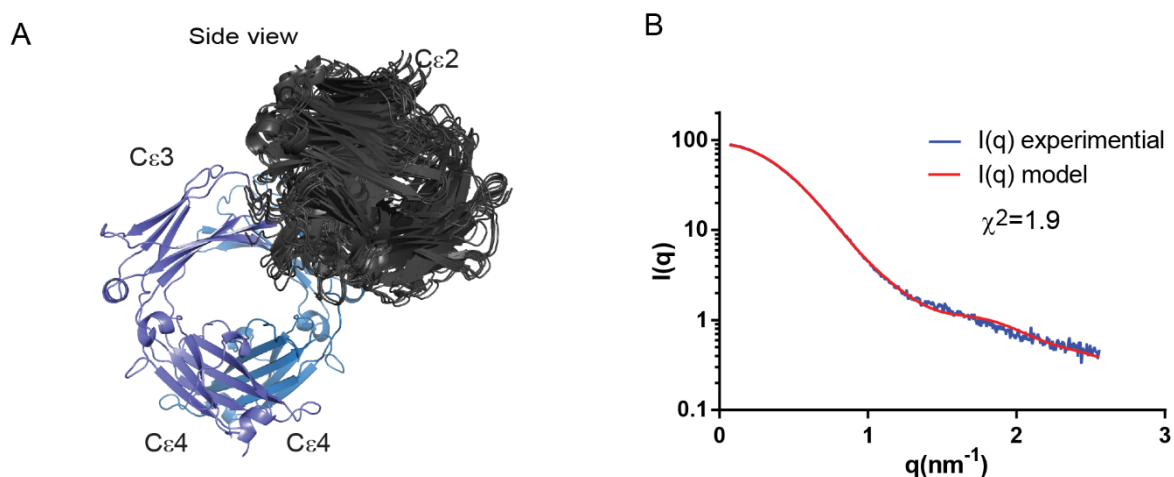
Figure 40: SAXS analysis of free IgE Fc.
A: Side view of 20 superimposed rigid body models obtained with IgE Fc Cε3-4 in the closed conformation (blue), and Cε2 domain (grey). **B:** Fit of the scattering curve calculated from a representative rigid body model to the experimental curve.

In roughly 95% of the output models with the Cε3 domains in the closed conformation a significant overlap between the Cε2 domains and the bound IgE026 would occur. The crystal structure of the IgE026:IgE Fc complex compared with unbound IgE Fc (PDB: 2WQR) revealed that the IgE Fc must adopt a significantly less bent conformation to avoid overlap between the Cε2 domains and the bound IgE026 (Fig. 41).
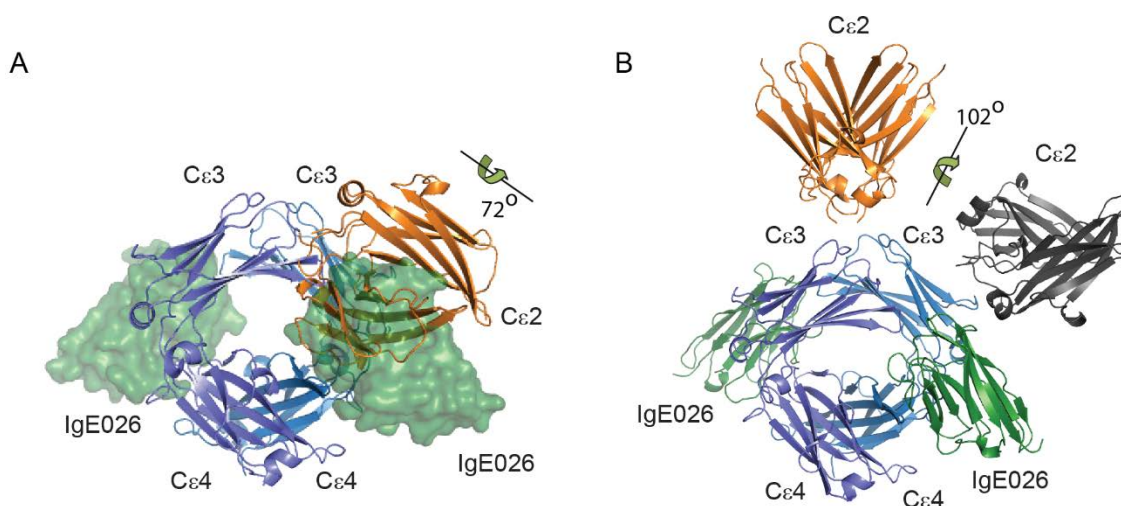
Figure 41: Conformational state of IgE026:IgE Fc in SAXS analysis.
A: Overlay of the fully bent conformation of free IgE Fc (PDB: 2WQR) with IgE026:IgE Fc revealed substantially overlap of Cε2 (orange) with the single domain antibody (green). **B:** Comparison of the extended IgE Fc conformation (Cε2 in orange; PDB: 4J4P) and the slightly bent conformation of the IgE Fc in complex with IgE026 observed in SAXS (Cε2 in grey).

71

Overall the SAXS data provide evidence for IgE026 mediated displacement of the Cε2 and unbending of the IgE Fc resulting in a so far undescribed conformation of the IgE Fc Cε2-4 domains, but still an approx. 100° rotation would be required to reach the fully extended conformation of IgE Fc (Fig. 41).

4.2 Structural and functional analysis of ligelizumab Fab

Ligelizumab, currently under clinical trials, was designed to obtain greater suppression of free IgE and IgE bound to mast cells and basophils compared to omalizumab, which might overcome some limitations of omalizumab and lead to better clinical outcomes [108,109].

4.2.1 Cloning, expression and purification of ligelizumab Fab

In order to analyse the structure of ligelizumab Fab, the Fab was expressed in insect cells. Therefore, the variable heavy and light chain of ligelizumab were amplified from a synthetic gene with the restrictions sites NotI/SgsI for the V_L and SfiI/XhoI for the V_H. Then, the variable heavy and light chain were cloned into the pFastBac Dual expression vector for baculovirus-mediated insect cell expression. The pFastBac Dual expression vector has two multiple cloning sites for the simultaneous expression of two proteins, which is beneficial for antibody expression. The expression of the light chain is initiated by the p10 promoter and the expression of the heavy chain by the polyhedrin promoter, which both are strong promoters. Heavy and light chains are expressed as fusion proteins with the gp67 signal sequence to ensure an efficient secretion. The expression cassette of ligelizumab Fab in pFastBac Dual is shown in Fig. 42.

Figure 42: Schematic representation of expression cassette of ligelizumab Fab in pFastBac Dual.

After the successful cloning, the recombinant ligelizumab Fab bacmid was generated, and *Sf*9 insect cells were transfected. Cryoprotected cell stocks were produced after three rounds of amplification and the titre determined in test expression. The immunoblot of the ligelizumab Fab test expression shows no difference in expression rate between the different volumes of cryostock, therefore 0.5 mL of cryostock were used for 1 L expression volume.
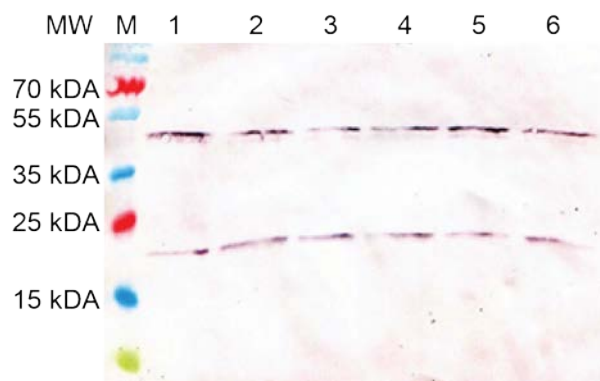
Figure 43: SDS-PAGE analysis of recombinant ligelizumab Fab test expression.
100 µL ligelizumab Fab cryostock was diluted in 5 mL HyClone™ SFX-Insect™ media. Different amounts (1-6: 1, 10, 25, 50, 75, 100 µL) of the diluted cryostock were used for expression in $1·10^6$ *Sf*9 cells/mL. Cells were incubated for 5 days at 27 °C, and the supernatant was analysed on 12% TRIS-glycine gel, which was used for immunoblot. 2 µL marker (M) and 20 µL non-reduced samples were used. Immunoblot was detected using anti-human κ-light chain conjugated with alkaline phosphatase (1:20,000), and NBT/BCIP substrate solution.

10 L ligelizumab Fab were expressed in *Sf*9 insect cells for 5 days shaking at 27 °C. The supernatant was centrifuged and purified by affinity chromatography using the ÄKTA Start system. The elution fractions, together with the supernatant and flow-through, were analysed on a 10% polyacrylamide gel stained with Coomassie and ligelizumab Fab specifically detected with anti-human κ-light chain antibody by immunoblot.
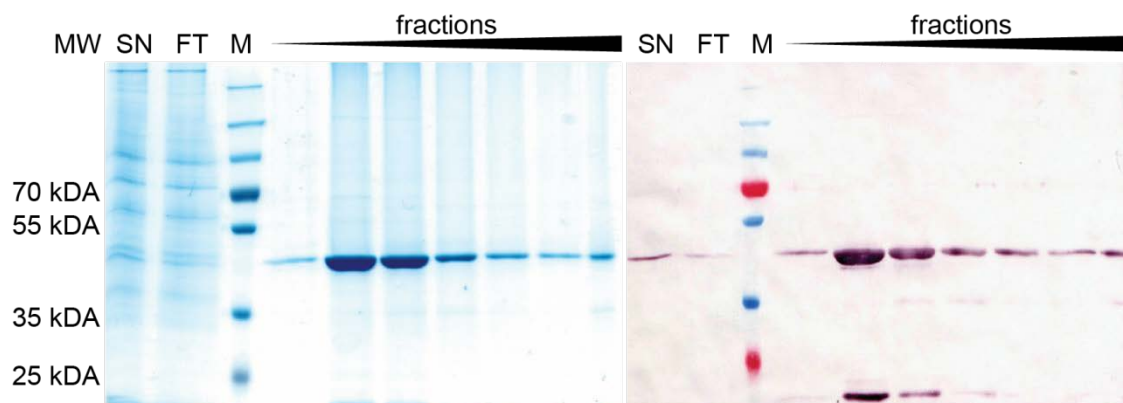

Figure 44: SDS-PAGE analysis of recombinant ligelizumab Fab purified with affinity chromatography.
Ligelizumab Fab was expressed in 1 L *Sf*9 cells, purified with 1 mL KappaSelect column (GE Healthcare), and supernatant (SN), flow-through (FT) and elution fractions were analysed on 10% TRIS-glycine gels, which were stained with Coomassie brilliant blue (left) and used for immunoblot (right). 2 µL marker (M) and 20 µL non-reduced samples were used. Immunoblot was detected using anti-human κ-light chain conjugated with alkaline phosphatase (1:20,000), and NBT/BCIP substrate solution.

Fig. 44 shows the analysis of the affinity chromatography of ligelizumab Fab purified from 1 L *Sf*9 insect cell supernatant. The intense band at approx. 50 kDa in the Coomassie-stained gel as well as in the immunoblot represents ligelizumab Fab, which has a theoretical molecular weight of 49 kDa.

The elution fractions contain minor impurities and degradation products of the protein, for example, the light chain specifically detected in the immunoblot at approx. 20 kDa. The protein has an expression rate of max. 2.5 mg/L, which corresponds to an overall yield of approx. 25 mg out of 10 L. Furthermore, the purification efficiency and reactivity of ligelizumab Fab against human IgE Fc was verified by ELISA. Ligelizumab Fab was efficiently purified from the cell culture supernatant and showed pronounced reactivity against the IgE Fc in fraction F2 - F5 (Fig. 45).
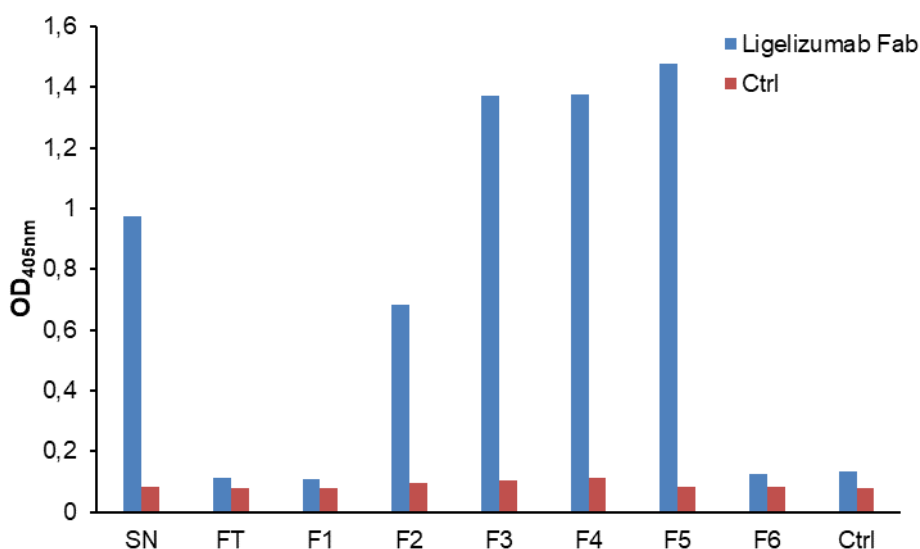

Figure 45: Immunoreactivity of ligelizumab Fab fractions against human IgE Fc in ELISA.
25 µL (100 ng/µL) human IgE Fc was coated overnight. The wells were blocked with 4% MPBS for 30 min at rt. After the wells had been washed with TPBS and PBS, 50 µL of the supernatant (SN), flow-through (FT) and elution fractions (F1-F6) including an antibody control (Ctrl) were incubated for 2 hours at rt. For detection 100 µL anti-human κ-light chain (1:20,000) conjugated with alkaline phosphatase were used. The development was performed with pNPP and detected at 405 nm.

These fractions were pooled, dialysed against 20 mM MES, 50 mM NaCl, pH 6.0, and subsequently applied to a 1 mL MonoS 5/50 cation exchange column using the ÄKTA pure 25 system. Ligelizumab Fab was eluted with a 0 - 50% gradient of 20 mM MES, 1 M NaCl, pH 6.0 and the elution fractions were analysed on a polyacrylamide gel.
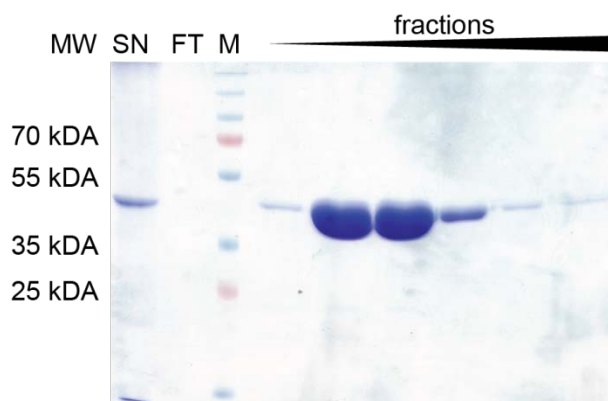
Figure 46: SDS-PAGE analysis of recombinant ligelizumab Fab purified with IEX.
Ligelizumab Fab was purified with 1 mL MonoS 5/50 GL column (GE Healthcare), and supernatant (SN), flow-through (FT) and elution fractions were analysed on 12% TRIS-glycine gel, which was stained with Coomassie brilliant blue. 2 µL marker (M) and 20 µL non-reduced samples were used.

Compared to the supernatant, all major contaminants were removed using the cation exchange chromatography (Fig. 46). The elution fractions containing ligelizumab Fab were pooled, concentrated and applied to a Superdex 75 10/300 GL gel filtration column. The protein was eluted isocratically with 20 mM HEPES, 50 mM NaCl, pH 7.2 and elution fractions were analysed with SDS-PAGE, depicted in Fig. 47.
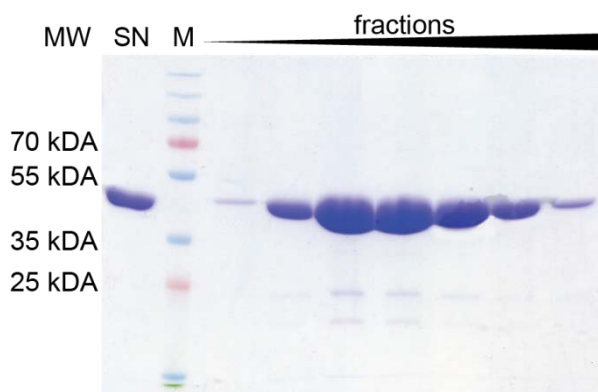

Figure 47: SDS-PAGE analysis of ligelizumab Fab purified with gel filtration.
Ligelizumab Fab was purified with Superdex 75 10/300 GL column (GE Healthcare), and the elution fractions were analysed on 12% TRIS-glycine gel, which was stained with Coomassie brilliant blue. 2 µL marker (M) and 20 µL non-reduced samples were used.

4.2.2 Effect of ligelizumab Fab on FcεRI binding in mediator release assay

In order to analyse the inhibitory effect of ligelizumab Fab a mediator release assay was performed. RBL-SX38 cells are basophil leukaemia cells from rats, which were stably transfected with human FcεRI. Due to the expression of the high-affinity receptor on the cell surface, this cell line is used as an allergy model to imitate the

IgE-mediated degranulation of human mast cells and basophil granulocytes by cross-linking the FcεRI.

The degranulation releases inflammatory mediators like histamine, serotonin and β-hexosaminidase. The latter together with sodium carbonate converts the chromogenic substrate 4-nitrophenyl *N*-acetyl-β-D-glucosaminide (pNAG), which can be detected at 405 nm. In order to verify the inhibitory effect of ligelizumab Fab in the context of allergic reactions, the Fab was incubated with recombinant M5huIgE prior to the incubation with the RBL cells. M5huIgE is a CCD-specific antibody that recognises the CCDs present on horseradish peroxidase (HRP). Hence, the release of β-hexosaminidase was measured and revealed the efficient inhibition of FcεRI cross-linking by binding the IgE antibodies, as represented in Fig. 48. The inhibitory effect is even more pronounced compared to the anti-IgE sdab IgE026. 3 µM ligelizumab Fab were sufficient to inhibit the cross-linking and to prevent the cells to release inflammatory mediators.
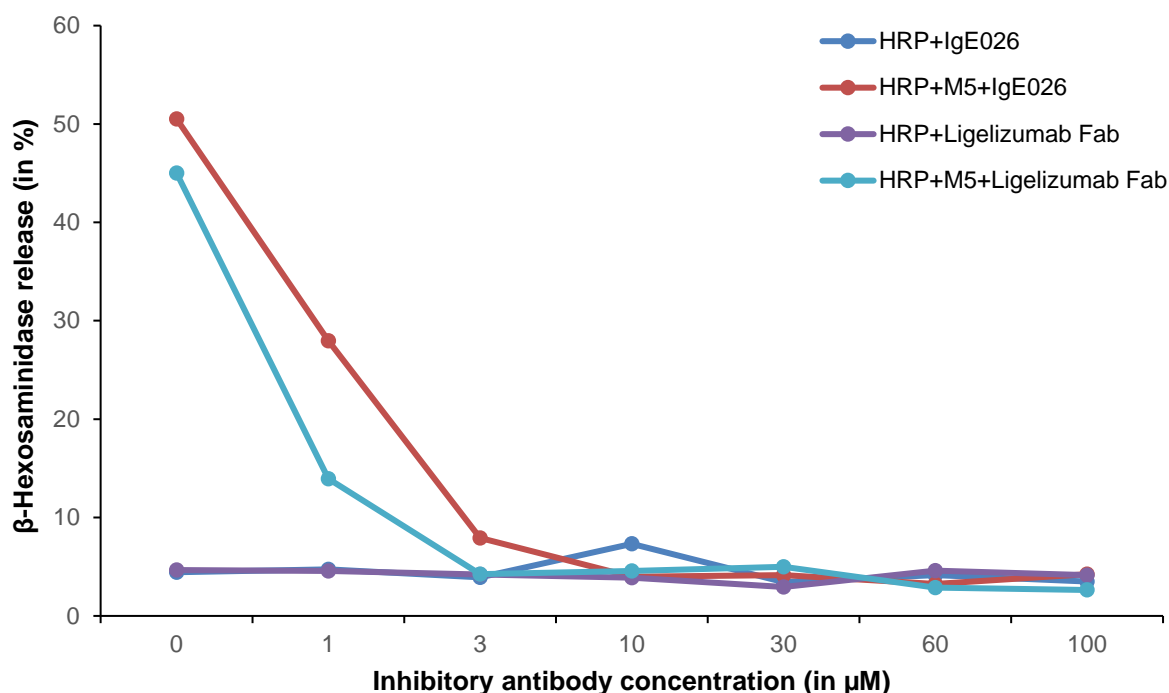

Figure 48: Analysis of the inhibitory efficiency of ligelizumab Fab in mediator release assay of RBL cells. RBL-SX38 cells were incubated for 120 minutes with 1 µg/mL M5huIgE preincubated with different concentrations of ligelizumab Fab and IgE026 for 30 min. Degranulation was induced by addition of 0.3 µg/mL HRP, and the release of the mediator β-hexosaminidase was detected after addition of the substrate pNAG at 405 nm. The IgE-induced release of β-hexosaminidase was calculated from the total amount after cell lysis in percent. No anti-IgE was added for the positive control and the negative control for each anti-IgE antibody was without M5huIgE.

4.2.3 Crystallisation of ligelizumab Fab in complex with human IgE Fc

The complex was formed with a molar ratio of 1:2 in which 1 mg IgE Fc was incubated with 2 mg of ligelizumab Fab overnight at 4 °C. After the complex was concentrated, it was applied to a Superdex 200 10/300 GL gel filtration column and eluted isocratically with 20 mM HEPES, 50 mM NaCl, pH 7.2. In Fig. 49 and Fig. 50, the chromatogram of the size exclusion chromatography compared to the elution profile of IgE Fc alone and the corresponding Coomassie gel of ligelizumab Fab:IgE Fc is illustrated.
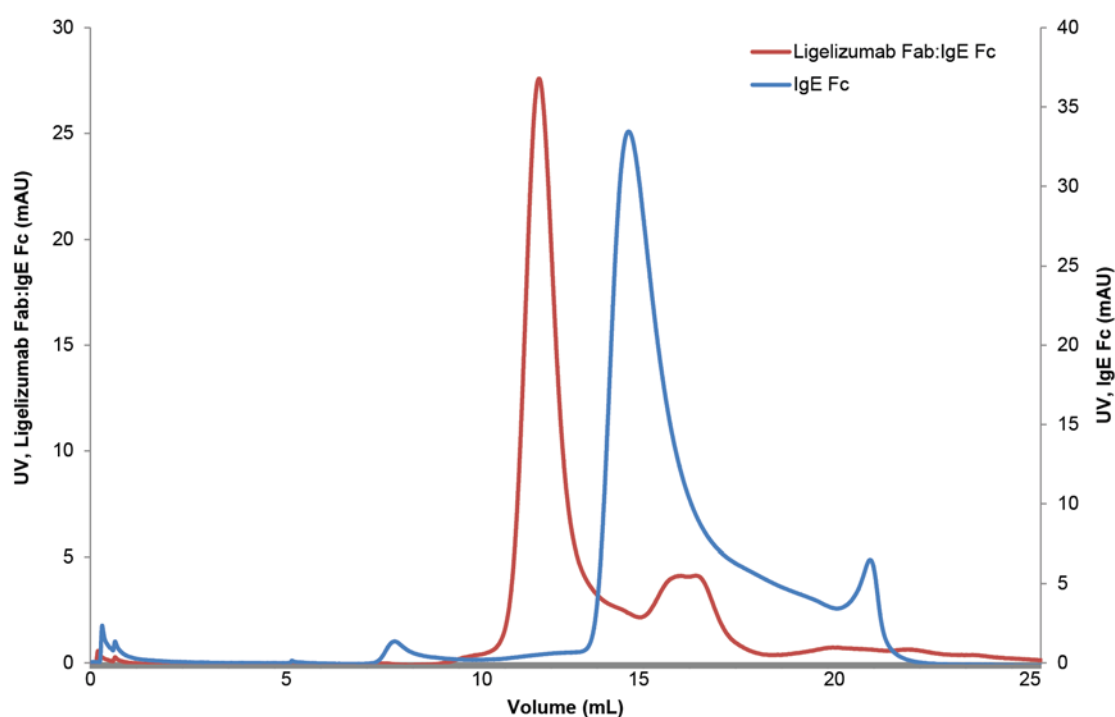

Figure 49: Purification of the ligelizumab:IgE Fc complex for crystallisation with gel filtration.
The ligelizumab Fab:IgE Fc (red) was formed with a 2:1 ratio overnight and purified with Superdex 200 10/300 GL column (GE Healthcare) compared to IgE Fc alone (blue) demonstrating the formation of the complex.

The shift to an earlier retention volume indicated the formation of the complex, which was confirmed in the Coomassie gel showing the IgE Fc between 70 and 100 kDa and ligelizumab Fab between 35 and 55 kDa. The peak between 15 and 20 mL in the chromatogram represents the excess ligelizumab Fab.
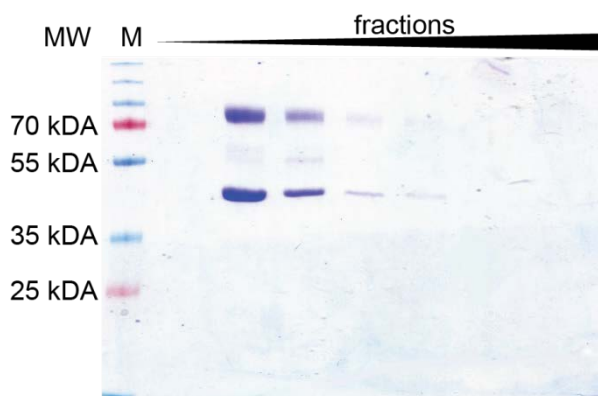
Figure 50: SDS-PAGE analysis of ligelizumab Fab:IgE Fc purified with gel filtration.
The complex ligelizumab Fab:IgE Fc was purified with Superdex 200 10/300 GL column (GE Healthcare), and the elution fractions were analysed on 12% TRIS-glycine gel, which was stained with Coomassie brilliant blue. 2 µL marker (M) and 20 µL non-reduced samples were used.

After concentrating to 10 mg/mL, the ligelizumab Fab:IgE Fc complex was crystallised by vapour diffusion in sitting drops formed by mixing protein and reservoir solution in the ratio 1:1. Initial commercial crystallisation trays (Structure, INDEX, and ProPlex) were set up with 200 nL protein solution and 200 nL reservoir solution at 4 °C and 19 °C using the mosquito® Crystal dispenser. After three days needle-shaped crystals were obtained in two different conditions (Structure F9: 0.1 M NaH$_2$PO$_3$, 0.1 M KH$_2$PO$_3$, 0.1 M MES pH 6.5, 2 M NaCl and Structure G2: 0.2 M (NH$_4$)$_2$SO$_4$, 0.1 M MES pH 6.5, 30% (w/v) PEG 5K MME) at 4 °C and 19 °C (Fig. 51).
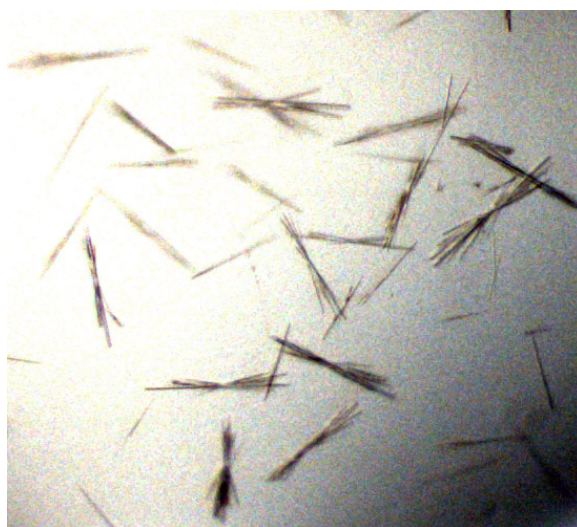

Figure 51: Microscopic image of the ligelizumab Fab:IgE Fc crystals (8x magnification).
Ligelizumab Fab:IgE Fc complex was concentrated to 10 mg/mL in 20 mM HEPES, 50 mM NaCl, pH 7.2, and crystallised by vapour diffusion in sitting drops formed by mixing 200 nL protein and 200 nL reservoir solution containing 0.2 M (NH$_4$)$_2$SO$_4$, 0.1 M MES pH 6.5, 30% (w/v) PEG 5K MME at 19 °C.

The crystallisation conditions were optimised with grid screens resulting in additional crystals and crystalline material, but no improvement in crystal morphology or size was obtained. In order to change the morphology of the crystals, an anti-IgE nanobody should be introduced into the complex structure. Therefore, a llama was immunized with the recombinant, CCD-specific M5huIgE and the nanobody 7-1 was selected with phage display and cloned into pET22b(+)-vector by M. MIEHE [117]. A 50 mL *E. coli* culture was inoculated with 50 µL of the overnight culture and cultured until cells reached the logarithmic phase at 37 °C. Protein expression was induced with IPTG and incubated at 30 °C overnight. The supernatant was purified with 1 mL Ni-NTA resin, and the elution fraction was analysed on a SDS-PAGE gel stained with Coomassie.
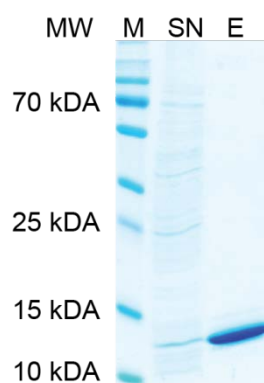

Figure 52: SDS-PAGE analysis of sdab 7-1 purified with IMAC.
The sdab 7-1 was expressed in 50 mL *E. coli* cells, purified with 1 mL Ni-NTA resin, and supernatant (SN) and the elution fraction (E) were analysed on 15% TRIS-glycine gel, which was stained with Coomassie brilliant blue. 2 µL marker (M) and 20 µL non-reduced samples were used.

As evident from the band in the gel between 10 and 15 kDa, the nanobody was purified efficiently from the supernatant without major contaminations. The biological activity was verified in ELISA with recombinant M5huIgE and human IgE Fc. Here, the nanobody 7-1 showed high reactivity to both IgE constructs suggesting a binding site in the IgE Fc domain compared to the nanobody IgE026.
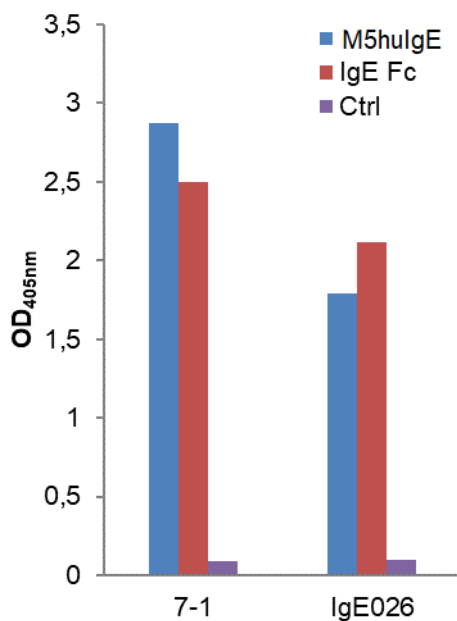
Figure 53: Immunoreactivity of sdab 7-1 against recombinant human IgE and human IgE Fc in ELISA.
25 µL (100 ng/µL) recombinant M5huIgE and human IgE Fc were coated overnight. The wells were blocked with 4% MPBS for 30 min at rt. After the wells had been washed with TPBS and PBS, 50 µL of the sdab 7-1 and sdab IgE026 were incubated for 2 hours at rt. For detection 100 µL anti-Penta His (1:5,000) and anti-mouse IgG (whole molecule)-AP (1:30,000) were used. The development was performed with pNPP and detected at 405 nm.

In order to crystallise the nanobody in complex with ligelizumab Fab:IgE Fc, the competition between ligelizumab Fab and 7-1 to the IgE Fc was proven by ELISA. Therefore, the nanobody alone, ligelizumab Fab alone or both together were incubated with IgE Fc coated on the plate. Advantageously, both antibodies could be detected independently with specific antibodies, anti-V5 and anti-kappa for the nanobody and ligelizumab Fab, respectively. As diagrammed in Fig. 54, both antibodies were able to bind to IgE Fc at the same time suggesting no competition for the same binding epitope.
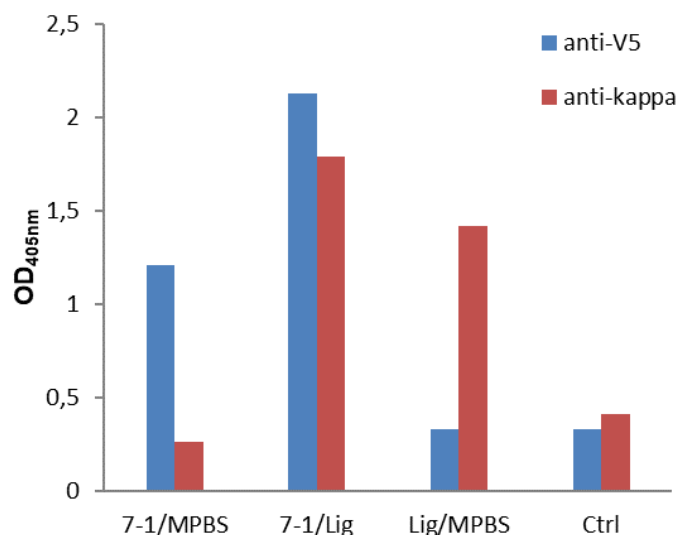
Figure 54: Competition analysis of sdab 7-1 and ligelizumab Fab in ELISA.
50 µL (100 ng/µL) human IgE Fc were coated overnight. The wells were blocked with 4% MPBS for 30 min at rt. After the wells had been washed with TPBS, 50 µL of the sdab 7-1 alone (7-1/MPBS), 7-1 and ligelizumab Fab together (7-1/Lig), ligelizumab Fab alone (Lig/MPBS) and an antibody control (Ctrl) were incubated for 2 hours at rt. Both antibodies were detected independently; 7-1 was detected with 100 µL anti-V5 (1:5,000) and anti-rabbit IgG (whole molecule)-AP (1:30,000), and ligelizumab Fab was detected with 100 µL anti-human κ-light chain (1:20,000) conjugated with alkaline phosphatase. The development was performed with pNPP and detected at 405 nm.

4.2.4 Crystallisation of ligelizumab Fab in complex with IgE Fc and sdab 7-1

The complex was formed with a molar ratio of 2:1:2 in which 2 mg ligelizumab Fab were incubated with 1 mg IgE Fc and 0.5 mg 7-1 overnight at 4 °C. After the complex was concentrated, it was applied to a Superdex 200 10/300 GL gel filtration column and eluted isocratically with 20 mM HEPES, 50 mM NaCl, pH 7.2. In Fig. 55, the chromatogram of the size exclusion chromatography of ligelizumab Fab:IgE Fc:7-1 is illustrated compared to the elution profile of ligelizumab Fab:IgE Fc alone. The shift to an earlier retention volume indicated the formation of the complex. The peak at ~16 mL represents the excess ligelizumab Fab and at ~19 mL represents the excess nanobody.
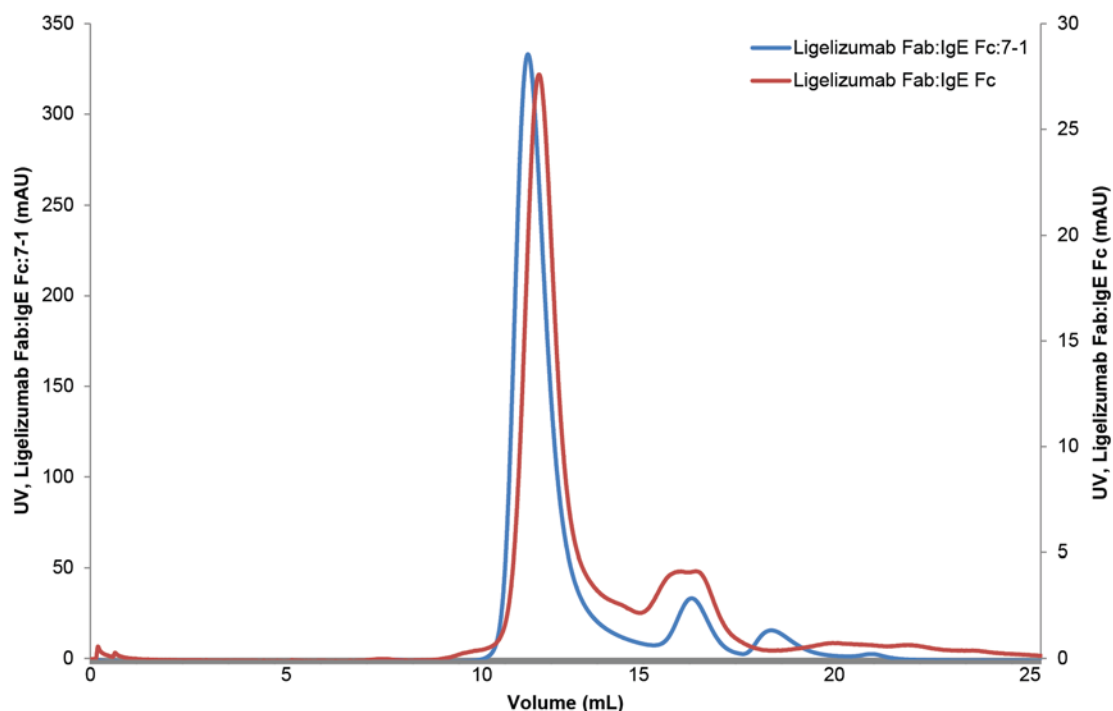
Figure 55: Purification of the ligelizumab:IgE Fc:7-1 complex for crystallisation with gel filtration.
The ligelizumab Fab:IgE Fc:7-1 complex (red) was formed with a 2:1:2 ratio overnight and purified with Superdex 200 10/300 GL column (GE Healthcare) compared to ligelizumab Fab:IgE Fc complex (blue) demonstrating the formation of the complex with the sdab.

The elution fractions were analysed on a polyacrylamide gel stained with Coomassie showing the successful formation of the complex and the excess proteins with IgE Fc at ~100 kDa, ligelizumab Fab between 40 and 55 kDa, and 7-1 at ~15 kDa. The observed double band of the nanobody might be the protein without V5-tag (Fig. 56).
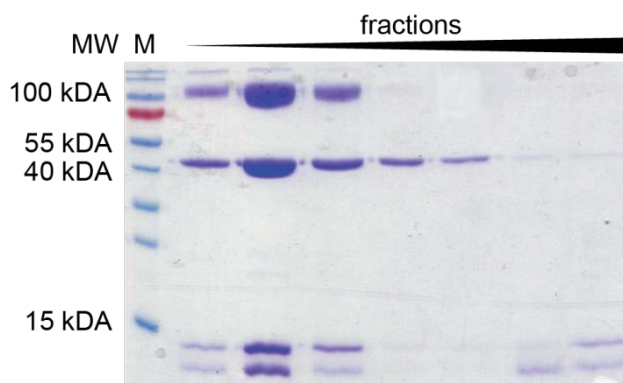

Figure 56: SDS-PAGE analysis of ligelizumab Fab:IgE Fc:7-1 purified with gel filtration.
The complex ligelizumab Fab:IgE Fc:7-1 was purified with Superdex 200 10/300 GL column (GE Healthcare), and the elution fractions were analysed on 15% TRIS-glycine gel, which was stained with Coomassie brilliant blue. 2 µL marker (M) and 20 µL non-reduced samples were used.

83

The ligelizumab Fab:IgE Fc:7-1 complex was crystallised by vapour diffusion in sitting drops formed by mixing protein and reservoir solution in the ratio 1:1. Initial commercial crystallisation trays (INDEX, Structure, and ProPlex) were set up with 200 nL protein solution and 200 nL reservoir solution at 4 °C and 19 °C using the mosquito® Crystal dispenser. After three days cubic shaped crystals were obtained in condition INDEX E6 (0.05 M $CaCl_2 \cdot 2\ H_2O$, 30% v/v PEG 550 MME, 0.1 M BIS TRIS pH 6.5) at 19 °C (Fig. 57).
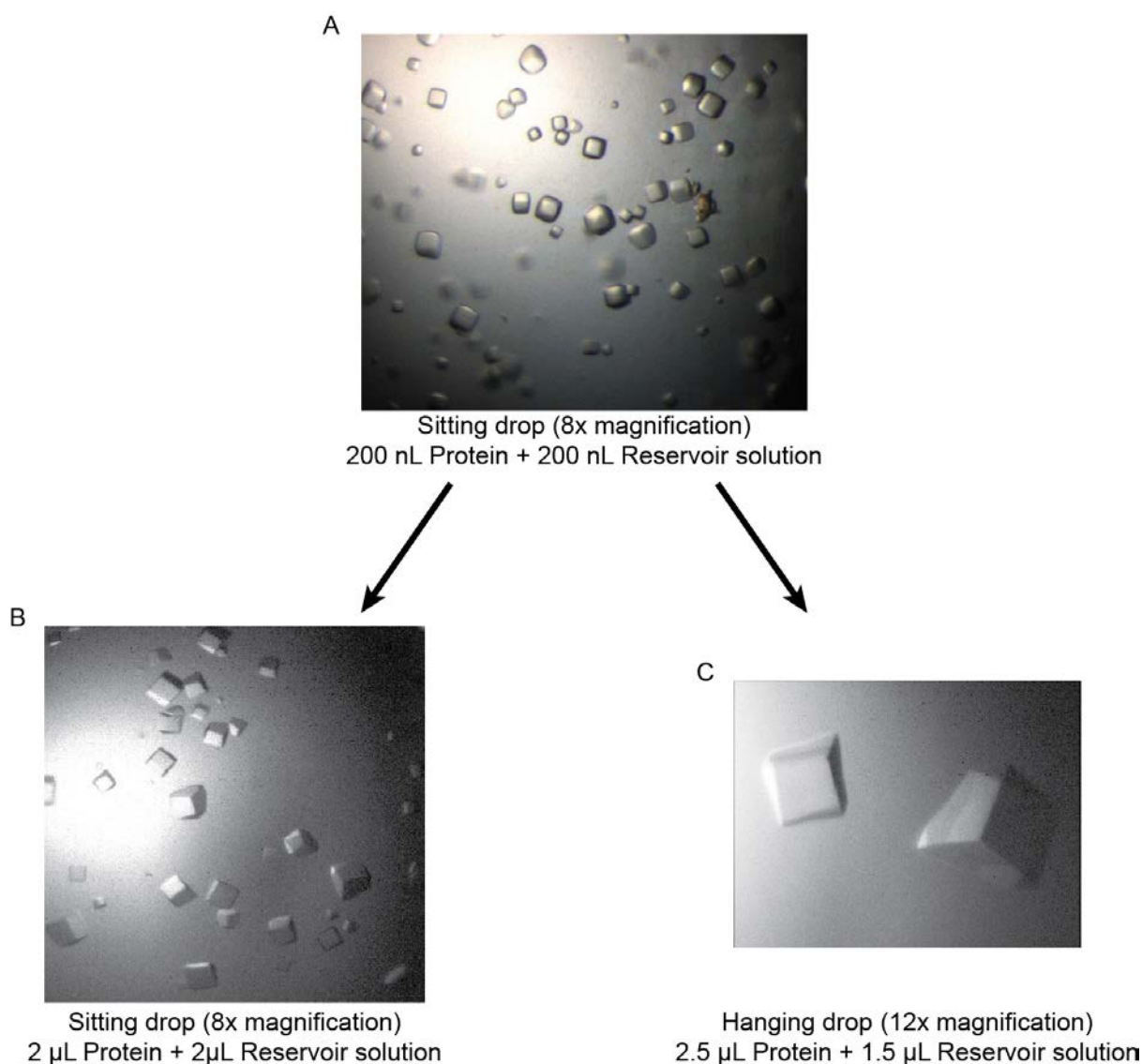

Figure 57: Microscopic image of ligelizumab Fab:IgE Fc:7-1 crystals.
Ligelizumab Fab:IgE Fc:7-1 complex was concentrated to 6.4 mg/mL in 20 mM HEPES, 50 mM NaCl, pH 7.2, and crystallised by vapour diffusion in 0.1 M BIS-TRIS pH 6.5, 30% PEG 550 MME, and 0.05 M $CaCl_2 \cdot 2\ H_2O$ at 19 °C. **A:** Initial crystals obtained from sitting drops formed by mixing 200 nL protein and 200 nL reservoir solution (8x magnification). **B:** Crystals obtained from sitting drops formed by mixing 2 µL protein and 2 µL reservoir solution (8x magnification). **C:** Crystals obtained from hanging drops formed by mixing 2.5 µL protein and 1.5 µL reservoir solution (12x magnification).

Initial data collection of the crystals resulted in a max. resolution of >11 Å. Therefore, the crystallisation conditions were optimised with grid screens, streak seeding and hanging drops resulting in bigger and sharper crystals (Fig. 57). Suitable crystals were cryoprotected in the reservoir solution, mounted and cryo-cooled in liquid nitrogen. The data were collected at the P13 beamline at DESY Hamburg (Hamburg, Germany), and processed with XDS[125]. The improved crystals diffracted in X-rays to a maximum resolution of 7.1 Å which is not sufficient for structure determination, but the space group F$4_1$3 2 could be determined. However, new crystals are needed to improve the resolution.

4.3 Structural and functional analysis of recombinant anti-alpha-Gal antibodies

Anti-alpha-Gal antibodies are from great interest because anti-alpha-Gal IgGs are the most abundant natural antibodies in humans and a major immunological barrier in xenotransplantation [5,73]. Additionally, anti-alpha-Gal IgE antibodies are associated with severe allergic reactions to red meat and cetuximab. Therefore, structural analyses of these interactions could help understanding the alpha-Gal-mediated immunological reactions in humans. The only anti-alpha-Gal antibody so far available is the monoclonal M86 derived from alpha-1,3-galactosyltransferase knockout mice selected by GALILI et al. [142]. The M86 clone was secreted as monoclonal anti-alpha-Gal IgM antibody and was cloned and expressed as chimeric Fab fragment. Furthermore, the M86 Fab should be crystallised alone and in complex with the alpha-Gal antigen to analyse the interaction.

4.3.1 Expression, purification and crystallisation of M86 Fab

The variable heavy and light chain were amplified and cloned as human IgE and IgG in the expression vector pcDNA3.1/Zeo for expression in HEK293 cells by PLUM et al.[143]. Due to a low expression rate in HEK293 cells, the M86 Fab was cloned into the pFastBac Dual vector for baculovirus-mediated insect cell expression analogue to the ligelizumab Fab. The transfection of Sf9 insect cells was performed according to the manufacturer's protocol. Therefore, the recombinant bacmid was generated and transfected into Sf9 insect cells. After the first round of amplification, cryoprotected cell stocks were produced, and the optimal titre for large-scale expression was determined in test expression. The immunoblot of the M86 Fab test expression shows the highest expression rate with 25 µL of the cryostock (lane 3, Fig. 58), which equals 1.2 L of expression volume with 1 mL cryostock.
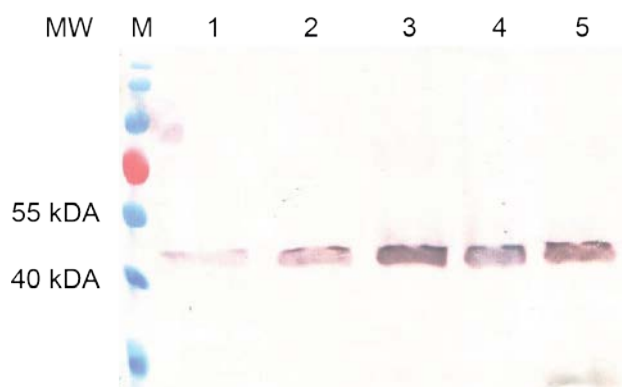
Figure 58: SDS-PAGE analysis of recombinant M86 Fab test expression.
100 µL M86 Fab cryostock was diluted in 5 mL HyClone™ SFX-Insect™ media. Different amounts (1-5: 1, 10, 25, 50, 100 µL) of the diluted cryostock were used for expression in $1 \cdot 10^6$ Sf9 cells/mL. Cells were incubated for 5 days at 27 °C, and the supernatant was analysed on 12% TRIS-glycine gel, which was used for immunoblot. 2 µL marker (M) and 20 µL non-reduced samples were used. Immunoblot was detected using anti-human κ-light chain conjugated with alkaline phosphatase (1:20,000), and NBT/BCIP substrate solution.

In total, 5 L M86 Fab were expressed in Sf9 insect cells for 5 days shaking at 27 °C. The remaining cells were removed by centrifugation, and the filtered supernatant was purified by affinity chromatography using the ÄKTA Start system. The elution fractions were analysed on a polyacrylamide gel stained with Coomassie and M86 Fab specifically detected with anti-human κ-light chain antibody in immunoblot.
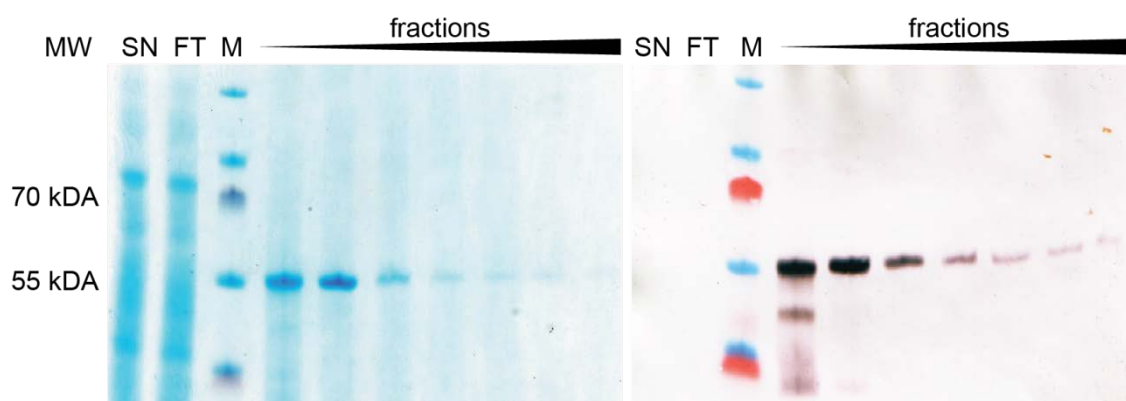

Figure 59: SDS-PAGE analysis of recombinant M86 Fab purified with affinity chromatography.
M86 Fab was expressed in 2.5 L Sf9 cells, purified with 1 mL KappaSelect column (GE Healthcare), and supernatant (SN), flow-through (FT) and elution fractions were analysed on 10% TRIS-glycine gels, which were stained with Coomassie brilliant blue (left) and used for immunoblot (right). 2 µL marker (M) and 20 µL non-reduced samples were used. Immunoblot was detected using anti-human κ-light chain conjugated with alkaline phosphatase (1:20,000), and NBT/BCIP substrate solution.

Fig. 59 shows the analysis of the affinity chromatography of M86 Fab purified out of 2.5 L *Sf*9 insect cell supernatant. The band at approx. 55 kDa in the Coomassie-stained gel as well as in the immunoblot represents the M86 Fab, which has a theoretical molecular weight of 50 kDa. The elution fractions contain minor impurities and degradation products of the protein.

The protein has a low expression rate of max. 1.6 mg/L that corresponds to an overall yield of approx. 8 mg out of 5 L. The elution fractions were pooled, dialysed against 20 mM NaOAc, 50 mM NaCl, pH 6.5, and subsequently applied to a 1 mL MonoS 5/50 cation exchange column. M86 Fab was eluted with a 0 - 50% gradient of 20 mM NaOAc, 1 M NaCl, pH 6.5 and the elution fractions were analysed on a polyacrylamide gel stained with Coomassie.
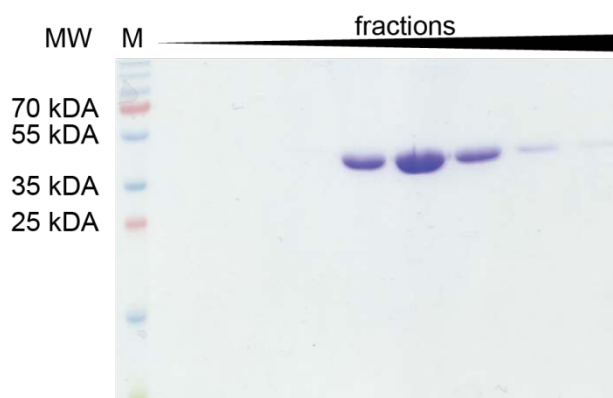

Figure 60: SDS-PAGE analysis of recombinant M86 Fab purified with ion exchange chromatography.
Recombinant M86 Fab was purified with 1 mL MonoS 5/50 GL column (GE Healthcare), and elution fractions were analysed on 15% TRIS-glycine gel, which was stained with Coomassie brilliant blue. 2 µL marker (M) and 20 µL non-reduced samples were used.

The elution fractions were pooled, the buffer exchanged to 20 mM HEPES, 50 mM NaCl, pH 7.2, and the sample concentrated to 8 mg/mL.

M86 Fab was crystallised by vapour diffusion in sitting drops formed by mixing protein and reservoir solution in the ratio 1:1. Initial commercial crystallisation trays (INDEX, Structure, and PEGION) were set up with 200 nL protein solution and 200 nL reservoir solution at 4 °C and 19 °C using the mosquito® Crystal dispenser. After ca. 14 days needle-shaped crystals were obtained in 20% (v/v) isopropanol, 20% (w/v) PEG4K, 0.1M NaOAc, pH 5.6 at 19 °C (Fig. 61).
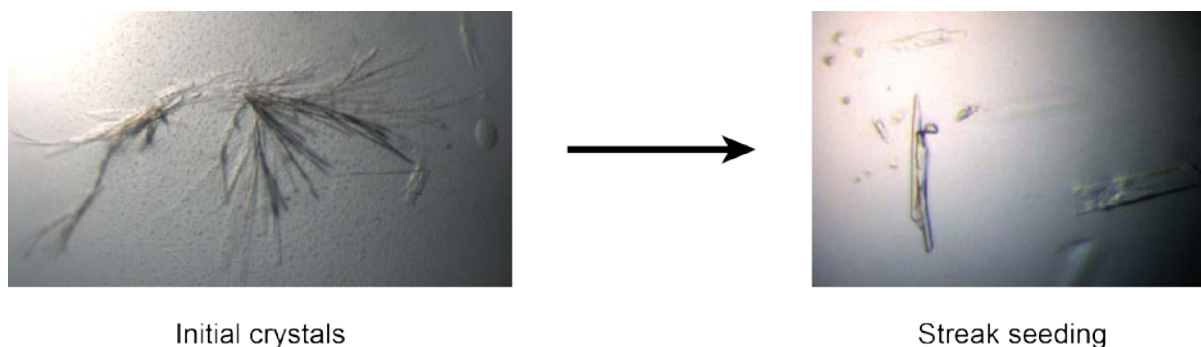
Initial crystals   Streak seeding

Figure 61: Microscopic image of M86 Fab crystals (8x magnification).
M86 Fab was concentrated to 8 mg/mL in 20 mM HEPES, 50 mM NaCl, pH 7.2, and crystallised by vapour diffusion in sitting drops formed by mixing 200 nL protein and 200 nL reservoir solution containing 20% (v/v) isopropanol, 20% (w/v) PEG4K, 0.1M NaOAc, pH 5.6 at 19 °C. On the left initial crystals and on the right crystals obtained from streak seeding in the same condition.

The thin needles were too fragile to mount, therefore the crystallisation condition was optimised with grid screens and streak seeding resulting in rod-shaped crystals after three days (Fig. 61). Suitable crystals were cryoprotected in 38% PEG 400, 0.1 M monosodium citrate pH 5.5, mounted and cryo-cooled in liquid nitrogen. The data were collected at ESRF (Grenoble, France), and processed with XDS[125]. Crystals diffracted in X-rays to a maximum resolution of 3.4 Å. The structure was determined by molecular replacement with PHASER[126] using the PDB entry 1T66 and 5I8K as search models for the variable and constant domains, respectively. The model was rebuild in Coot[127] and refined with Phenix.refine[128]. The asymmetric unit contained two M86 Fab molecules organized in opposite positions, as represented in Fig. 62A. The refinement parameters, listed in the appendix 7.4, were used for evaluation of the preliminary model. The Fab diffracted in X-rays to 3.4 Å in the orthorhombic space group $P2_12_12_1$. Iterative rebuilding and refinement resulted in a preliminary structure with R_{work}/R_{free} values of 0.287/0.316. Clear electron density present for the majority of residues and a complete data set (99%) allowed tracing of the amino acids with confidence.

For the first time, the structure of an alpha-Gal-specific antibody was determined as evident from the M86 Fab cartoon representation, depicted in Fig. 62B. This structure can be used for docking experiments with alpha-Gal saccharides or used as a search model in future co-crystallisation experiments.

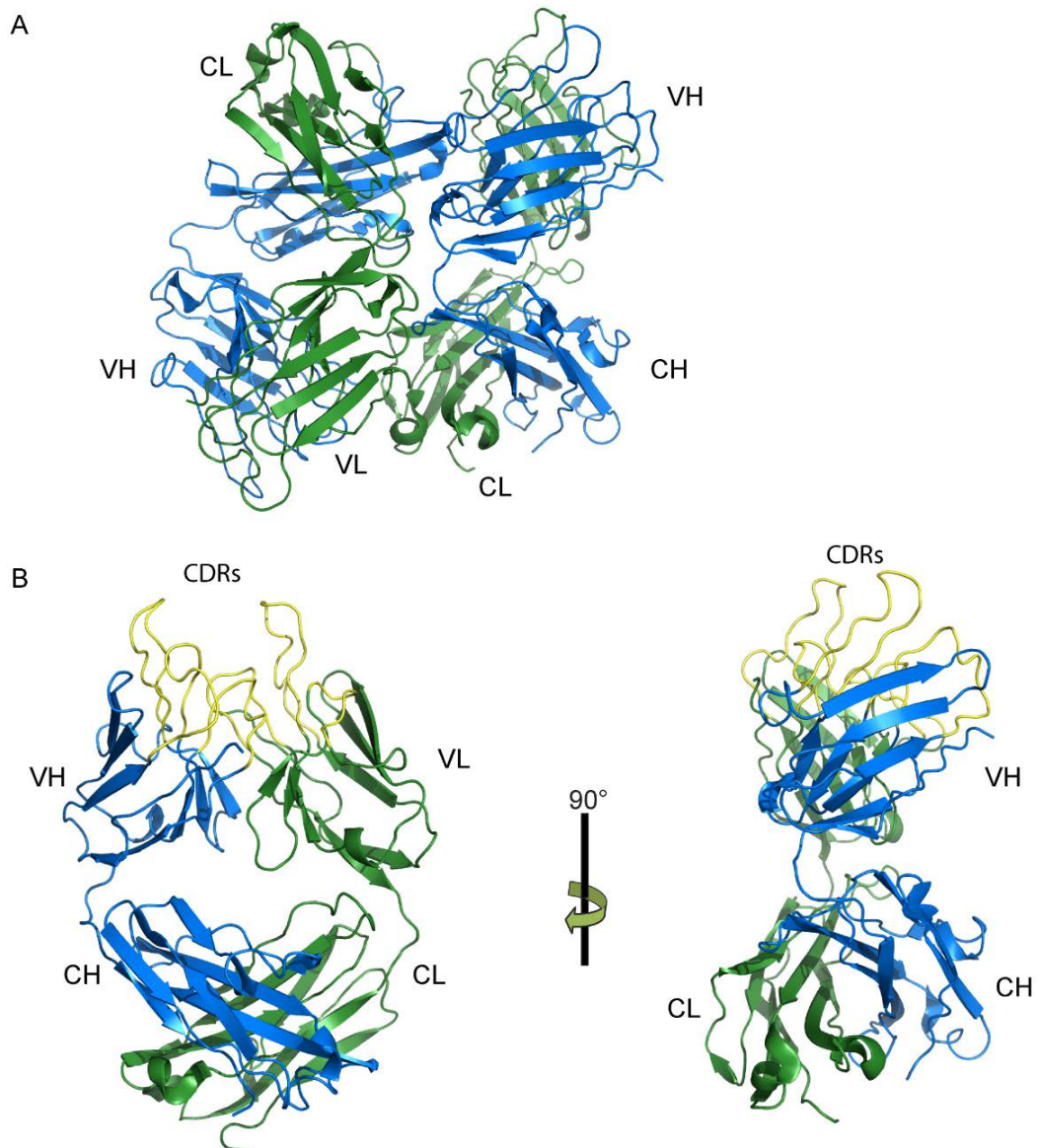**Figure 62: Cartoon representation of M86 Fab.**
A: The cartoon representation shows the asymmetric unit containing two M86 Fab molecules in opposite positions. **B:** The cartoon representation shows a single M86 Fab molecule with the constant and the variable domains. The side view shows the organisation of the two chains and the CDR regions. (heavy chain: blue, light chain: green, and CDRs: yellow).

4.3.2 Cloning, expression and purification of M86huIgE

In order to compare the IgE reactivity of red meat allergic patient with a recombinant monoclonal anti-alpha-Gal antibody, the chimeric M86 Fab was converted into a human IgE antibody in the pFastBac Dual expression vector for baculovirus-mediated insect cell expression. Therfore, the constant region of the Fab was exchanged with the human IgE heavy chain. The expression cassette of the M86huIgE is shown in Fig. 63.
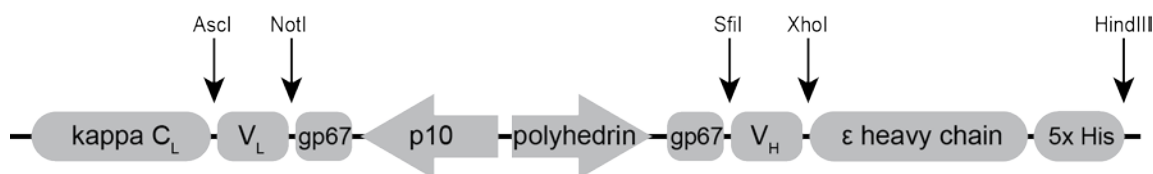

Figure 63: Schematic representation of expression cassette of human IgE in pFastBac Dual.

After the successful cloning, the recombinant M86huIgE bacmid was generated, and *Sf*9 insect cells were transfected. Cryoprotected cell stocks were produced after the first round of amplification and the titre determined in test expression. The immunoblot of the M86huIgE test expression shows the highest expression rate with 50 µL of the cryostock (lane 4, Fig. 64), which equals 600 mL of expression volume with 1 mL cryostock.
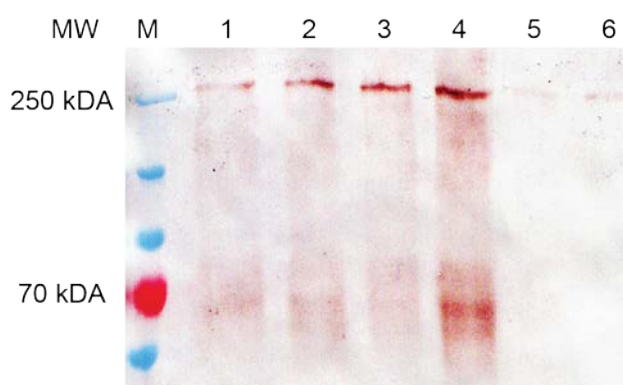
Figure 64: SDS-PAGE analysis of recombinant M86huIgE test expression.
100 µL M86huIgE cryostock was diluted in 5 mL HyClone™ SFX-Insect™ media. Different amounts (1-6: 1, 10, 25, 50, 75, 100 µL) of the diluted cryostock were used for expression in $1 \cdot 10^6$ *Sf*9 cells/mL. Cells were incubated for 5 days at 27 °C, and the supernatant was analysed on 7.5% TRIS-glycine gel, which was used for immunoblot. 2 µL marker (M) and 20 µL non-reduced samples were used. Immunoblot was detected using anti-human IgE conjugated with alkaline phosphatase (1:30,000), and NBT/BCIP substrate solution.

M86huIgE was expressed in 1 L *Sf*9 insect cells for 5 days shaking at 27 °C. The cell-free and filtered supernatant was purified by affinity chromatography using the ÄKTA Start system. The elution fractions were analysed on a SDS-PAGE gel stained with Coomassie, and M86huIgE specifically detected with anti-human IgE antibody in immunoblot (Fig. 65).
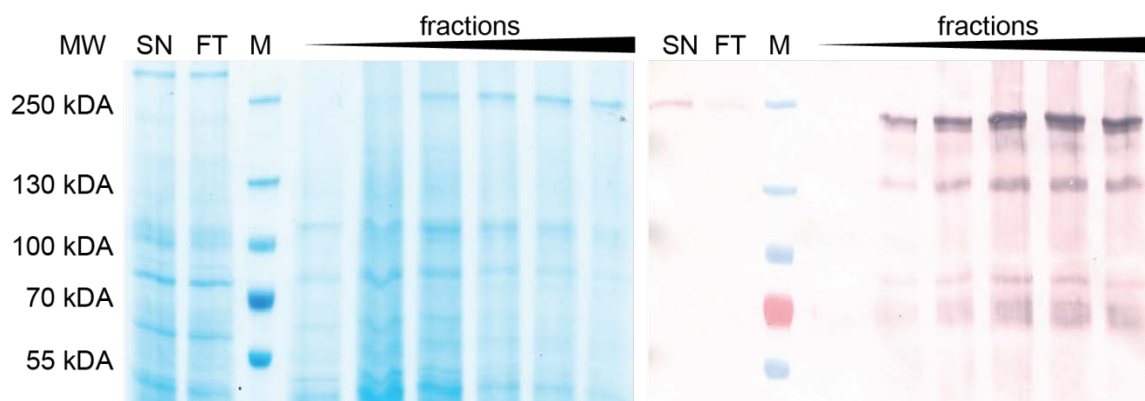

Figure 65: SDS-PAGE analysis of recombinant M86huIgE purified with IMAC.
M86huIgE was expressed in 1 L *Sf*9 cells, purified with 1 mL HisTrap column (GE Healthcare), and supernatant (SN), flow-through (FT) and elution fractions were analysed on 7.5% TRIS-glycine gels, which were stained with Coomassie brilliant blue (left) and used for immunoblot (right). 2 µL marker (M) and 20 µL non-reduced samples were used. Immunoblot was detected using anti-human IgE conjugated with alkaline phosphatase (1:30,000), and NBT/BCIP substrate solution.

The band at approx. 250 kDa represents the M86huIgE in the Coomassie-stained gel as well as in the immunoblot, which has a theoretical molecular weight of 167 kDa but shows different migration behaviour in SDS-PAGE probably due to the heavy glycosylation of the molecule. Smaller fragments at ~70 kDa and ~130 kDa were also detected with anti-human IgE antibody in the immunoblot and presumably are parts of the heavy chain.
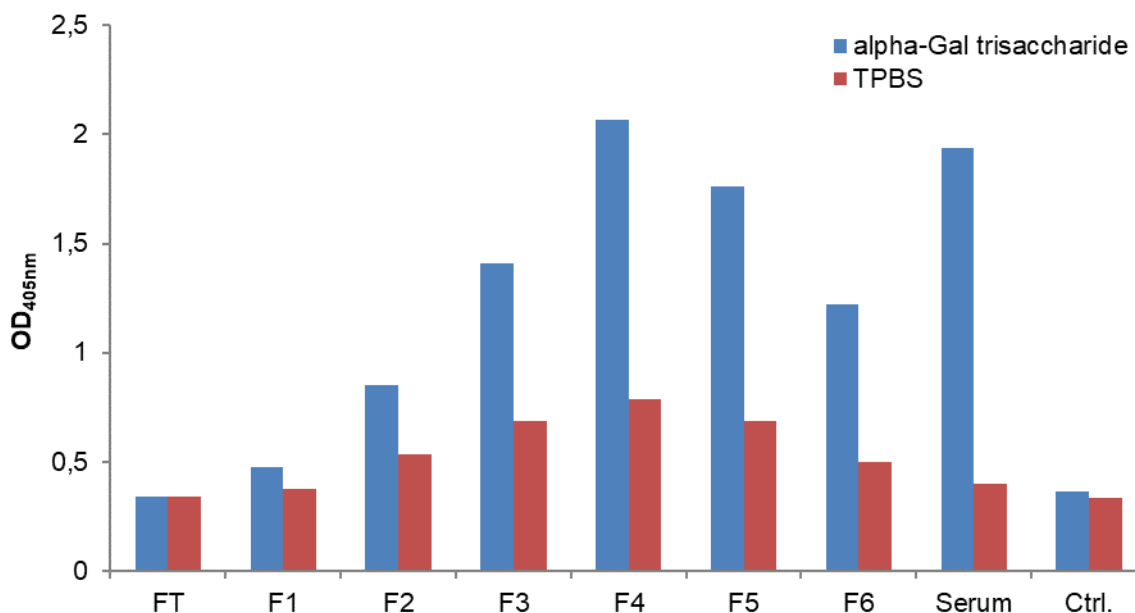
Figure 66: Immunoreactivity of M86huIgE fractions against alpha-Gal trisaccharide in ELISA.
25 µL (100 ng/µL) alpha-Gal trisaccharide were coated overnight. The wells were blocked with 4% TPBS for 30 min at rt. After the wells had been washed with TPBS and PBS, 50 µL of the flow-through (FT), elution fractions (F1-F6) and serum of a red meat allergic patient were incubated for 2 hours at rt. For detection 100 µL anti-human IgE (1:30,000) conjugated with alkaline phosphatase were used. The development was performed with pNPP and detected at 405 nm.

The reactivity of the purification fractions was verified against the alpha-Gal trisaccharide coupled to HSA in ELISA shown in Fig. 66. The elution fractions exhibited reactivity to the alpha-Gal antigen comparable with the reactivity of a red meat allergic patient serum that was used as a positive control.

In total the max. expression yield was 1 mg per litre. The pooled fractions were concentrated to 1 mg/mL and used to verify the biological activity of M86huIgE in mediator release assay. The mediator release assay in Fig. 67 shows the capability of M86huIgE to activate and degranulate basophils compared to M5huIgE, while cross-linked with anti-human IgE. The M86huIgE is able to initiate a degranulation of the basophils with a minimum concentration of 10 ng/mL.
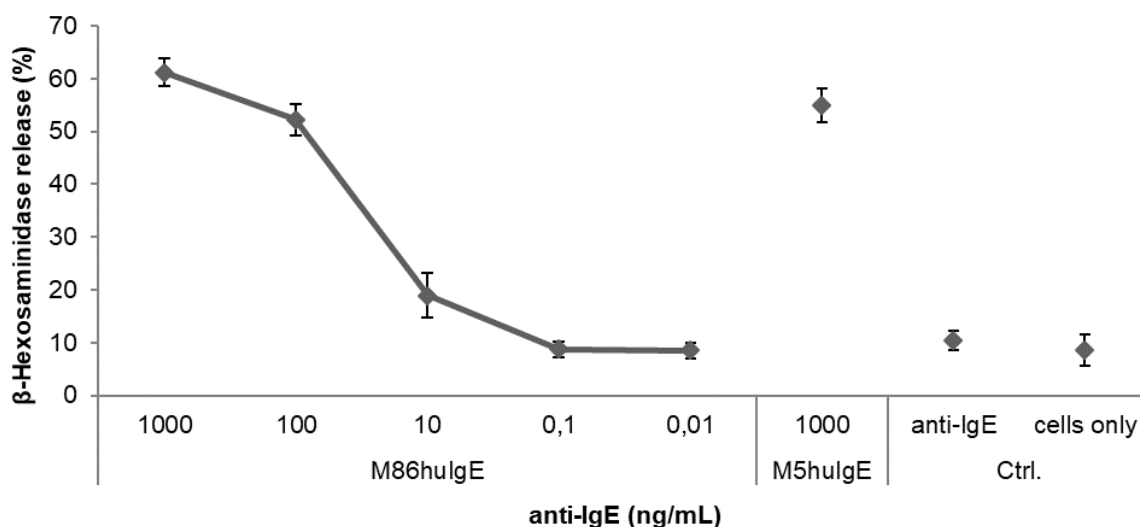
Figure 67: Analysis of the biological activity of M86huIgE cross-linked with anti-human IgE in mediator release assay of RBL-SX38 cells.
RBL-SX38 cells were incubated 60 minutes with M86huIgE and M5huIgE as a positive control. Degranulation was induced by addition of anti-human IgE antibody in decreasing concentrations. The release of the mediator β-hexosaminidase was detected after addition of the substrate pNAG at 405 nm. The IgE-induced release of β-hexosaminidase was calculated from the total amount after cell lysis in percent. The assay was performed in triplicates, and the error bars represent the standard deviation.

Allergen-dependent activation of monoclonal IgE usually is difficult to achieve, because in most cases, only one epitope per allergen is available. In order to link two identical paratopes, a multivalent protein bearing at least two independent alpha-Gal epitopes is needed. Therefore, the alpha-Gal rich bovine thyroglobulin and alpha-Gal-HSA conjugate were used in mediator release assay, but no antigen was able to induce significant mediator release compared to anti-IgE cross-linking of the human IgE antibodies shown in Fig. 68.

These results suggest that the recombinant monoclonal alpha-Gal-specific M86huIgE exhibits intrinsic potential to activate effector cells by cross-linking the FcεRI with anti-IgE, which is not translated into an antigen-dependent manner suggesting an impact of affinity.
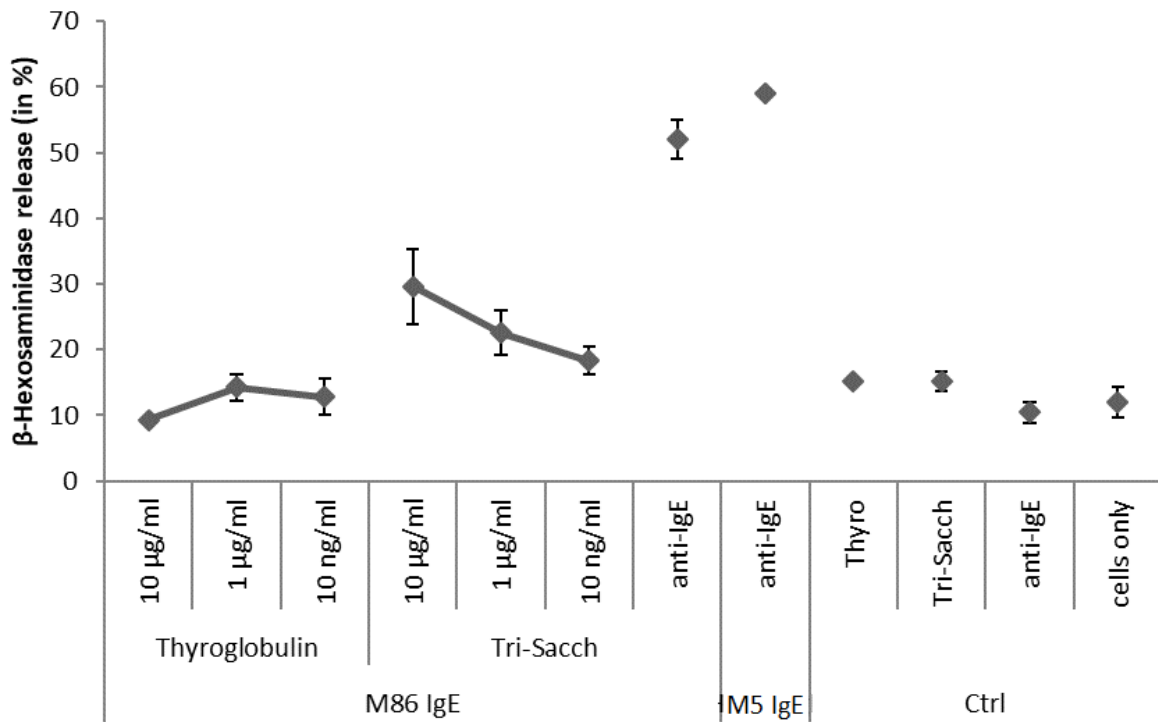
Figure 68: Analysis of the biological activity of M86huIgE with mediator release of RBL-SX38 cells.
RBL-SX38 cells were incubated 60 minutes with M86huIgE and M5huIgE as a positive control. Degranulation was induced by addition of thyroglobulin, alpha-Gal trisaccharide and anti-human IgE antibody in decreasing concentrations. The release of the mediator β-hexosaminidase was detected after addition of the substrate pNAG at 405 nm. The IgE-induced release of β-hexosaminidase was calculated from the total amount after cell lysis in percent. The assay was performed in triplicates, and the error bars represent the standard deviation.

4.4 Functional analysis of red meat allergic patient sera in glycan array

It has been reported that IgE reactivity to alpha-Gal is related with low titres of sIgE to blood group antigen B, and that red meat allergic patients display sIgE to alpha-Gal without concomitant sensitization to three unrelated carbohydrate epitopes [144,145]. However, the presence of broader IgE responses to carbohydrate epitopes and the fine specificity of the alpha-Gal-directed immune response in allergic patients remain open. Therefore, the molecular profile of the recombinant monoclonal alpha-Gal-specific M86huIgE and human IgE from sera of red meat allergic patients with an elevated level of sIgE to alpha-Gal were analysed in glycan arrays using a large panel of displayed carbohydrate structures.

4.4.1 Analysis of IgE reactivity of red meat allergic patients

Seven patients were identified based on ImmunoCAP sIgE levels to alpha-Gal and clinical history of allergy to red meat, gelatine and other animal-derived materials from Southern Germany, Sweden, and Norway (Tab. 4).

Table 4: Overview of patients IgE level and reactivity to carbohydrate structures.

Patient ID	Origin	Total IgE	sIgE alpha-Gal	sIgE CCD	Recognition of α-Gal structures	Recognition of other carbohydrate structures
1	Germany	1040	60	<0.35	88, 17, 10	44, 57, 62, 26
2	Germany	1826	>100	0.60	88, 17, 10	1, 66, 53, 59, 62, 55, 92, 69, 26, 83, 85, 86, 90, 29, 56, 96, 98, 99
3	Germany	91	2	<0.35	88, 17	1, 5, 87, 57, 59, 25, 26, 84, 85, 86, 29, 8, 56, 96, 98, 99
4	Germany	120	9	1.44	17	1, 5, 66, 51, 62, 25, 67, 18, 26, 74, 20, 77, 85, 29, 96, 98, 99
5	Sweden	370	100	<0.35	17	31, 41, 21
6	Sweden	180	121	0.49	17	1, 5, 6, 7, 31, 16, 27, 28, 53, 25, 95, 18, 26, 74, 85, 86, 29
7	Norway	600	70	0.38	88, 17	4, 5, 16, 44, 62, 92, 26, 90, 96, 98, 99
8	Germany	340	<0.35	60	-	72, 75, 78, 80

The sera were applied to the glycan array containing 100 synthetic carbohydrate epitopes including several alpha-Gal structures and a variety of carbohydrates with galactose in 1,2-, 1,3-, and 1,4-glycosidic linkages in α- and β-anomeric state (Tab. 7 in the appendix). The alpha-Gal-specific M86huIgE was used as a reference. As a negative control, allergic patient serum with an elevated level of total IgE and high sIgE to CCD, but no sIgE to alpha-Gal was included. The IgE reactivity was detected with monoclonal anti-human IgE antibody conjugated to biotin and Cy3 fluorescence dye conjugated to streptavidin. The fluorophore was excited using a Typhoon Trio Plus laser scanner at 532 nm.
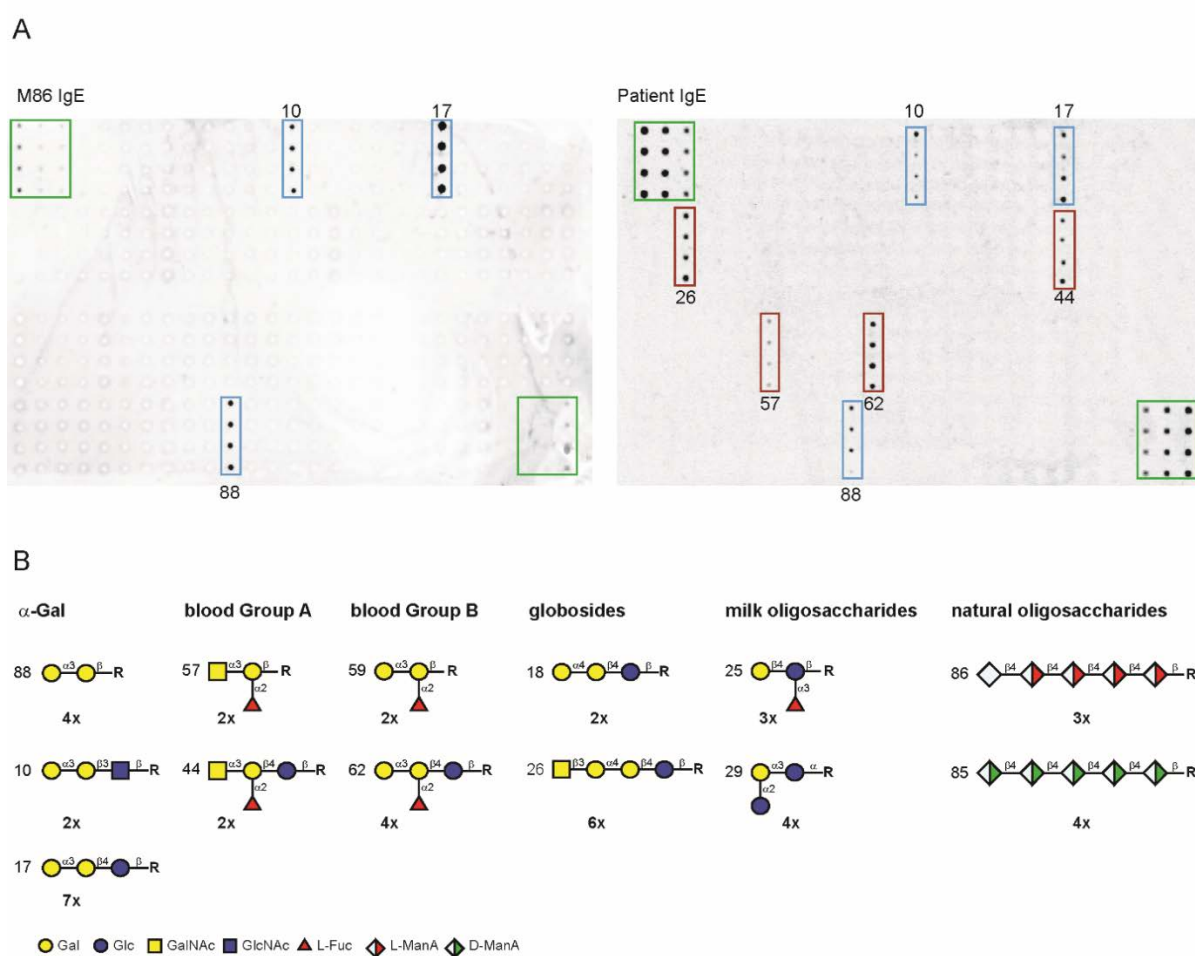
Figure 69: IgE reactivity to carbohydrate epitopes on a glycan array (183x147 mm; 300x300 dpi).
A: Red meat allergic patient sera (exemplary array, right) and the monoclonal alpha-Gal-specific M86huIgE (left) were applied to glycan arrays. IgE reactivity was detected with monoclonal biotinylated anti-human IgE and Cy3-conjugated streptavidin. Fluorescence was measured using a Typhoon Trio Plus laser scanner at 532 nm. **B:** Depicted are the structures of carbohydrate epitopes that were recognised by several of the patients' sera. Important, structurally related carbohydrates are also included. The frequency of recognition is indicated.

The monoclonal M86hugE showed pronounced reactivity to the three alpha-Gal carbohydrates presented on the array (No. 10, 17, 88, Fig. 69). Remarkably, the alpha-Gal trisaccharide with glucose at the reducing end (No. 17) displayed a slightly higher IgE reactivity than the one with *N*-acetyl glucosamine at the reducing end (No. 10) or the alpha-Gal disaccharide (No. 88). Neither reactivity to carbohydrates with galactose in 1,2-, 1,3-, and 1,4-glycosidic linkages in α- and β-anomeric state nor to any other carbohydrate were detected supporting a highly defined specificity of alpha-Gal recognition.

All seven alpha-Gal positive patient sera recognised alpha-Gal structures, but only two sera showed IgE reactivity to all three alpha-Gal structures (ID 1 and ID 2; Tab. 4), which is illustrated in Fig. 69. The alpha-Gal trisaccharide with glucose at the reducing end (No. 17) was recognised by all patients, compared to the trisaccharide with *N*-acetyl glucosamine at the reducing end (No. 10), which was detected only by two patient sera. Also, serum IgE reactivity beyond alpha-Gal was detected in the glycan arrays. Some patient sera (ID 1, 2, 3, 4, and 7) showed pronounced reactivity to the structurally related blood group antigen B, which is present as a tri- and tetramer on the glycan array (No. 59 and 62). The structurally unrelated blood group A antigen was also recognised by patient ID 1, 3 and 7. Furthermore, significant IgE reactivity against globosides (No. 18 and 26), human milk oligosaccharides (No. 25 and 29) and natural oligosaccharides (No. 85 and 86) were observed. The control serum (ID 8) exhibited IgE reactivity to entirely different structures supporting the specificity of alpha-Gal positive sera detected on the array.

The IgE reactivity against the alpha-Gal di- and trisaccharide and the blood group antigens was compared in ELISA using bovine thyroglobulin, neoglycoconjugates with HSA of an alpha-Gal di- and trisaccharide, and blood group antigens A and B (Fig. 70).
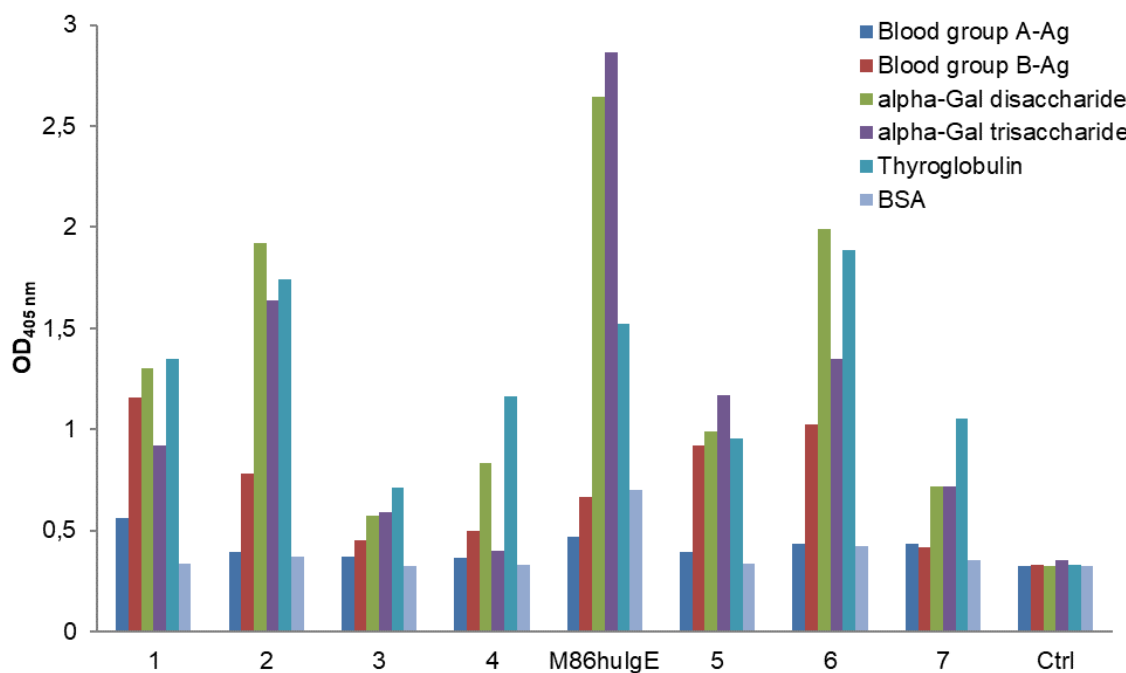
Figure 70: Immunoreactivity of different red meat allergic patient sera in ELISA.
25 µL (50 ng/µL) of blood group antigens and alpha-Gal carrying antigens were coated overnight. The wells were blocked with 1% BSA for 1 hour at rt. After the wells had been washed with TPBS and PBS, 20 µL of the red meat allergic patient sera (ID 1-7) and M86huIgE (1:2) were added and incubated overnight at 4 °C. For detection 50 µL anti-human IgE (1:30,000) conjugated with alkaline phosphatase were used. The development was performed with pNPP and detected at 405 nm.

In accordance with the sIgE levels, all sera exhibited pronounced IgE reactivity to both alpha-Gal saccharides. The trisaccharide shows a reduced IgE reactivity compared to the disaccharide, which shows only minor signals in the glycan array but a pronounced IgE reactivity in ELISA. Patient sera ID 1 shows IgE reactivity to blood group antigen A in ELISA, which was the only patient sera detecting both blood group A structures in the glycan array. In contrast, blood group B antigen was recognised by nearly all patient sera in ELISA but showed limited reactivity in the glycan array suggesting a limited accessibility of the glycans on the array. This also suggests that the variant IgE reactivities of the patient sera emphasise a different reactivity of individual sera, which underlines the high specificity of the recognition of galactose-based epitopes by IgE.

5. Discussion

5.1 Structural and functional analysis of anti-IgE antibodies

Allergic disorders like allergic rhinitis, atopic dermatitis, allergic asthma and anaphylaxis are increasingly prevalent in the developed world, and more than 25% of individuals in industrialised countries are affected [1]. It is well known that these allergic diseases can be linked to IgE antibodies present in the circulation and on the surface of a variety of cell types [13]. IgE antibodies are evolutionarily conserved and heavily glycosylated heterotetramers with the ε-heavy chain containing four constant domains [32,35]. In atopic individuals, allergen-specific IgE is bound to the high-affinity IgE receptor on mast cells and basophils after previous sensitization with the respective allergen. Upon subsequent exposure to the allergen, IgE antibodies bound to the FcεRI are cross-linked by the allergen triggering degranulation of the effector cell, release of proinflammatory mediators, and immediate reactions [17,18]. IgE can also bind to the low-affinity receptor (CD23), which is able to regulate IgE synthesis in stimulated B cells [49]. Essential for receptor binding is the IgE Fc, which can adopt different conformational states ranging from closed to open. FcεRI binds to the open and CD23 to the closed conformation of IgE Fc making binding of both receptors mutually exclusive as each is dependent on the conformational state of the IgE antibody and preventing overlap of the two pathways [41].

Generally, in anti-IgE therapy, the key to intervention in allergic diseases is the reduction of IgE in the serum and eventually on effector cells. Therefore, anti-IgE therapeutics are supposed to bind in proximity to the FcεRI binding site in order to interfere with the receptor binding. The only approved anti-IgE antibody, omalizumab, primarily prevents interaction of free IgE with its receptor on effector cells [95,96]. However, roughly 39% of patients receiving omalizumab did not respond to the treatment. Hence, antagonistic anti-IgE antibodies, antibody alternatives including a DARPin, and interesting antibody formats like the single domain antibody IgE026 were developed [101]. Furthermore, second-generation anti-IgE molecules such as ligelizumab are currently in clinical trials, but initial results suggest limited improvements [4].

In this thesis, the interaction of human IgE in complex with the anti-IgE antibodies IgE026 and ligelizumab should be analysed by biophysical and functional methods

exploring the conformational states of IgE with respect to future anti-IgE drug development.

5.1.1 Structural and functional analysis of IgE026:IgE Fc complex

The single domain antibody IgE026, recently developed for IgE targeting in allergic diseases, was successfully cloned, expressed in *Escherichia coli* and purified from the supernatant with a high yield of max. 80 mg/L as a soluble and nonaggregating recombinant protein. An even higher production yield of single domain antibodies could be obtained by expression in *Saccharomyces cerevisiae* with over 100 mg/L [146]. The introduced His-Tag allowed the purification of the protein with IMAC followed by IEX yielding the pure IgE026 with only minor contaminations. The efficiently purified protein was assessed pure enough for complex formation.

The human IgE Fc was expressed in the mammalian cell line HEK293 to obtain proper human posttranslational modifications and an authentic IgE Fc to minimise the risk of trapping the molecules in a rare or artificial conformation. The IgE Fc was purified from cell culture supernatant with a yield of up to 10 mg/L. Other research groups expressed the human IgE Fc in a stabilised form having artificial disulphide bridges or reduced glycosylation in Chinese hamster ovary (CHO) cells with a 10-fold higher expression yield [147]. Besides the higher expression yield, the authentic nature of the IgE Fc is not preserved, and mutations of glycosylation sites might lead to artificial conformations. Nevertheless, expression rates of up to 120 mg/L for different human proteins in HEK293 cells are reported suggesting room for optimisation for the IgE Fc production [148]. The IgE Fc was efficiently purified from the supernatant with IMAC followed by IEX. All major contaminants were successfully removed, besides a small fraction of IgE Fc lacking the Cε2 domains. The IgE Fc Cε3-4 fragment was probably co-expressed or the product of a degraded Cε2-4 and due to a similar pI value not entirely removed by IEX. Having a relatively small difference in molecular size, both fragments did not separate in gel filtration, but due to the structural similarity, it was assessed of sufficient purity for complex formation and crystallisation. The immunoreactivity of both proteins was verified by ELISA prior to complex formation. The complex was formed, purified by gel filtration and crystallised by vapour diffusion in sitting drops. After three days, complex crystals were obtained that diffracted in X-rays to a maximum resolution of 3.4 Å comparable with the IgE Fc complex structures in the RCSB Protein Data Bank. The structure

was determined by molecular replacement showing that the asymmetric unit contains two copies of the sdab IgE026 and one IgE Fc molecule. During structure determination, it became evident that the crystallised complex contained the IgE Fc Cε3-4 fragment and not the full IgE Fc Cε2-4 as expected. Apparently, the degraded IgE Fc lacking the Cε2 domains is kinetically favoured in the crystallisation process. Notably, most of the complex structures for IgE Fc available in literature contain only the IgE Fc Cε3-4 domains, and likewise, the complex with the entire IgE Fc was not obtained, probably because the flexibility of the Cε2 domains prevent the full IgE Fc complex from crystallising. Recently, the structure of a mutated IgE Fc Cε2-4 in complex with omalizumab Fab was determined indicating the feasibility of crystallising the full IgE Fc in complex [149]. Iterative rebuilding and refinement of the complex structure resulted in a final structure with R_{work}/R_{free} values of 0.212/0.241, which allowed tracing of most residues with confidence and the presence of clear electron density for the majority of residues at the IgE026:IgE Fc interface. The R-value is a measure of the quality of the atomic model obtained from the crystallographic data and measures how well the simulated diffraction pattern matches the experimentally observed ones [150]. In this case, the R-value is comparable to the published IgE Fc complex structures with respect to the resolution.

The sdab bridges the Cε3 and Cε4 domains from each ε-chain in the IgE Fc dimer with the Cε3 and Cε4 domains contributing with 30% and 70%, respectively. It binds symmetrically to the IgE Fc Cε3-4 forming a 2:1 complex where each sdab buries ~800 Å^2 upon complex formation, which is slightly larger than the omalizumab epitope [42]. Mutational analysis identified that residues in the CDR3 of the IgE026 play a critical role in the interaction, which supports the fact that the extended CDR3 regions found in sdabs are essential. Although omalizumab is roughly 3-fold bigger (~50 kDa vs ~15 kDa) than the sdab, the enlarged CDR3 region of the sdab contributes to a more significant buried surface. Omalizumab mainly binds the Cε3 domains in the open conformation directly inhibiting the FcεRI binding site and sterically interfering with CD23 binding [42]. Both the epitope and the inhibition mode of IgE026 are different from omalizumab and other anti-IgE molecules, e.g. DARPin or MEDI4212. As evident from the structural overlay of different anti-IgE complex structures depicted in the appendix Fig. 72, all anti-IgE molecules aim for the direct

inhibition of the FcεRI binding site by binding to the Cε3 domains in the open conformation. However, the sdab IgE026 binds in close proximity to the CD23 binding site and shows significant overlap, which directly inhibits the CD23 binding. The FcεRI binding is inhibited by IgE026 trapping the IgE Fc in the closed conformation, which represents a so far undescribed mechanism in anti-IgE therapy.

Despite the overall resolution of 3.4 Å, the IgE Fc is well resolved. For the first time in an IgE Fc complex structure, an oligomannosidic heptasaccharide at position N394 was resolved. The heptasaccharide was observed as an (N-acetyl-glucosamine)$_2$(mannose)$_5$ glycan which is essential for biological activity of the IgE. Recently, SHADE *et al.* demonstrated that the selective removal of the oligomannosidic glycan at position N394 diminished the interaction with FcεRI by altering the conformation of IgE [53]. Thus, the glycosylation of IgE at this position is an absolute requirement for initiation of the allergic cascade. Besides the occurrence in the IgE026:IgE Fc structure, this glycan has also been reported for the structure of free IgE Fc (PDB: 5LGJ), and in both structures, the glycans contact the same residues suggesting limited flexibility of the glycan. Despite the proximity of the sdab epitope to the glycan, there is no direct contact, but water-mediated contacts may be present that are not visible at this resolution. A glycoproteomic analysis was performed to get deeper insights into the glycosylation pattern of the IgE Fc. The denatured or with trypsin digested IgE Fc was analysed with an ESIq/TOF mass spectrometer and verified the presence of the heptasaccharide at position N394 with a ratio of 34%. Furthermore, octa-, nona-, deca- and undecasaccharides were identified in ratios of 6 - 26%. These findings are supported by the glycoproteomic analyses of PLOMP *et al.* who discovered the same oligomannosidic distribution on three different IgE antibodies with the heptasaccharide as the most common glycan at this crucial position [52]. Surprisingly, analysis of the tryptic digestion, as well as the denatured IgE Fc, suggested the glycosylation of only one out of three possible *N*-glycosylation sites. In the analyses of PLOMP *et al.*, complex-type glycans were found at position N265 and N371 [52]. Generally, glycosylation of IgE has been shown to affect binding affinity for the IgE receptors [52], but nevertheless lacking the glycans at these positions did not affect the binding of IgE Fc as evident from the functional assays in this thesis.

As mentioned before, the complex of IgE026 bound to the full IgE Fc did not crystallise, hence the complex was analysed using small angle X-ray scattering (SAXS). SAXS is a technique used for the three-dimensional low-resolution characterisation of biological macromolecules in solution under physiological conditions complementary to high-resolution methods like X-ray crystallography and nuclear magnetic resonance (NMR) [130]. In 1990, the first SAXS model of a rat IgE was determined and recently a chimeric human IgE antibody was analysed with SAXS in our group suggesting a compact, unflexible molecule [141,151].

In order to analyse a sample with SAXS, the production of a good quality, monodisperse preparation is required. The sample preparation for the crystallisation contained minor amounts of IgE Fc Cε3-4, which were successfully removed by hydrophobic interaction chromatography. Both, the newly formed complex and the IgE Fc alone were purified with size exclusion chromatography, and synchrotron SAXS data were collected for different dilutions to avoid attractive and repulsive interactions between the molecules. For the IgE026:IgE Fc complex a concentration of 1.7 mg/mL and for the IgE Fc alone the concentrations 2.2 and 9.0 mg/mL were merged and used for further modelling. The Guinier plot is a reliable indicator of sample quality, and it showed no sign of interparticle effects for both preparations. Furthermore, the radius of gyration was estimated to 3.3 nm for the IgE Fc similar to values previously observed for IgE Fc[140] and 3.6 nm for the IgE026:IgE Fc complex. The proteins were well folded and had limited flexibility as evident from the Kratky plot. The limited flexibility of both molecules might be a result of the missing hinge-region replaced by the Cε2 domains compared to IgG antibodies.

For the first time, the models obtained from rigid body refinements allowed insights into the characteristics of free IgE Fc and IgE Fc in complex with IgE026 in solution. The free IgE Fc adopted the bent conformation with the Cε2 domains located towards the Cε3 domains. Early FRET studies[152], X-ray solution scattering studies[140] and crystal structures[153] of IgE Fc confirmed the compact, bent structure. A substantial overlap between the Cε2 domains and IgE026 occurred by superimposing the output model of the SAXS analysis with the complex structure obtained by X-ray crystallography. Hence, the IgE Fc must adopt a significantly less bent conformation to avoid a sterical clash. The modelling suggested an IgE026 mediated displacement of the Cε2 domains and unbending of the IgE Fc resulting in a so far undescribed conformation in between the bent and extended conformation

of the IgE Fc. In order to reach the fully extended conformation a 102° rotation of the Cε2 domains is required. Similar observations were reported for a mutated omalizumab Fab binding a mutated IgE Fc adopting a partially bent conformation. Molecular dynamics simulation revealed energy basins corresponding to this finding [154]. In general, the bent conformation is stabilising the IgE:FcεRI complex where the bound IgE has a half-life of several weeks. Disruption of the interaction of the Cε2 domains with the FcεRI or Cε3 domains profoundly enhances the off-rate and decreases the half-life of IgE [155]. Besides locking the IgE Fc in a closed conformation, IgE026 forces the Cε2 domains in a partially bent conformation, which probably also contributes to the inhibitory effect. Recently, the determination of IgE Fc in complex with CD23 also revealed the partial dislocation of the Cε2 domains [40], which supports our results.

In order to validate the observed overlap between the IgE026 and CD23 epitopes in functional assays, the capability of the sdab interfering with the CD23 binding of IgE was assessed in enzyme-linked facilitated antigen binding (ELIFAB) assays. The ELIFAB assay is an ELISA-based method for analysing the allergen:IgE complex interactions with the low-affinity receptor CD23 developed by SHAMJI et al. [122]. This assay is an enhancement of the IgE-FAB assay and is independent of Epstein-Barr virus-transformed B cells used in the IgE-FAB assay. The ELIFAB assay is based on the detection of the binding of preformed oligovalent IgE:allergen complexes to CD23. Binding of these complexes to CD23 is crucial for facilitated antigen presentation and transport across the epithelium and amplifies specific IgE [38,156]. The CD23 binding of IgE:allergen complexes is inhibited by blocking IgG$_4$ antibodies, an indicator for successful allergen immunotherapy, which makes it a useful tool in allergy diagnostics [122]. Sera of patients with an elevated level of specific IgE (> 100 kUA/L) against three different allergens were incubated with the respective allergen to form the IgE:allergen complexes and then applied to CD23. In the first experiment, the sdab was preincubated with the IgE:allergen complexes to assess the competition with the CD23. IgE026 efficiently prevented binding of the IgE:allergen complexes to CD23 in a concentration range of 8 - 12 µg/mL. The monovalent sdab has a significantly higher affinity to IgE as compared to monovalent CD23 (K_D = 1.4 nM vs 1 µM) explaining the inhibitory effect of IgE026 [47]. In order to investigate a potential disruptive effect of IgE026, preformed

106

IgE:allergen complexes were incubated with CD23, and then IgE026 was added. Within ten minutes the CD23 binding was significantly reduced, and after 60 minutes almost no binding was detected suggesting the efficient displacement of IgE:allergen complexes from CD23. As observed in the ELIFAB analyses the inhibition of IgE binding to CD23 and displacement of IgE from CD23 strongly supports the observed epitope in the IgE026:IgE Fc structure and proposed mode of action of the anti-IgE sdab.

However, the primary target of anti-IgE therapy remains interference with FcεRI-mediated immediate reactions. Therefore, the effect of IgE026 on IgE bound to the FcεRI was assessed in basophil activation test (BAT). A panel of six birch pollen allergic patients was analysed with and without preincubation of the peripheral blood with IgE026, and the basophil activation threshold sensitivity (CDsens) was investigated. Invented as an anti-IgE therapeutic to prevent binding to the FcεRI, IgE026 efficiently reduced the basophil activation resulting in a CDsens for patients' basophils of 50 - 95% indicating a potent indirect inhibition mechanism of IgE026 without steric competition to the FcεRI. The correlation of CDsens and the IgE level of the patients indicated a pronounced reduction of CDsens with a small ratio of sIgE/tIgE. This might point toward the fact that patients with a specific ratio benefit from the treatment with IgE026 by reducing the cellular sensitivity. With respect to the IgE ratio, affinity and repertoire complexity as well as patient-specific sensitization profiles (mono- and polysensitized) need to be taken into account when talking about the efficiency of a potential anti-IgE therapeutic [157].

The displacement of IgE from FcεRI by DARPin E2_79 and omalizumab at high concentrations was described recently [94]. Flow cytometry analysis of surface IgE on human basophils obtained from three allergic patients sensitized to birch pollen or insect venom showed that treatment with 45 µmol/L IgE026 for 15 minutes reduced the amount of surface IgE to approx. 30%. Further incubation reduced the surface IgE to approx. 20% after 60 minutes showing a potent disruption. This data suggests a more efficient displacement of IgE from FcεRI than the IgE026 mutant Y112A and omalizumab Fab, which showed no comparable effect in the same experiment at a concentration of 90 µmol/L conformable with the findings of other groups [94]. The observed disruptive effect is most likely driven by the conformational rearrangement induced by the binding of IgE026 to the FcεRI bound IgE. The sdab operates with a novel dissociation strategy compared to the DARPin E2_79 which disrupts

preformed IgE:FcεRI complexes by the facilitated dissociation mechanism [104]. The described removal of IgE from both circulation and effector cells could represent a benefit, but the *in vivo* effect has not been sufficiently proven yet, and it has been shown that the reduction is counterbalanced by increased sensitivity [158]. The capability for displacing IgE could become an important strategy for improving the efficacy of anti-IgE therapeutics by increasing this activity [94], but additional studies are needed to address the consequences and implications in detail.

In general, single domain antibodies exhibit high production yields in simple expression systems such as *E. coli* or *S. cerevisiae* and an extraordinary stability, which render them as interesting molecules for biotechnological and biomedical applications [110]. As described in this thesis, the targeting of IgE antibodies in allergic patients with sdabs could offer a variety of benefits. The small size which is about 10-fold smaller compared to IgG allows the efficient targeting of antigenic sites that are usually not recognised by conventional antibodies. Furthermore, the extended CDR3 loop contributes to the ability to penetrate into such sites. In addition to the targeting of less accessible sites, the small size results in a fast tissue penetration and a rapid renal clearance, which is a disadvantage for therapeutic applications [110]. Omalizumab has a roughly 300-fold higher serum half-life (up to 26 days[159] vs several hours[160]) rendering one injection per month sufficient for treatment of, e.g. allergic asthma. Therefore, the coupling of sdabs to albumin or polyethylene glycol could extend the half-life significantly when applying intravenously [117]. Delivery in the functional form via mucosal and airway tissues, for instance as an aerosol spray targeting local inflammatory reaction sites is possible and could improve the use of challenging routes in anti-IgE applications [161].

The mode of action described in this thesis for the sdab IgE026 could open up for the development of novel anti-IgE molecules of even lower molecular weight that target the same epitope on the IgE Fc leading to similar conformational rearrangements. Thus, the fundamental research of IgE026 in complex with IgE Fc done in this thesis could accelerate the development of anti-allergy and asthma drugs in the future.

5.1.2 Structural and functional analysis of ligelizumab Fab:IgE Fc complex

Ligelizumab, developed as a monoclonal human IgG1 antibody alternative to omalizumab, was successfully cloned as an IgG1 Fab, expressed in *Sf*9 insect cells and purified from cell supernatant with a moderate expression rate of max. 2.5 mg/L. Higher expression yields of 5 - 20 mg/L[162,163] for Fab fragments are reported in the literature suggesting room for improvement, e.g. with additional virus amplification rounds to obtain a higher virus titre stock for expression. The protein was efficiently purified with IMAC followed by IEX and gel filtration yielding the pure ligelizumab Fab with minor degradation products that was assessed pure enough for complex formation. IgE Fc was expressed and purified as mentioned before for the IgE026:IgE Fc complex (chapter 5.1.1). The immunoreactivity of ligelizumab Fab to IgE Fc was verified by ELISA prior to complex formation. The mediator release assay demonstrated the inhibitory effect of ligelizumab Fab compared to IgE026. Additional functional assays such as basophil activation test or ELIFAB assays are needed to validate the efficiency of ligelizumab in anti-IgE therapy which might help to evaluate clinical trials in the future.

The complex was formed, purified by gel filtration and crystallised by vapour diffusion in sitting drops. The crystallisation resulted in needle-shaped crystals, which were too fragile for X-ray diffraction analysis and no change in morphology of the crystals was obtained after seeding and optimisation screens. In the literature, the potential of single domain antibodies as chaperones supporting the crystallisation of difficult proteins and protein complexes is well documented [164,165]. Therefore, a single domain antibody should be crystallised in complex with ligelizumab Fab and IgE Fc, in order to obtain a different morphology.

The anti-IgE single domain antibody 7-1 was successfully selected from a llama library and expressed in *E. coli* in high yields similar to the sdab IgE026. After purification with IMAC, the reactivity to IgE Fc was verified, and competition with ligelizumab Fab was excluded in ELISA. Ligelizumab was developed to interfere with the FcεRI binding site suggesting the binding epitope in the Cε3 domain. Hence, the single domain antibody 7-1 probably binds to the Cε2 or Cε4 domain preventing a sterical clash with ligelizumab Fab.

The complex between ligelizumab Fab, IgE Fc and sdab 7-1 was successfully formed and crystallised by vapour diffusion in sitting drops. Obtained cubic crystals

diffracted in X-rays to a maximum resolution of 11 Å. Introduction of the single domain antibody changed significantly the morphology resulting in a highly symmetric order in the crystal. Analysis of the crystals on a silver stained SDS-gel (data not shown) indicated the presence of all three proteins including the unmutated IgE Fc Cε2-Cε4 suggesting no interference of the flexible Cε2 domains with the crystallisation process confirmed by recent publications of IgE Fc complex structures [40,149]. Probably ligelizumab Fab stabilises the Cε2 domains similar to a Fab structure reported by DRINKWATER *et al.* that binds to the IgE Fc in an extended conformation [37].

Improvement of the crystal size with hanging drops increased the resolution to a maximum of 7.1 Å, but a resolution better than 5 Å is still needed to determine the structure with confidence. Nevertheless, the collected data were processed revealing the space group $F\,4_1\,3\,2$, which is according to the crystal morphology a face-centered cubic space group. Furthermore, initial molecular replacement with different search models indicated that the IgE Fc might engage the previously described extended conformation, but still better diffracting crystals are needed.

To circumvent the crystallisation process of proteins and protein complexes, a new technique gains increasing popularity. J. DUBOCHET, J. FRANK and R. HENDERSON were awarded the Nobel price 2017 in chemistry for developing the cryo-electron microscopy (cryo-EM) for the high-resolution structure determination of biomolecules in solution [166]. Structures with a resolution up to 1.5 Å were determined [167], which would be sufficient for the determination of protein complexes of therapeutic antibodies like the ligelizumab Fab complex. However, the high costs could slow the spread of cryo-EM at the moment, but the development in this area has not reached its limits, and it will be the state-of-the-art technique in the future revolutionising the X-ray crystallography.

5.2 Structural and functional analysis of recombinant anti-alpha-Gal antibodies

The alpha-Gal epitope (galactose-α-1,3-galactose) is a cross-reactive carbohydrate determinant with huge clinical relevance. It is a ubiquitous carbohydrate in cells and tissues of most non-primate mammals and New World monkeys, however, not in Old World monkeys, apes, and human beings [5]. Thus, alpha-Gal is associated with red meat induced delayed symptoms of anaphylaxis and is reported as a novel type of carbohydrate epitope that causes severe food allergy related to IgE antibodies. The delayed reaction remains enigmatic, but the prevailing hypothesis is that the digestion, absorption, and transit of glycoproteins and/or glycolipids are relevant [7]. Hard ticks are associated with the alpha-Gal IgE sensitization mechanism and recent studies identified alpha-Gal glycan modifications in the midgut and saliva [84,85]. Nevertheless, the sensitization mechanism is not entirely understood, and molecular data of the interaction of IgE with carbohydrate epitopes are still scarce. In order to analyse the binding characteristics as well as effector mechanisms, human/mouse chimeric antibodies were generated based on an alpha-Gal-specific antibody to obtain structural and molecular insights into its interaction with alpha-Gal. The well-established murine IgM antibody (M86) should be cloned as a Fab fragment and a monoclonal human IgE antibody. Prior to this work, both antibody fragments were expressed in HEK293 cells with insufficient expression rates (personal communication). Recloning and expression in *Sf*9 insect cells should gain access to large quantities of alpha-Gal-specific IgE and IgG Fab for extended structural and functional analyses.

5.2.1 Expression, purification and crystallisation of M86 Fab

M86 Fab was successfully cloned, expressed in *Sf*9 insect cells, and purified from the supernatant by kappa-chain-specific affinity chromatography. The low expression rate of 1.6 mg/L was comparable to the HEK cell expression. In addition, the expression in High Five insect cells was tested but yielded the same amount of M86 Fab (data not shown). The successful establishment of an efficient purification protocol for the M86 Fab with affinity chromatography followed by ion exchange made a total expression of 5 L (8 mg) sufficient for crystallisation trials. M86 Fab was crystallised by vapour diffusion in sitting drops resulting in needle-shaped crystals after 14 days (20% (v/v) isopropanol, 20% (w/v) PEG4K, 0.1 M NaOAc, pH 5.6 at

19 °C). The crystals were too fragile for mounting. Therefore, the effective optimisation of the condition with grid screens and streak seeding resulted in new rod-shaped crystals after three days. The crystals diffracted in X-rays to a maximum resolution of 3.4 Å and the structure was determined by molecular replacement revealing two Fab molecules in the asymmetric unit. For the first time, the structure of the alpha-Gal-specific antibody M86 Fab was determined giving first insights into the organisation of the CDR regions.

Recently, the structure of a disaccharide bound by a CCD-specific Fab antibody was determined and showed insights into the antibody-glycan interactions (PDB: 5I80). The same should be done for the alpha-Gal-specific M86 Fab with the corresponding di- or trisaccharide. Unfortunately, the M86 Fab crystal could not be reproduced, and optimisation of the conditions failed. Nevertheless, docking experiments with the obtained M86 Fab structure could be done instead, in order to get first molecular insights into a possible binding mechanism. PLUM *et al.* reported the first STD NMR-based epitope mapping of the alpha-Gal M86 IgE epitope and demonstrated the significance of the terminal galactose in the binding mechanism [143]. These results combined with the molecular modelling of an anti-galactan mAb with the alpha-Gal di- and trisaccharide docked in the binding pocket [168], can be used as a basis for the docking of the alpha-Gal saccharides into the binding pocket of the M86 Fab revealing the interaction of an alpha-Gal-specific Fab with its antigen. Nevertheless, crystallisation of the M86 Fab in complex with the glycan is still necessary to evaluate the actual interaction.

5.2.2 Expression, purification and functional analysis of M86huIgE

For the expression of the monoclonal alpha-Gal-specific human M86 IgE antibody in *Sf*9 insect cells, the M86 Fab was converted into a human IgE antibody. Although IgE can be successfully expressed in mammalian cells, this expression system is hampered by the demand for the time-consuming establishment of transfectants prior to larger scale production of recombinant proteins. In addition, the expression yield is not sufficient for e.g. structural analyses. Probably the high molecular weight, the additional domain and the extensive glycosylation inhibit the secretion of IgE from mammalian cells. Furthermore, three out of seven *N*-glycosylation sites are found in the $C\varepsilon 1$ domain, which is the interface of assembly with the light chain and

might pose higher threshold for folding and assembly of IgE. The most relevant difference in the use of lepidopteran cells compared to mammalian cells is the degree and nature of glycosylation. Oligomannose-type glycans represent the most frequent structures on glycoproteins expressed in lepidopteran cells, due to low levels or lack of some transferases together with the presence of a Golgi-associated *N*-acetylglucosaminidase [169]. BANTLEON *et al.* showed the expression of a leporid/human IgE in insect cells with high expression rates of up to 30 mg/L and the essential biological characteristics of the natural and the recombinant counterpart from mammalian cells [170]. Nevertheless, the M86huIgE had an expression yield of up to 1 mg/L that is 30-fold less than reported by BANTLEON *et al.* and comparable with the expression in HEK293 cells (according to personal communication). Additional rounds of amplification, which might also introduce mutations, can still optimise the expression rate. Furthermore, the IgE antibody used in the publication of BANTLEON *et al.* was a chimeric leporid/human IgE, which might have an advantage in expression rate in *Sf*9 cells over chimeric mouse/human antibodies.

The reactivity of the M86huIgE was verified in ELISA against the alpha-Gal trisaccharide conjugated to HSA, and the biological activity was assessed in mediator release assays. The different glycosylation pattern introduced by *Sf*9 cells compared to HEK293 did not influence the biological function of M86huIgE as it activated effector cells in an anti-IgE-dependent manner in mediator release assay. The same observation was reported for a leporid/human IgE antibody expressed in both cell lines by BANTLEON *et al.* [170]. Furthermore, the recombinant M86huIgE was unable to mediate basophil degranulation in the presence of multivalent alpha-Gal whereas the antibody was able to bind to the FcεRI as evident from the anti-IgE cross-linking. The architecture of the alpha-Gal epitope and the accessibility on the surface of different carriers might affect the basophil activation. It is known that limited affinities of allergen-specific IgE can significantly decrease the basophil sensitivity [157]. The affinity of M86huIgE derived from insect cells was not determined, but the monoclonal M86 derived from alpha-1,3-galactosyltransferase knockout mice was selected by GALILI *et al.*[142] and secreted as a monoclonal anti-alpha-Gal IgM antibody. The IgM origin suggests low to moderate affinities and might explain the behaviour in mediator release assays. In addition, the lack of allergen-dependent mediator release might reflect the delayed anaphylactic symptoms observed in

patients with red meat allergy, compared to the analysis of a murine C38-2 IgE antibody of medium affinity that showed cellular activation upon stimulation with a multivalent conjugate [143].

5.3 Analysis of IgE reactivity of red meat allergic patients

The association between red meat allergy with particular clinical features and specific IgE to alpha-Gal was discovered recently, and the diagnostic approaches for a putative meat allergy are limited [74]. Skin prick tests with commercial extracts with undefined amounts of alpha-Gal are often equivocal, and specific IgE tests to whole meat extracts have a low sensitivity [171]. For routine allergy diagnostics, the singleplex analysis test based on bovine thyroglobulin is available but might be false positive in parasitized and cat allergic patients [172]. Therefore, a new analysis method for detection of IgE profiles associated with alpha-Gal was established in this thesis. The glycan array technology has become a powerful tool for high-throughput determination of interactions of different carbohydrate structures with, e.g. antibodies, proteins, viruses and cells, but many challenges remain. Different array platforms can yield different results, and some screens show no binding at all. However, the glycan array technology was successfully used in different research fields to profile antibody responses in HIV infection, cancer patients and xenotransplants [173,174]. BLIXT et al. analysed sera of ten patients with type I diabetes who had a xenotransplant using a glycan array [175]. The group identified IgA, IgM and IgG antibodies against blood group A and B epitopes, but also alpha-Gal epitopes in the patients' sera. Based on these findings, seven patients with elevated levels of alpha-Gal-specific IgE were selected and analysed on a glycan array containing 100 synthetic carbohydrate epitopes. The M86huIgE antibody was used as a positive control and showed pronounced reactivity to all three alpha-Gal structures present on the array with a slightly higher IgE reactivity to the alpha-Gal trisaccharide with glucose at the reducing end. The antibody showed no reactivity to carbohydrates with galactose in different architectures supporting a highly defined specificity of alpha-Gal recognition. All analysed sera exhibited IgE reactivity to at least one of the three alpha-Gal structures, only two sera showed reactivity to all three structures suggesting a different recognition mode compared to the monoclonal IgE antibody. All sera recognized the alpha-Gal trisaccharide with glucose at the reducing end that is primarily found on glycolipids. Alpha-Gal in the form of glycolipids is present at the site of the tick lesion and is part of the putative sensitization mechanism as reported by WILSON et al. [7]. Thus, the alpha-Gal trisaccharide could represent a diagnostically interesting structure that might give further insights into the alpha-Gal sensitization

pathway. Besides the alpha-Gal reactivity of the sera, the glycan array allowed analysing the serum IgE reactivity beyond alpha-Gal. In a recent study, a selective IgE reactivity of red meat allergic patient sera towards alpha-Gal could be demonstrated without concomitant sensitization to three unrelated carbohydrate epitopes, fucose and xylose based CCDs, arabinose based CCDs and glycolylneuraminic acid (Neu5Gc) [145]. In contrast, several related and unrelated carbohydrate structures could be identified in the glycan arrays that showed pronounced IgE reactivities such as globosides and human milk oligosaccharides. Globosides are glycolipids, which reside in cellular membranes and can be found in human and bovine milk [176]. Allergic reactions to milk oligosaccharides were reported in an atopic population in Singapore, and the correlation of red meat and cow's milk allergy was observed but the relevance remains unclear [177,178]. In order to connect the broad IgE reactivity detected in the glycan array with its clinical relevance, additional diagnostical approaches need to be addressed, and the history of the patients needs to be studied further. Moreover, some patients showed pronounced IgE reactivity to the structurally related blood group B antigen and to the structurally unrelated blood group A antigen. In contrast, a recent study from RISPENS et al. reported the presence of low titres of anti-blood group B IgE in red meat allergic patients [148]. Further insights into the blood group of the patients are needed to draw a conclusion between the blood group and a potential alpha-Gal allergy. The IgE reactivities to the different alpha-Gal saccharides and the blood group antigens observed in the glycan array were confirmed by ELISA. Here, the alpha-Gal trisaccharide exhibited a clearly reduced IgE reactivity, while the disaccharide showed pronounce IgE reactivity, which is somehow antithetic to the glycan array results. That suggests that the variant IgE reactivities observed on the glycan array reflect a more limited accessibility and a varying reactivity of individual sera. Varying fine specificity in the context of immune responses to alpha-linked galactose epitopes by natural antibodies was reported already in the early 1990s and is influenced by a variety of factors [179]. Additionally, the variant IgE reactivities also emphasise high specificity of the recognition of galactose-based epitopes by IgE.

The analyses of red meat allergic patient sera using glycan arrays revealed individual differences between the sensitization profiles to different alpha-Gal structures and showed the broad recognition of additional carbohydrate structures.

These findings were supported by the study of Jappe *et al.* who used a dot blot assay to detect the individual differences in the sensitization profile [83].

The use of the glycan array technology is a robust multiplex method to analyse and identify conserved and individual reactivity patterns to carbohydrates. The limited accessibility of the glycans spotted on the array and the preferential detection of higher affinity IgE interactions limit this method, but with respect to the affinity, glycan arrays are similar to the allergen arrays (e.g. ISAC). Hence, they display the sensitization and cross-reactivity profiles to a broad panel of potentially relevant allergens. More profound insights into the individual patient IgE profiles might contribute to a better understanding of sensitization to additional antigenic carbohydrate epitopes and molecular mechanisms of carbohydrate-based allergies. Therefore, the use of glycan arrays might lead to the identification of risk-associated IgE binding patterns and in combination with other diagnostical approaches might show the whole clinical picture behind the mostly underdiagnosed red meat allergic patients.

6. References

1   Galli, S. J. *et al.*, The development of allergic inflammation. *Nature*. 454, 445-454, (**2008**).

2   Holgate, S. T., New strategies with anti-IgE in allergic diseases. *World Allergy Organ J.* 7, 17, (**2014**).

3   Kopp, M. V., Omalizumab: Anti-IgE therapy in allergy. *Curr Allergy Asthma Rep.* 11, 101-106, (**2011**).

4   AdisInsight. Ligelizumab. http://adisinsight.springer.com/drugs/800033626, (Last access: **07.09.2017**).

5   Macher, B. A. & Galili, U., The Galα1,3Galβ1,4GlcNAc-R (α-Gal) epitope: A carbohydrate of unique evolution and clinical relevance. *Biochimica et Biophysica Acta (BBA) - General Subjects*. 1780, 75-88, (**2008**).

6   Koike, C. *et al.*, Functionally important glycosyltransferase gain and loss during catarrhine primate emergence. *Proc Natl Acad Sci U S A*. 104, 559-564, (**2007**).

7   Wilson, J. M. *et al.*, Galactose-alpha-1,3-Galactose: Atypical Food Allergen or Model IgE Hypersensitivity? *Curr Allergy Asthma Rep.* 17, 8, (**2017**).

8   Huber, B., 100 Jahre Allergie: Clemens von Pirquet – sein Allergiebegriff und das ihm zugrunde liegende Krankheitsverständnis. *Wiener klinische Wochenschrift*. 118, 573-579, (**2006**).

9   Von Pirquet, C., Allergie. *Munch Med Wochenschr*. 53, 1457-1458, (**1906**).

10   European Academy for Allergy and Clinical Immunology. Advocacy Manifesto: Tackling the Allergy Crisis in Europe - Concerted Policy Action Needed. http://www.eaaci.org/outreach/public-declarations/3243-advocacy-manifesto-tackling-the-allergy-crisis-in-europe,-2015.html (Last access: **03.08.2017**).

11   Ring, J. *et al.*, Global Allergy Forum and Second Davos Declaration 2013 Allergy: Barriers to cure-challenges and actions to be taken. *Allergy*. 69, 978-982, (**2014**).

12   Gell, P. G. H. & Coombs, R. R. A., *The classification of allergic reactions underlying disease. Clinical aspects of immunology*. (Blackwell, **1963**).

13   Murphy, K. P. *et al.*, *Janeway's immuno biology*. 7th edn, (Garland Science, **2008**).

14   Valenta, R., The future of antigen-specific immunotherapy of allergy. *Nat Rev Immunol.* 2, 446-453, (**2002**).

15   Johansson, S. G. O. *et al.*, A revised nomenclature for allergy: An EAACI position statement from the EAACI nomenclature task force. *Allergy.* 56, 813-824, (**2001**).

16   Licona-Limon, P. *et al.*, TH2, allergy and group 2 innate lymphoid cells. *Nat Immunol.* 14, 536-542, (**2013**).

17   Stone, K. D. *et al.*, IgE, mast cells, basophils, and eosinophils. *J Allergy Clin Immunol.* 125, S73-80, (**2010**).

18   Galli, S. J. & Tsai, M., IgE and mast cells in allergic disease. *Nat Med.* 18, 693-704, (**2012**).

19   Larche, M. *et al.*, Immunological mechanisms of allergen-specific immunotherapy. *Nat Rev Immunol.* 6, 761-771, (**2006**).

20   Sarin, S. *et al.*, The role of the nervous system in rhinitis. *Journal of Allergy and Clinical Immunology.* 118, 999-1014, (**2006**).

21   Cevikbas, F. *et al.*, Neuroimmune interactions in allergic skin diseases. *Curr Opin Allergy Clin Immunol.* 7, 365-373, (**2007**).

22   Lalloo, U. G. *et al.*, Pathophysiology and clinical presentations of cough. *Journal of Allergy and Clinical Immunology.* 98, 91-97, (**1996**).

23   He, S. H. *et al.*, IL-9(+) IL-10(+) T cells link immediate allergic response to late phase reaction. *Clin Exp Immunol.* 165, 29-37, (**2011**).

24   Descotes, J. & Choquet-Kastylevsky, G., Gell and Coombs's classification: is it still valid? *Toxicology.* 158, 43-49, (**2001**).

25   Matricardi, P. M. *et al.*, EAACI Molecular Allergology User's Guide. *Pediatr Allergy Immunol.* 27 Suppl 23, 1-250, (**2016**).

26   Jakob, T. *et al.*, Component resolved diagnostics for hymenoptera venom allergy. *Curr Opin Allergy Clin Immunol*. 17(5), 363-372, (**2017**).

27   Werfel, T. *et al.*, Position paper of the EAACI: food allergy due to immunological cross-reactions with common inhalant allergens. *Allergy*. 70, 1079-1090, (**2015**).

28   Mescher, A. L. & Junqueira, L. C. U., *Junqueira's basic histology : text and atlas*. 13th edn, (McGraw-Hill Medical,, **2013**).

29   Irani, V. *et al.*, Molecular properties of human IgG subclasses and their implications for designing therapeutic monoclonal antibodies against infectious diseases. *Molecular Immunology*. 67, 171-182, (**2015**).

30   Johansson, S. G. O., The discovery of IgE. *J Allergy Clin Immunol*. 137, 1671-1673, (**2016**).

31   Kelly, B. T. & Grayson, M. H., Immunoglobulin E, what is it good for? *Ann Allergy Asthma Immunol*. 116, 183-187, (**2016**).

32   Amarasekera, M., Immunoglobulin E in health and disease. *Asia Pac Allergy*. 1, 12-15, (**2011**).

33   Pulendran, B. & Artis, D., New paradigms in type 2 immunity. *Science*. 337, 431-435, (**2012**).

34   Marichal, T. *et al.*, A beneficial role for immunoglobulin E in host defense against honeybee venom. *Immunity*. 39, 963-975, (**2013**).

35   Wurzburg, B. A. *et al.*, Structure of the Human IgE-Fc Cε3-Cε4 Reveals Conformational Flexibility in the Antibody Effector Domains. *Immunity*. 13, 375-385, (**2000**).

36   Wan, T. *et al.*, The crystal structure of IgE Fc reveals an asymmetrically bent conformation. *Nat Immunol*. 3, 681-686, (**2002**).

37   Drinkwater, N. *et al.*, Human immunoglobulin E flexes between acutely bent and extended conformations. *Nat Struct Mol Biol*. 21, 397-404, (**2014**).

38   Gould, H. J. & Sutton, B. J., IgE in allergy and asthma today. *Nat Rev Immunol*. 8, 205-217, (**2008**).

39   Holdom, M. D. *et al.*, Conformational changes in IgE contribute to its uniquely slow dissociation rate from receptor FcεRI. *Nat Struct Mol Biol.* 18, 571-576, (**2011**).

40   Dhaliwal, B. *et al.*, IgE binds asymmetrically to its B cell receptor CD23. *Scientific Reports.* 7, 45533, (**2017**).

41   Dhaliwal, B. *et al.*, Crystal structure of IgE bound to its B-cell receptor CD23 reveals a mechanism of reciprocal allosteric inhibition with high affinity receptor FcεRI. *Proc Natl Acad Sci U S A.* 109, 12686-12691, (**2012**).

42   Pennington, L. F. *et al.*, Structural basis of omalizumab therapy and omalizumab-mediated IgE exchange. *Nat Commun.* 7, 11610, (**2016**).

43   Kinet, J.-P., The high-affinity IgE receptor (FcεRI): From Physiology to Pathology. *Annual Review of Immunology.* 17, 931-972, (**1999**).

44   Letourneur, O. *et al.*, Glycosylation of human truncated FcεRI alpha chain is necessary for efficient folding in the endoplasmic reticulum. *J Biol Chem.* 270, 8249-8256, (**1995**).

45   Shin, J.-S. & Greer, A. M., The role of FcεRI expressed in dendritic cells and monocytes. *Cellular and Molecular Life Sciences.* 72, 2349-2360, (**2015**).

46   Kraft, S. & Kinet, J.-P., New developments in FcεRI regulation, function and inhibition. *Nat Rev Immunol.* 7, 365-378, (**2007**).

47   Acharya, M. *et al.*, CD23/FcεRII: molecular multi-tasking. *Clin Exp Immunol.* 162, 12-23, (**2010**).

48   Lemieux, G. A. *et al.*, The low affinity IgE receptor (CD23) is cleaved by the metalloproteinase ADAM10. *J Biol Chem.* 282, 14836-14844, (**2007**).

49   McCloskey, N. *et al.*, Soluble CD23 monomers inhibit and oligomers stimulate IGE synthesis in human B cells. *J Biol Chem.* 282, 24083-24091, (**2007**).

50   Hibbert, R. G. *et al.*, The structure of human CD23 and its interactions with IgE and CD21. *J Exp Med.* 202, 751-760, (**2005**).

51   Vercelli, D. *et al.*, The B-cell binding site on human immunoglobulin E. *Nature.* 338, 649-651, (**1989**).

52   Plomp, R. *et al.*, Site-specific N-glycosylation analysis of human immunoglobulin e. *J Proteome Res.* 13, 536-546, (**2014**).

53   Shade, K. T. *et al.*, A single glycan on IgE is indispensable for initiation of anaphylaxis. *J Exp Med.* 212, 457-467, (**2015**).

54   Spiro, R. G., Protein glycosylation: nature, distribution, enzymatic formation, and disease implications of glycopeptide bonds. *Glycobiology.* 12, 43-56, (**2002**).

55   Marino, K. *et al.*, A systematic approach to protein glycosylation analysis: a path through the maze. *Nat Chem Biol.* 6, 713-723, (**2010**).

56   Lodish, H. F., *Molecular cell biology.* 4th edn, (Freeman, **2000**).

57   Aebi, M., N-linked protein glycosylation in the ER. *Biochim Biophys Acta.* 1833, 2430-2437, (**2013**).

58   Furmanek, A. & Hofsteenge, J., Protein C-mannosylation: facts and questions. *Acta Biochim Pol.* 47, 781-789, (**2000**).

59   Roth, J. *et al.*, Protein N-glycosylation, protein folding, and protein quality control. *Mol Cells.* 30, 497-506, (**2010**).

60   Haltiwanger, R. S. & Lowe, J. B., Role of glycosylation in development. *Annu Rev Biochem.* 73, 491-537, (**2004**).

61   Freeze, H. H., Human disorders in N-glycosylation and animal models. *Biochim Biophys Acta.* 1573, 388-393, (**2002**).

62   Altmann, F., The role of protein glycosylation in allergy. *Int Arch Allergy Immunol.* 142, 99-115, (**2007**).

63   Aalberse, R. C. *et al.*, Immunoglobulin E antibodies that crossreact with vegetable foods, pollen, and Hymenoptera venom. *J Allergy Clin Immunol.* 68, 356-364, (**1981**).

64   Wilson, I. B. *et al.*, Analysis of Asn-linked glycans from vegetable foodstuffs: widespread occurrence of Lewis a, core alpha1,3-linked fucose and xylose substitutions. *Glycobiology.* 11, 261-274, (**2001**).

65   Kleine-Tebbe, J. & Jakob, T., *Molecular Allergy Diagnostics: Innovation for a Better Patient Management.* (Springer International Publishing, **2017**).

66   Altmann, F., Coping with cross-reactive carbohydrate determinants in allergy diagnosis. *Allergo J Int.* 25, 98-105, (**2016**).

67   Jappe, U. *et al.*, In vitro hymenoptera venom allergy diagnosis: improved by screening for cross-reactive carbohydrate determinants and reciprocal inhibition. *Allergy.* 61, 1220-1229, (**2006**).

68   Worm, M. *et al.*, Food allergies resulting from immunological cross-reactivity with inhalant allergens: Guidelines from the German Society for Allergology and Clinical Immunology (DGAKI), the German Dermatology Society (DDG), the Association of German Allergologists (AeDA) and the Society for Pediatric Allergology and Environmental Medicine (GPA). *Allergo J Int.* 23, 1-16, (**2014**).

69   Holzweber, F. *et al.*, Inhibition of IgE binding to cross-reactive carbohydrate determinants enhances diagnostic selectivity. *Allergy.* 68, 1269-1277, (**2013**).

70   Jin, C. *et al.*, Affinity of IgE and IgG against cross-reactive carbohydrate determinants on plant and insect glycoproteins. *J Allergy Clin Immunol.* 121, 185-190 e182, (**2008**).

71   Carballada, F. J. *et al.*, Low prevalence of IgE to cross-reactive carbohydrate determinants in beekeepers. *J Allergy Clin Immunol.* 128, 1350-1352 e1352, (**2011**).

72   Mertens, M. *et al.*, Cross-reactive carbohydrate determinants strongly affect the results of the basophil activation test in hymenoptera-venom allergy. *Clin Exp Allergy.* 40, 1333-1345, (**2010**).

73   Sandrin, M. & McKenzie, I. F. C., Galα(1,3)Gal, the Major Xenoantigen(s) Recognised in Pigs by Human Natural Antibodies. *Immunological Reviews.* 141, 169-190, (**1994**).

74   Chung , C. H. *et al.*, Cetuximab-Induced Anaphylaxis and IgE Specific for Galactose-α-1,3-Galactose. *New England Journal of Medicine.* 358, 1109-1117, (**2008**).

75   Qian, J. *et al.*, Structural characterization of N-linked oligosaccharides on monoclonal antibody cetuximab by the combination of orthogonal matrix-assisted laser desorption/ionization hybrid quadrupole-quadrupole time-of-flight tandem mass spectrometry and sequential enzymatic digestion. *Anal Biochem.* 364, 8-18, (**2007**).

76   Wiegandt, A. & Meyer, B., Unambiguous characterization of N-glycans of monoclonal antibody cetuximab by integration of LC-MS/MS and (1)H NMR spectroscopy. *Anal Chem.* 86, 4807-4814, (**2014**).

77   Commins, S. P. *et al.*, Delayed anaphylaxis, angioedema, or urticaria after consumption of red meat in patients with IgE antibodies specific for galactose-α-1,3-galactose. *Journal of Allergy and Clinical Immunology.* 123, 426-433.e422, (**2009**).

78   Van Nunen, S. A. *et al.*, An association between tick bite reactions and red meat allergy in humans. *Med J Aust.* 190, 510-511, (**2009**).

79   Apostolovic, D. *et al.*, The red meat allergy syndrome in Sweden. *Allergo J Int.* 25, 49-54, (**2016**).

80   Sekiya, K. *et al.*, Delayed anaphylactic reaction to mammalian meat. *J Investig Allergol Clin Immunol.* 22, 446-447, (**2012**).

81   Lee, J. H. *et al.*, Delayed mammalian meat-induced anaphylaxis confirmed by skin test to cetuximab. *The Journal of Dermatology.* 40, 577-578, (**2013**).

82   Wickner, P. G. & Commins, S. P., The First 4 Central American Cases Of Delayed Meat Allergy With Galactose-Alpha-1,3-Galactose Positivity Clustered Among Field Biologists In Panama. *Journal of Allergy and Clinical Immunology.* 133, AB212, (**2014**).

83   Jappe, U. *et al.*, Meat allergy associated with galactosyl-alpha-(1,3)-galactose (alpha-Gal)-Closing diagnostic gaps by anti-alpha-Gal IgE immune profiling. *Allergy*, (**2017**).

84   Hamsten, C. *et al.*, Identification of galactose-α-1,3-galactose in the gastrointestinal tract of the tick Ixodes ricinus; possible relationship with red meat allergy. *Allergy.* 68, 549-552, (**2013**).

85   Araujo, R. N. *et al.*, Amblyomma sculptum tick saliva: α-Gal identification, antibody response and possible association with red meat allergy in Brazil. *International Journal for Parasitology.* 46, 213-220, (**2016**).

86   Pulendran, B. & Artis, D., New Paradigms in Type 2 Immunity. *Science.* 337, 431-435, (**2012**).

87   Preston, S. G. *et al.*, Novel immunomodulators from hard ticks selectively reprogramme human dendritic cell responses. *PLoS Pathog.* 9, e1003450, (**2013**).

88   Bowman, A. S. *et al.*, A Novel Phospholipase A2Activity in Saliva of the Lone Star Tick,Amblyomma americanum(L.). *Experimental Parasitology.* 87, 121-132, (**1997**).

89   Oliveira, C. J. *et al.*, Deconstructing tick saliva: non-protein molecules with potent immunomodulatory properties. *J Biol Chem.* 286, 10960-10969, (**2011**).

90   Segal, M. *et al.*, Anti-immunoglobulin e therapy. *World Allergy Organ J.* 1, 174-183, (**2008**).

91   Baird, B. *et al.*, Interaction of IgE with its high-affinity receptor. Structural basis and requirements for effective cross-linking. *Int Arch Allergy Appl Immunol.* 88, 23-28, (**1989**).

92   Froehlich, J. *et al.*, Initial human study with a humanized recombinant anti-IgE monoclonal antibody: safety, tolerance and pharmacokinetic (PK)/dynamic profile. *Clinical Pharmacology & Therapeutics.* 57, 162-162, (**1995**).

93   Schulman, E. S., Development of a monoclonal anti-immunoglobulin E antibody (omalizumab) for the treatment of allergic respiratory disorders. *Am J Respir Crit Care Med.* 164, S6-11, (**2001**).

94   Eggel, A. *et al.*, Accelerated dissociation of IgE-FcεRI complexes by disruptive inhibitors actively desensitizes allergic effector cells. *J Allergy Clin Immunol.* 133, 1709-1719, (**2014**).

95   Kopp, M. V., Omalizumab: Anti-IgE Therapy in Allergy. *Current Allergy and Asthma Reports.* 11, 101-106, (**2011**).

96   Xolair Prescribing information. https://www.gene.com/download/pdf/xolair_prescribing.pdf, (Last access: **17.11.2017**).

97   Kawakami, T. & Blank, U., From IgE to Omalizumab. *J Immunol.* 197, 4187-4192, (**2016**).

98   Long, A. *et al.*, Incidence of malignancy in patients with moderate-to-severe asthma treated with or without omalizumab. *J Allergy Clin Immunol.* 134, 560-567 e564, (**2014**).

99   Hamilton, R. G. *et al.*, Immunological methods for quantifying free and total serum IgE levels in allergy patients receiving omalizumab (Xolair) therapy. *Journal of immunological methods.* 303, 81-91, (**2005**).

100   Liu, J. *et al.*, Characterization of complex formation by humanized anti-IgE monoclonal antibody and monoclonal human IgE. *Biochemistry.* 34, 10474-10482, (**1995**).

101   Bousquet, J. *et al.*, Predicting and evaluating response to omalizumab in patients with severe allergic asthma. *Respir Med.* 101, 1483-1492, (**2007**).

102   Binz, H. K. *et al.*, High-affinity binders selected from designed ankyrin repeat protein libraries. *Nat Biotechnol.* 22, 575-582, (**2004**).

103   Baumann, M. J. *et al.*, DARPins against a functional IgE epitope. *Immunol Lett.* 133, 78-84, (**2010**).

104   Kim, B. *et al.*, Accelerated disassembly of IgE-receptor complexes by a disruptive macromolecular inhibitor. *Nature.* 491, 613-617, (**2012**).

105   Cohen, E. S. *et al.*, A novel IgE-neutralizing antibody for the treatment of severe uncontrolled asthma. *MAbs.* 6, 756-764, (**2014**).

106   Sheldon, E. *et al.*, Pharmacokinetics, Pharmacodynamics, and Safety of MEDI4212, an Anti-IgE Monoclonal Antibody, in Subjects with Atopy: A Phase I Study. *Adv Ther.* 33, 225-251, (**2016**).

107   Singh, S. *et al.* High affinity anti-human IgE antibodies. US 7531169 B2 (**2009**).

108   Arm, J. P. *et al.*, Pharmacokinetics, pharmacodynamics and safety of QGE031 (ligelizumab), a novel high-affinity anti-IgE antibody, in atopic subjects. *Clin Exp Allergy.* 44, 1371-1385, (**2014**).

109   Gauvreau, G. M. *et al.*, Efficacy and safety of multiple doses of QGE031 (ligelizumab) versus omalizumab and placebo in inhibiting allergen-induced early asthmatic responses. *J Allergy Clin Immunol.* 138, 1051-1059, (**2016**).

110   Saerens, D. & Muyldermans, S., *Single domain antibodies : methods and protocols.* (Humana Press, **2012**).

111   Siontorou, C. G., Nanobodies as novel agents for disease diagnosis and therapy. *Int J Nanomedicine.* 8, 4215-4227, (**2013**).

112   Hamers-Casterman, C. *et al.*, Naturally occurring antibodies devoid of light chains. *Nature.* 363, 446-448, (**1993**).

113   Alexander, A. *et al.*, gamma Heavy chain disease in man: cDNA sequence supports partial gene deletion model. *Proc Natl Acad Sci U S A.* 79, 3260-3264, (**1982**).

114   Greenberg, A. S. *et al.*, A new antigen receptor gene family that undergoes rearrangement and extensive somatic diversification in sharks. *Nature.* 374, 168-173, (**1995**).

115   Arbabi-Ghahroudi, M. *et al.*, Prokaryotic expression of antibodies. *Cancer Metastasis Rev.* 24, 501-519, (**2005**).

116   Rajabi-Memari, H. *et al.*, Expression and characterization of a recombinant single-domain monoclonal antibody against MUC1 mucin in tobacco plants. *Hybridoma (Larchmt).* 25, 209-215, (**2006**).

117   Muyldermans, S., Nanobodies: natural single-domain antibodies. *Annu Rev Biochem.* 82, 775-797, (**2013**).

118   Meerts, P. *et al.* Immunoglobulin single variable domains directed against IgE. WO 2012175740 A1 (**2012**).

119   Jansohn, M. *et al.*, *Gentechnische Methoden: Eine Sammlung von Arbeitsanleitungen für das molekularbiologische Labor.* (Spektrum Akademischer Verlag, **2011**).

120   Inoue, H. *et al.*, High efficiency transformation of Escherichia coli with plasmids. *Gene.* 96, 23-28, (**1990**).

121   Ciccarone, V. C. *et al.*, Generation of Recombinant Baculovirus DNA in E.coli Using a Baculovirus Shuttle Vector. *Methods Mol Med*. 13, 213-235, (**1998**).

122   Shamji, M. H. *et al.*, Cell-free detection of allergen-IgE cross-linking with immobilized phase CD23: inhibition by blocking antibody responses after immunotherapy. *J Allergy Clin Immunol*. 132, 1003-1005 e1001-1004, (**2013**).

123   Johansson, S. G. *et al.*, Passive IgE-sensitization by blood transfusion. *Allergy.* 60, 1192-1199, (**2005**).

124   McPherson, A. & Gavira, J. A., Introduction to protein crystallization. *Acta Crystallogr F Struct Biol Commun*. 70, 2-20, (**2014**).

125   Kabsch, W., XDS. *Acta crystallographica. Section D, Biological crystallography.* 66, 125-132, (**2010**).

126   McCoy, A. J. *et al.*, Phaser crystallographic software. *Journal of applied crystallography.* 40, 658-674, (**2007**).

127   Emsley, P. & Cowtan, K., Coot: model-building tools for molecular graphics. *Acta crystallographica. Section D, Biological crystallography.* 60, 2126-2132, (**2004**).

128   Adams, P. D. *et al.*, PHENIX: a comprehensive Python-based system for macromolecular structure solution. *Acta crystallographica. Section D, Biological crystallography.* 66, 213-221, (**2010**).

129   Croll, T. I. & Andersen, G. R., Re-evaluation of low-resolution crystal structures via interactive molecular-dynamics flexible fitting (iMDFF): a case study in complement C4. *Acta crystallographica. Section D, Structural biology.* 72, 1006-1016, (**2016**).

130   Mertens, H. D. & Svergun, D. I., Structural characterization of proteins and complexes using small-angle X-ray solution scattering. *J Struct Biol*. 172, 128-141, (**2010**).

131   Brennich, M. E. *et al.*, Online data analysis at the ESRF bioSAXS beamline, BM29. *Journal of applied crystallography.* 49, 203-212, (**2016**).

132   Franke, D. *et al.*, Automated acquisition and analysis of small angle X-ray scattering data. *Nucl Instrum Meth A*. 689, 52-59, (**2012**).

133   Svergun, D. I., Determination of the Regularization Parameter in Indirect-Transform Methods Using Perceptual Criteria. *Journal of applied crystallography*. 25, 495-503, (**1992**).

134   Petoukhov, M. V. *et al.*, New developments in the ATSAS program package for small-angle scattering data analysis. *Journal of applied crystallography*. 45, 342-350, (**2012**).

135   Svergun, D. *et al.*, CRYSOL - A program to evaluate x-ray solution scattering of biological macromolecules from atomic coordinates. *Journal of applied crystallography*. 28, 768-773, (**1995**).

136   Hayward, S. & Berendsen, H. J., Systematic analysis of domain motions in proteins from conformational change: new results on citrate synthase and T4 lysozyme. *Proteins*. 30, 144-154, (**1998**).

137   Braren, I. *et al.*, Generation of human monoclonal allergen-specific IgE and IgG antibodies from synthetic antibody libraries. *Clin Chem*. 53, 837-844, (**2007**).

138   Krissinel, E. & Henrick, K., Inference of macromolecular assemblies from crystalline state. *J Mol Biol*. 372, 774-797, (**2007**).

139   Wurzburg, B. A. & Jardetzky, T. S., Conformational flexibility in immunoglobulin E-Fc 3-4 revealed in multiple crystal forms. *J Mol Biol*. 393, 176-190, (**2009**).

140   Beavil, A. J. *et al.*, Bent domain structure of recombinant human IgE-Fc in solution by X-ray and neutron scattering in conjunction with an automated curve fitting procedure. *Biochemistry*. 34, 14449-14461, (**1995**).

141   Davis, K. G. *et al.*, A model for the solution conformation of rat IgE. *Biochem Soc Trans*. 18, 935-936, (**1990**).

142   Galili, U. *et al.*, A sensitive assay for measuring alpha-Gal epitope expression on cells by a monoclonal anti-Gal antibody. *Transplantation*. 65, 1129-1132, (**1998**).

143   Plum, M. *et al.*, Close-up of the immunogenic alpha1,3-galactose epitope as defined by a monoclonal chimeric immunoglobulin E and human serum using saturation transfer difference (STD) NMR. *J Biol Chem.* 286, 43103-43111, (**2011**).

144   Rispens, T. *et al.*, IgE production to alpha-gal is accompanied by elevated levels of specific IgG1 antibodies and low amounts of IgE to blood group B. *PLoS One.* 8, e55566, (**2013**).

145   Apostolovic, D. *et al.*, Red meat allergic patients have a selective IgE response to the alpha-Gal glycan. *Allergy.* 70, 1497-1500, (**2015**).

146   Frenken, L. G. *et al.*, Isolation of antigen specific llama VHH antibody fragments and their high level secretion by Saccharomyces cerevisiae. *J Biotechnol.* 78, 11-21, (**2000**).

147   Young, R. J. *et al.*, Secretion of recombinant human IgE-Fc by mammalian cells and biological activity of glycosylation site mutants. *Protein Eng.* 8, 193-199, (**1995**).

148   Subedi, G. P. *et al.*, High Yield Expression of Recombinant Human Proteins with the Transient Transfection of HEK293 Cells in Suspension. *J Vis Exp*, e53568, (**2015**).

149   Davies, A. M. *et al.*, Allosteric mechanism of action of the therapeutic anti-IgE antibody omalizumab. *J Biol Chem.* 292, 9975-9987, (**2017**).

150   Wang, J., Estimation of the quality of refined protein crystal structures. *Protein Sci.* 24, 661-669, (**2015**).

151   Wolf, S. V., Interaktion und strukturelle Aspekte humaner IgE-Antikörper im Kontext der Allergie. PhD thesis, University of Hamburg, (**2015**).

152   Zheng, Y. *et al.*, Conformations of IgE bound to its receptor FcεRI and in solution. *Biochemistry.* 30, 9125-9132, (**1991**).

153   Wan, T. *et al.*, The crystal structure of IgE Fc reveals an asymmetrically bent conformation. *Nature Immunology.* 3, 681-686, (**2002**).

154   Davies, A. M. *et al.*, Allosteric mechanism of action of the therapeutic anti-IgE antibody omalizumab. *Journal of Biological Chemistry.* 292, 9975-9987, (**2017**).

155 McDonnell, J. M. *et al.*, The structure of the IgE Cϵ2 domain and its role in stabilizing the complex with its high-affinity receptor FcϵRIα. *Nat Struct Biol.* 8, 437-441, (**2001**).

156 Clement, M. J. *et al.*, Toward a better understanding of the basis of the molecular mimicry of polysaccharide antigens by peptides: the example of Shigella flexneri 5a. *J Biol Chem.* 281, 2317-2332, (**2006**).

157 Christensen, L. H. *et al.*, Several distinct properties of the IgE repertoire determine effector cell degranulation in response to allergen challenge. *J Allergy Clin Immunol.* 122, 298-304, (**2008**).

158 Macglashan, D. W., Jr. & Saini, S. S., Omalizumab increases the intrinsic sensitivity of human basophils to IgE-mediated stimulation. *J Allergy Clin Immunol.* 132, 906-911 e901-904, (**2013**).

159 Luu, M. *et al.*, Pharmacokinetics, pharmacodynamics and clinical efficacy of omalizumab for the treatment of asthma. *Expert Opin Drug Metab Toxicol.* 12, 1503-1511, (**2016**).

160 Harmsen, M. M. & De Haard, H. J., Properties, production, and applications of camelid single-domain antibody fragments. *Appl Microbiol Biotechnol.* 77, 13-22, (**2007**).

161 Detalle, L. *et al.*, Generation and Characterization of ALX-0171, a Potent Novel Therapeutic Nanobody for the Treatment of Respiratory Syncytial Virus Infection. *Antimicrob Agents Chemother.* 60, 6-13, (**2015**).

162 Bes, C. *et al.*, The chimeric mouse-human anti-CD4 Fab 13B8.2 expressed in baculovirus inhibits both antigen presentation and HIV-1 promoter activation. *Hum Antibodies.* 10, 67-76, (**2001**).

163 Abrams, C. *et al.*, Determinants of specificity of a baculovirus-expressed antibody Fab fragment that binds selectively to the activated form of integrin alpha IIb beta 3. *J Biol Chem.* 269, 18781-18788, (**1994**).

164 Koide, S., Engineering of recombinant crystallization chaperones. *Curr Opin Struct Biol.* 19, 449-457, (**2009**).

165 Lam, A. Y. *et al.*, Nanobody-aided structure determination of the EpsI:EpsJ pseudopilin heterodimer from Vibrio vulnificus. *J Struct Biol.* 166, 8-15, (**2009**).

166   Nobelprize.org. The 2017 Nobel Prize in Chemistry - Press Release. https://www.nobelprize.org/nobel_prizes/chemistry/laureates/2017/press.html, (Last access: **07.11.2017**).

167   Yuan, Y. *et al.*, Cryo-EM structures of MERS-CoV and SARS-CoV spike glycoproteins reveal the dynamic receptor binding domains. *Nat Commun.* 8, 15092, (**2017**).

168   Milland, J. *et al.*, Carbohydrate residues downstream of the terminal Galalpha(1,3)Gal epitope modulate the specificity of xenoreactive antibodies. *Immunol Cell Biol.* 85, 623-632, (**2007**).

169   Altmann, F. *et al.*, Insect cells contain an unusual, membrane-bound beta-N-acetylglucosaminidase probably involved in the processing of protein N-glycans. *J Biol Chem.* 270, 17344-17349, (**1995**).

170   Bantleon, F. *et al.*, Human IgE is efficiently produced in glycosylated and biologically active form in lepidopteran cells. *Mol Immunol.* 72, 49-56, (**2016**).

171   Michel, S. *et al.*, Skin prick test and basophil reactivity to cetuximab in patients with IgE to alpha-gal and allergy to red meat. *Allergy.* 69, 403-405, (**2014**).

172   Arkestal, K. *et al.*, Impaired allergy diagnostics among parasite-infected patients caused by IgE antibodies to the carbohydrate epitope galactose-alpha 1,3-galactose. *J Allergy Clin Immunol.* 127, 1024-1028, (**2011**).

173   Liang, C. H. & Wu, C. Y., Glycan array: a powerful tool for glycomics studies. *Expert Rev Proteomics.* 6, 631-645, (**2009**).

174   Oyelaran, O. & Gildersleeve, J. C., Glycan arrays: recent advances and future challenges. *Curr Opin Chem Biol.* 13, 406-413, (**2009**).

175   Blixt, O. *et al.*, Anticarbohydrate Antibody Repertoires in Patients Transplanted with Fetal Pig Islets Revealed by Glycan Arrays. *American Journal of Transplantation.* 9, 83-90, (**2009**).

176   Newburg, D. S. & Chaturvedi, P., Neutral glycolipids of human and bovine milk. *Lipids.* 27, 923-927, (**1992**).

177   Soh, J. Y. *et al.*, Anaphylaxis to galacto-oligosaccharides--an evaluation in an atopic population in Singapore. *Allergy.* 70, 1020-1023, (**2015**).

178   Werfel, S. J. *et al.*, Clinical reactivity to beef in children allergic to cow's milk. *J Allergy Clin Immunol.* 99, 293-300, (**1997**).

179   Wieslander, J. *et al.*, Specificity of human antibodies against galα1-3gal carbohydrate epitope and distinction from natural antibodies reacting with galα1-2gal or galα1-4 gal. *Glycoconjugate Journal.* 7, 85-100, (**1990**).

7. Appendix

7.1 Data collection and refinement statistics of the IgE026:IgE Fc complex

Table 5: Data collection and refinement statistics.
Values in parentheses are for the highest-resolution shell. Statistics were calculated by XSCALE (scaling), phenix.refine (refinement) and MOLPROBITY (validation).

Data collection	
Dataset	IgE026:IgE Fc
X-ray source	Diamond I24
Space group	$P4_12_12$
Unit cell parameters	a=102.0, b=102.0, c=300.4 Å
	$\alpha=\beta=\gamma=90°$
Resolution (Å)	19.96-3.40 (3.52-3.40)
Unique reflections	22564 (2190)
Multiplicity	12.3 (10.5)
$I/\sigma(I)$	8.3 (1.11)
Completeness	0.99 (1.00)
R_{meas}	0.35 (2.37)
R_{pim}	0.10 (0.71)
R_{merge}	0.34 (2.25)
$CC_{1/2}$	0.99 (0.76)
Refinement statistics	
Reflections in refinement	22560
R_{work}	0.2123
R_{free}	0.2408
Average B-value (Å^2)	111.4
Macromolecule (Å^2)	111.4
Carbohydrates (Å^2)	121.7
Wilson B-value (Å^2)	108.2
Protein atoms	5226
Carbohydrate atoms	166
Ramachandran statistics (%)	
Favored	97.12
Allowed	2.88
Outliers	0.00
RMSD from ideal geometry	
Bond angles (°)	0.86
Bond length (Å)	0.004
Clashscore	3.76
PDB ID	5NQW

7.2 Observed electron density from the IgE026:IgE Fc interface
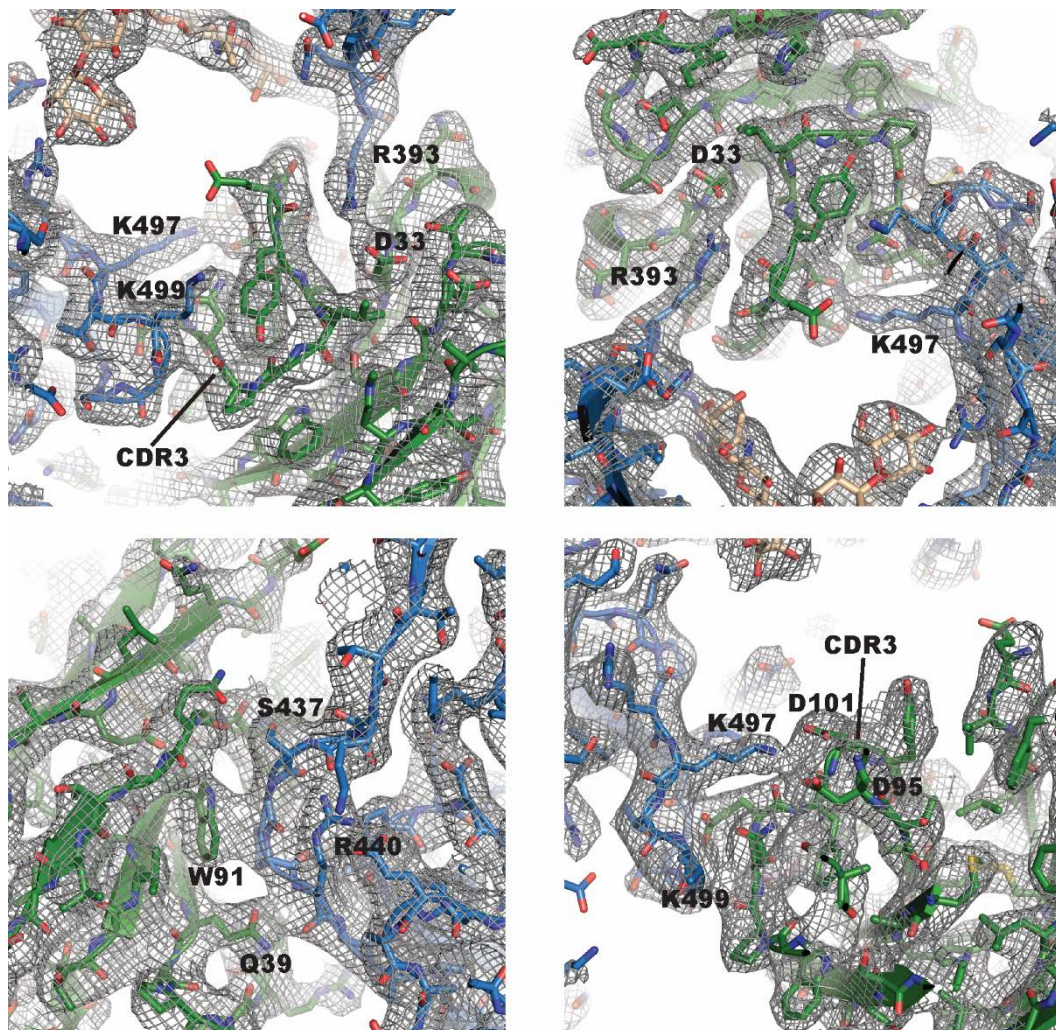
Figure 71: Electron density from the intermolecular interface.
A 2mF$_o$-DF$_c$ electron density map contoured at 1σ at different interface regions in the complex. The IgE026 is shown in green and IgE Fc in blue.

7.3 Comparison of the epitopes of several IgE binding molecules
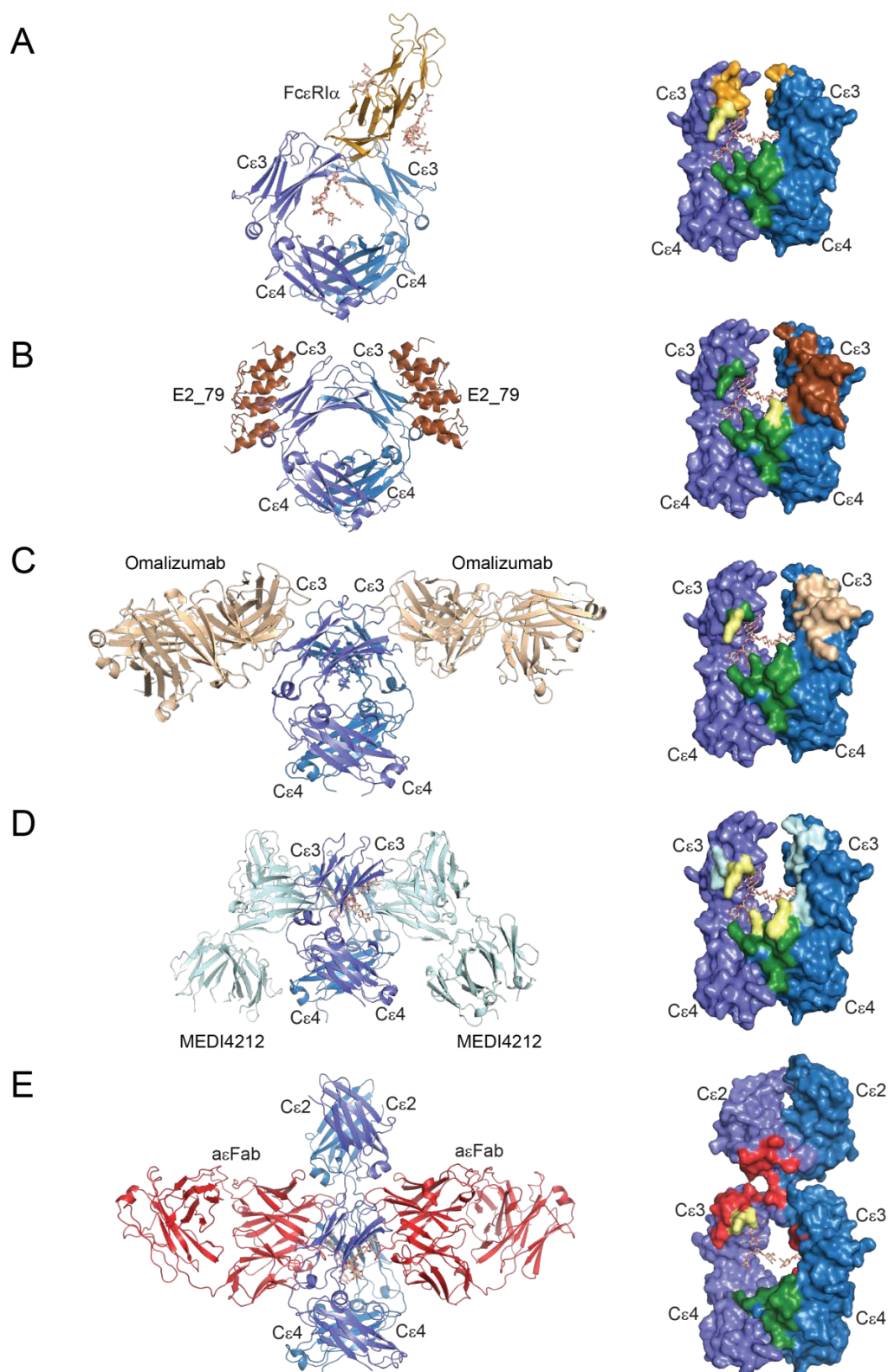
Figure 72: The epitopes of several IgE binding molecules and their overlap with the IgE026 sdab epitope.
Cartoon representations are shown to the left with the IgE Fc in blue and other Fc binding proteins in other colours. To the right are displayed surface representations with the sdab epitope in green, the epitope of the other IgE binder in individual colours, and overlapping epitope residues in yellow. Comparison of the IgE026:IgE Fc complex with **A:** FcεRI complex (PBD: 1F6A), **B:** IgE Fc:E2_79 complex (PDB: 4GRG), **C:** IgE Fc:Omalizumab Fab (PDB: 5HYS), **D:** IgE Fc:MEDI4212 Fab (PDB: 5ANM), and **E:** another IgE Fc:anti-IgE Fab (PDB: 4J4P).

7.4 Data collection and refinement statistics of M86 Fab

Table 6: Data collection and refinement statistics.
Values in parentheses are for the highest-resolution shell. Statistics were calculated by XSCALE (scaling), phenix.refine (refinement) and MOLPROBITY (validation).

Data collection	
Dataset	M86 Fab
X-ray source	ESRF Grenoble
Space group	$P2_12_12_1$
Unit cell parameters	a=64.0 b=97.7, c=157.2 Å
	$α$=$β$=$γ$=90°
Resolution (Å)	49.61-3.41 (3.52-3.40)
Unique reflections	13998 (2707)
Completeness	0.99 (0.98)
Refinement statistics	
Reflections in refinement	13994
R_{work}	0.2878
R_{free}	0.3160
Average B-value ($Å^2$)	67.88
Wilson B-value ($Å^2$)	74.62
Ramachandran statistics (%)	
Favored	92.75
Outliers	1.04
RMSD from ideal geometry	
Bond angles (°)	0.93
Bond length (Å)	0.004
Clashscore	10.61

7.5 The 100 different carbohydrates represented on the glycan array

Table 7: Carbohydrates represented on the glycan array.

1 β-Glc-	2 β-Gal-	3 α-Man-	4 α-Fuc-
5 α-Rha-	6 β-GlcNAc-	7 β-GalNAc-	8 Tobramycin
9 Gal-β-1,3-GlcNAc-β-	10 Gal-α-1,3-Gal-β-1,3-GlcNAc-β-	11 Neu5Ac-α-2,3-Gal-β-1,3-GlcNAc-β-	12 Neu5Ac-α-2,6-Gal-β-1,3-GlcNAc-β-
13 Neu5Gc-α-2,3-Gal-β-1,3-GlcNAc-β-	14 Neu5Gc-α-2,6-Gal-β-1,3-GlcNAc-β-	15 Gal-β-1,3-(Fuc-α-1,4)-GlcNAc-β- [Lewis A]	16 Gal-β-1,4-Glc-β-
17 Gal-α-1,3-Gal-β-1,4-Glc-β-	18 Gal-α-1,4-Gal-β-1,4-Glc-β-	19 GlcNAc-β-1,3-Gal-β-1,4-Glc-β-	20 GalNAc-β-1,3-Gal-β-1,4-Glc-β-
21 Neu5Ac-α-2,3-Gal-β-1,4-Glc-β-	22 Neu5Ac-α-2,6-Gal-β-1,4-Glc-β-	23 Neu5Gc-α-2,3-Gal-β-1,4-Glc-β-	24 Neu5Ac-α-2,6-Gal-β-1,4-Glc-β-
25 Gal-β-1,4-(Fuc-α-1,3)-Glc-β-	26 GalNAc-β-1,3-Gal-α-1,4-Gal-β-1,4-Glc-β-	27 GlcNAc-β-1,6-GlcNAc-β-	28 4-P-GlcNAc-β-1,4-Man-β-.
29 Glc-α-1,2-Gal-α-1,3-Glc-α-	30 Gal-β-1,3-GalNAc-α-	31 Gal-β-1,4-GlcNAc-β-	32 Gal-β-1,4 -(Fuc-α-1,3)-GlcNAc-β- [Lewis X]
33 Neu5Ac-α-2,3-Gal-β-1,4-(Fuc-α-1,3)-GlcNAc-β- [Sialyl Lewis X]	34 Neu5Ac-α-2,3-Gal-β-1,3 -(Fuc-α-1,4)-GlcNAc-β- [Sialyl Lewis A]	35 Neu5Gc-α-2,3-Gal-β-1,3-(Fuc-α-1,4)-GlcNAc-β- [Sialyl Lewis A]	36 Gal-α-1,4-Gal-β-1,3-GlcNAc-β-
37 Gal-β-1,4-GlcNAc-β-1,3-Gal-β-1,4-Glc-β- [LNnT]	38 GlcA-β-1,4-GlcNAc-α-1,4-GlcA-β-	39 GlcNAc-β-1,6-(Gal-β-1,3)-GalNAc-α-O-Ser	40 Neu5Ac-α-2,3Gal-β-1,4-(6S)GlcNAc-β-
41 GalNAc-β-1,4-GlcNAc-β-	42 Neu5Ac-α-2,8-Neu5Ac-α-2,3-Gal β-1,4-Glc-β-	43 Neu5Gc-α-2,8-Neu5Ac-α-2,3-Gal-β-1,4-Glc-β-	44 GalNAc-α-1,3-(Fuc-α-1,2)-Gal-β-1,4-Glc-β- [Blood A antigen tetrose]
45 GlcNAc-β-1,2-Man-α-	46 Neu5Ac-α-2,3-Gal-β-	47 Gal-β-1,3 -GalNAc-β-1,3-Gal-β-	48 Glc-α-1,2-Gal-α-
49 Gal-β-1,4-(Fuc-α-1,3)-GlcNAc-β-1,3-Gal-β-	50 Neu5Ac-α-2,3-Gal-β-1,4-(Fuc-α-1,3)-Glc-β- [3-Sialyl-3-fucosyllactose/ F-SL]	51 GlcNAc-β-1,4-GlcNAc-β-	52 β-D-GlcA-
53 Gal-β-1,4-(6S)GlNAc-β-	54 GlcNAc-α-1,3-(Glc-α-1,2-Glc-α-1,2)-Gal-α-1,3-Glc-α-	55 Gal-β-1,3-GalNAc-β-1,4-(Neu5Gc-α-2,3)-Gal-β-1,4-Glc-β-	56 Sisomicin Sulphate
57 GalNAc-α-1,3-(Fuc-α-1,2)-Gal-β- [Blood A antigen trisaccharide]	58 Fuc-α-1,2-Gal-β-1,4-GlcNAc-β- [Blood H antigen trisaccharide]	59 Gal-α-1,3-(Fuc-α-1,2)-Gal-β- [Blood B antigen trisaccharide]	60 Fuc-α-1,2-Gal-β-1,3-GlcNAc-β-1,3-Gal-β-1,4-Glc-β- [LNFP I]
61 Fuc-α-1,2-Gal-β-1,4-Glc-β- [Blood H antigen trisaccharide]	62 Gal-α-1,3-(Fuc-α-1,2)-Gal-β-1,4-Glc-β- [Blood B antigen tetrasaccharide]	63 (Fuc-α-1,2)-Gal-β-1,4-(Fuc-α-1,3)-GlcNAc-β- [Lewis Y]	64 (Fuc-α-1,2)-Gal-β-1,3-(Fuc-α-1,4)-GlcNAc-β- [Lewis B]
65 Gal-β-1,3-(Fuc-α-1,4)-GlcNAc-β-1,3-Gal-β-1,4-(Fuc-α-1,4)-Glc-β- [Lewis A]	66 Gal-β-1,3-GalNAc-β-	67 Gal-β-1,3-(Neu5Ac-α-2,6)-GalNAc-β-	68 Neu5Ac-α-2,6-Gal-β-1,3-GalNAc-β-
69 Neu5Ac-α-2,6-Gal-β-1,3-(Neu5Ac-α-2,6)-GalNAc-β-	70 Neu5Ac-α-2,3-Gal-β-1,3-(Neu5Ac-α-2,6)-GalNAc-β-	71 Neu5Ac-α-2,6-(Neu5Ac-α-2,3)-Gal-β-1,3-GalNAc-β-	72 GalNAc-β-1,4-(Neu5Ac-α-2,3)-Gal-β-1,4-Glc-β- [GM2]
73 GalNAc-β-1,4-(Neu5Ac-α-2,8-Neu5Ac-α-2,3)-Gal-β-1,4-Glc-β- [GD2]	74 Gal-α-1,4-Gal-β-1,4-GlcNAc-β-	75 β-D-Rha-	76 Glc-α-1,4-Glc-β-
77 Glc-α-1,6-Glc-α-1,4-Glc-β-	78 Maltotriose-β-	79 Glc-α-1,6-Glc-α-1,6-Glc-β-	80 Maltotetraose-β-

81   GlcNAc-α-1,4-GlcA-β-1,4-GlcNAc-α1,4-GlcA-β-

82 Maltohexaose-β-

83 Maltoheptaose-β-

84 Acarbose-β-

85 D-pentamannuronic acid-β-

86 L-pentaguluronic acid-β-

87 D-cellose-β-

88 Gal-α-1,3-Gal-β-

89 β-1,4-Xylotetrose

90 Chitin-trisaccharide

91 KDN-α-2,8-Neu5Ac-α-2,3-Gal-β-1,4-Glc-β-

92   Neu5Ac-α-2,8-Neu5Gc-α-2,3-Gal-β-1,4-Glc-β-

93   Neu5Ac-α-2,8-Neu5Ac-α-2,8-Neu5Ac-α-2,3-Gal-β-1,4-Glc-β-

94   Neu5Ac-α-2,8-Neu5Ac-α-2,6-Gal-β-1,4-Glc-

95   Gal-β-1,3-GalNAc-β-1,4-(Neu5Ac-α-2,3)-Gal-β-1,4-Glc-β-

96   Gentamicin Sulphate

97 Kanamycin sulphate

98 Geneticin Disulphate Salt (G418)

99 Neomycin trisulphate

100 SGP

7.6 Sequence information

IgE026 (synthetic gene)

ccatggaggttcagctgctggaaagcggtggtggtctggttcagcctggtggtagcctgcgtctgagctgtgcagcaa

gcggttttacctttggtaattatgatatggcatgggttcgtcaggcaccgggtaaacgtccggaatgggttagcagcattg

ataccggtggtgatatcacacattatgccgatagcgttaaaggtcgttttaccattagccgtgataatgccaaaaatacc

ctgtacctgcagatgaatagtctgcgtccggaagataccgcagtttattggtgtgcaaccgatgaagaatatgcactgg

gtccgaatgagtttgattattatggtcagggcaccctggttaccgttagctcagcggccgcagatc

Ligelizumab scFv (synthetic gene)

gatcggcgcgccccgcttgatttccaccttggtgccgcctccaaaggtggtgggccaggaccagctctgctggcaata

atacacggcaaagtcctcggactgcagggagctgattgtcagggtgaactcggtgccagagccgctgccggaaaat

ctggcggggatgccgctgatgctctcgctggcgtagtagatcagcagtctgggggcctgtccgggcttctgctgatacc

agtggatgttggtgccgatgctctgagaggctctgcaggacagggtggctctttcgcctggagacacactcagggtgg

cggggctctgggtcatcacgatctcaagtgcactgccgccacttccgcctccgccagatcctccgccgccactcgag

actgtcacgagggtgccctggccccagtagtcgaagtagtcgtagttgctgccgctgaagtggctgaaccgggcgca

gtagtacacggcggtgtcctcgctccgcaggctgctcagttccatgtaggcggtggaggtgctggtgtcggcggtgaa

ggtcactctggccttgaacttctcgttgtagttggtggtgaaggtgccggggtcgatctcgcccatccattccaggccatg

tccaggggcctggcgcacccattccagccagtaccagctaaaggtgtagccgctggccttgcaggacaccttcacg

ctgctgccaggcttcatcacttcggcgccagactgcaccagctgcacctggcactgcacacatttaaatgatc

IgE026

MEVQLLESGGGLVQPGGSLRLSCAASGFTFGNYDMAWVRQAPGKRPEWVSSIDT
GGDITHYADSVKGRFTISRDNAKNTLYLQMNSLRPEDTAVYWCATDEEYALGPNEF
DYYGQGTLVTVSSAAAD

Human IgE Fc Cε2-4

ARDFTPPTVKILQSSCDGGGHFPPTIQLLCLVSGYTPGTINITWLEDGQVMDVDLST
ASTTQEGELASTQSELTLSQKHWLSDRTYTCQVTYQGHTFEDSTKKCADSNPRGV
SAYLSRPSPFDLFIRKSPTITCLVVDLAPSKGTVNLTWSRASGKPVNHSTRKEEKQR
NGTLTVTSTLPVGTRDWIEGETYQCRVTHPHLPRALMRSTTKTSGPRAAPEYAFAT
PEWPGSRDKRTLACLIQNFMPEDISVQWLHNEVQLPDARHSTTQPRKTKGSGFFV
FSRLEVTRAEWEQKDEFICRAVHEAASPSQTVQRAVSVNPGK

Ligelizumab Fab (huIgG1)

EIVMTQSPATLSVSPGERATLSCRASQSIGTNIHWYQQKPGQAPRLLIYYASESISGI
PARFSGSGSGTEFTLTISSLQSEDFAVYYCQQSWSWPTTFGGGTKVEIKRRTVGA
PSVFIFPPSDEQLKSGTASVVCLLNNFYPREAKVQWKVDNALQSGNSQESVTEQD
SKDSTYSLSSTLTLSKADYEKHKVYACEVTHQLSSPVTKSFNRGECQVQLVQSGAE
VMKPGSSVKVSCKASGYTFSWYWLEWVRQAPGHGLEWMGEIDPGTFTTNYNEKF
KARVTFTADTSTSTAYMELSSLRSEDTAVYYCARFSHFSGSNYDYFDYWGQGTLV
TVSSASTKGPSVFPLAPSSKSTSGGTAALGCLVKDYFPEPVTVSWNSGALTSGVHT
FPAVLQSSGLYSLSSVVTVPSSSLGTQTYICNVNHKPSNTKVDRRVEPKSCDKT

Single domain antibody 7-1

QVQLVESGGGLVQAGGPLRLSCAVFGSTFSNNVADWYRQAPGKQRELVARISAS
GATREYGDSVKGRFTISRDDAKNTMYLQMNNLKPEDTAVYRCHKIEWEDLSRKDY
WGQGTQVTVSS

M86 Fab (huIgG1)

DVVMTQTPLSLPVSLGDQASISCRSSQSLVHSDGNTYFHWYLQKPGQSPKLLIHRI
SNRFSGVPDRFSGSGSGTDFTLKISRVEAEDLGVYFCSQSTHIPWTFGGGTKLEIK
RTVGAPSVFIFPPSDEQLKSGTASVVCLLNNFYPREAKVQWKVDNALQSGNSQES
VTEQDSKDSTYSLSSTLTLSKADYEKHKVYACEVTHQGLSSPVTKSFNRGECEVKL
EESGGGLVQPGRSMKLSCVASGFIFSDYWMNWVRQSPEKGLEWIAQIRTNPYNY
ETYYSDSVKGRFTISRDDSKSSVYLQMKNLRSEDMGIYYCTWSHYALDNWGQGTS
VTVSSASTKGPSVFPLAPSSKSTSGGTAALGCLVKDYFPEPVTVSWNSGALTSGV
HTFPAVLQSSGLYSLSSVVTVPSSSLGTQTYICNVNHKPSNTKVDRRVEPKSCDKT

M86huIgE

DVVMTQTPLSLPVSLGDQASISCRSSQSLVHSDGNTYFHWYLQKPGQSPKLLIHRI
SNRFSGVPDRFSGSGSGTDFTLKISRVEAEDLGVYFCSQSTHIPWTFGGGTKLEIK
RTVGAPSVFIFPPSDEQLKSGTASVVCLLNNFYPREAKVQWKVDNALQSGNSQES
VTEQDSKDSTYSLSSTLTLSKADYEKHKVYACEVTHQGLSSPVTKSFNRGECDVV
MTQTPLSLPVSLGDQASISCRSSQSLVHSDGNTYFHWYLQKPGQSPKLLIHRISNR
FSGVPDRFSGSGSGTDFTLKISRVEAEDLGVYFCSQSTHIPWTFGGGTKLEIKRTV
GAPSVFIFPPSDEQLKSGTASVVCLLNNFYPREAKVQWKVDNALQSGNSQESVTE
QDSKDSTYSLSSTLTLSKADYEKHKVYACEVTHQGLSSPVTKSFNRGECRTVGAP
SVFIFPPSDEQLKSGTASVVCLLNNFYPREAKVQWKVDNALQSGNSQESVTEQDS
KDSTYSLSSTLTLSKADYEKHKVYACEVTHQGLSSPVTKSFNRGECASTQSPSVFP
LTRCCKNIPSNATSVTLGCLATGYFPEPVMVTWDTGSLNGTTMTLPATTLTLSGHY
ATISLLTVSGAWAKQMFTCRVAHTPSSTDWVDNKTFSVCSRDFTPPTVKILQSSCD
GGGHFPPTIQLLCLVSGYTPGTINITWLEDGQVMDVDLSTASTTQEGELASTQSELT
LSQKHWLSDRTYTCQVTYQGHTFEDSTKKCADSNPRGVSAYLSRPSPFDLFIRKS
PTITCLVVDLAPSKGTVNLTWSRASGKPVNHSTRKEEKQRNGTLTVTSTLPVGTRD
WIEGETYQCRVTHPHLPRALMRSTTKTSGPRAAPEVYAFATPEWPGSRDKRTLAC
LIQNFMPEDISVQWLHNEVQLPDARHSTTQPRKTKGSGFFVFSRLEVTRAEWEQK
DEFICRAVHEAASPSQTVQRAVSVNPGK

7.7 Vector maps
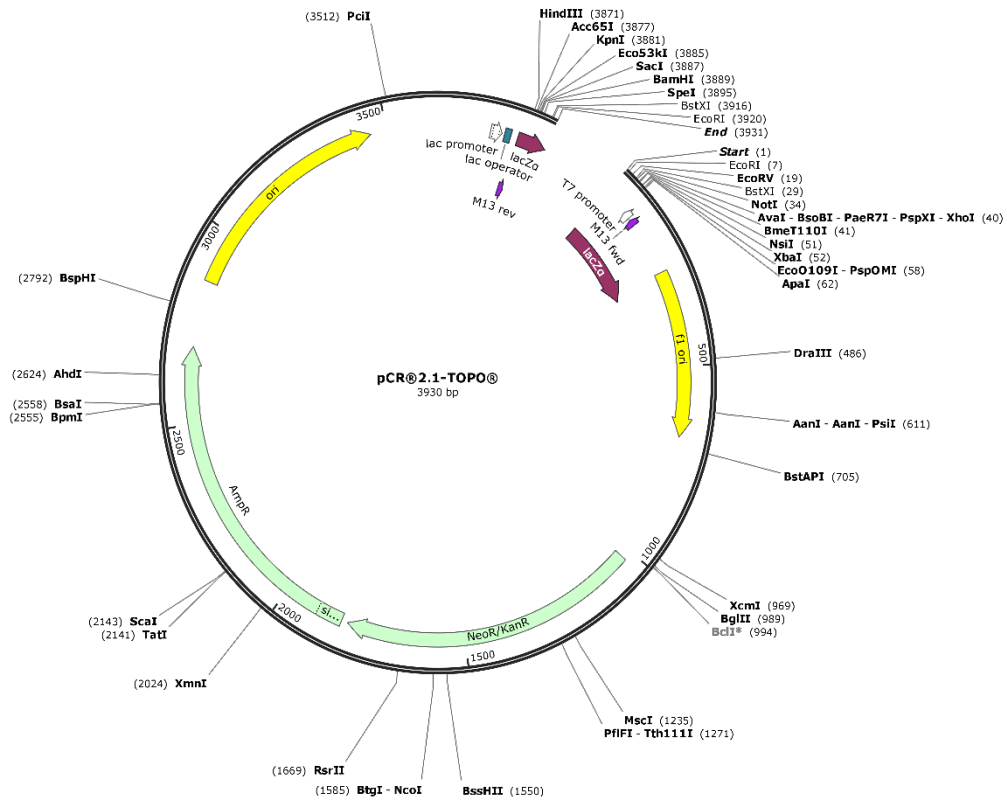
Figure 73: The pCR®2.1-TOPO® vector was used for subcloning of PCR fragments.
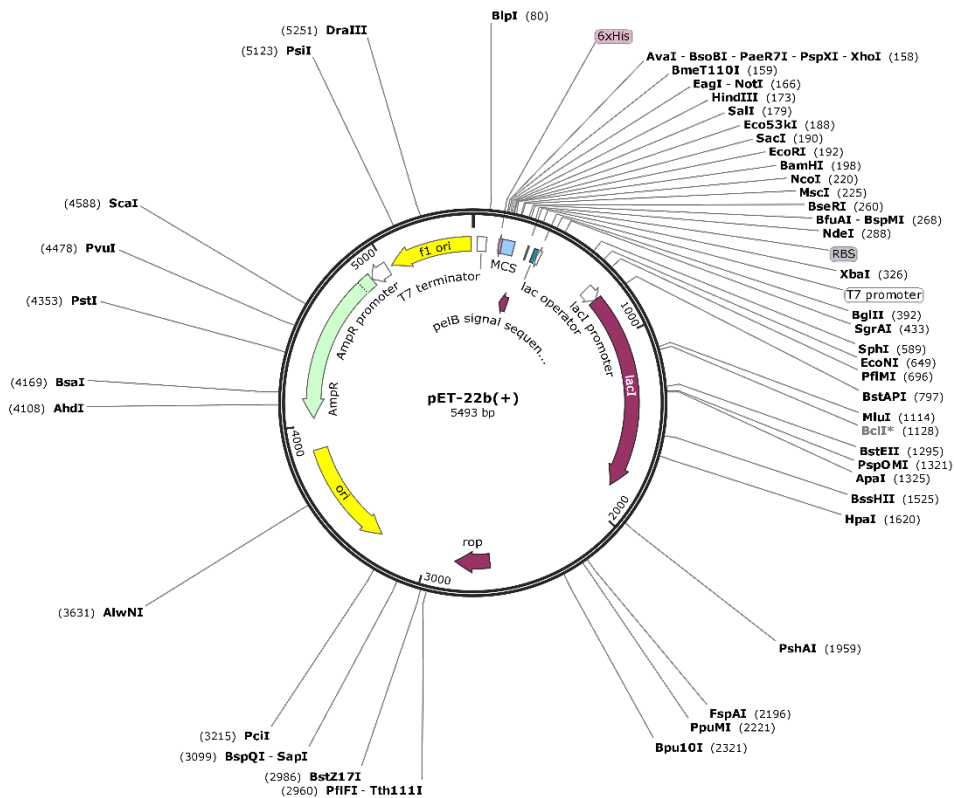
Figure 74: The pET-22b(+) vector was used for the expression of sdabs in *E. coli*.
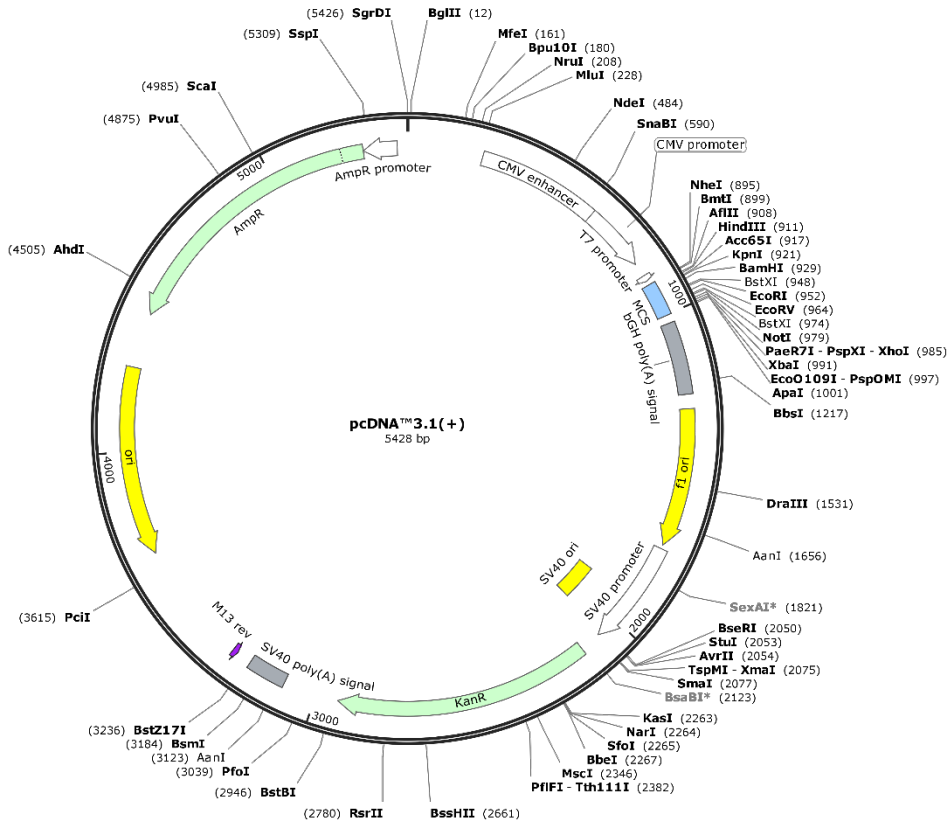
Figure 75: The pcDNA3.1(+)/Zeo vector was used for the expression of huIgE Fc in HEK293 cells.
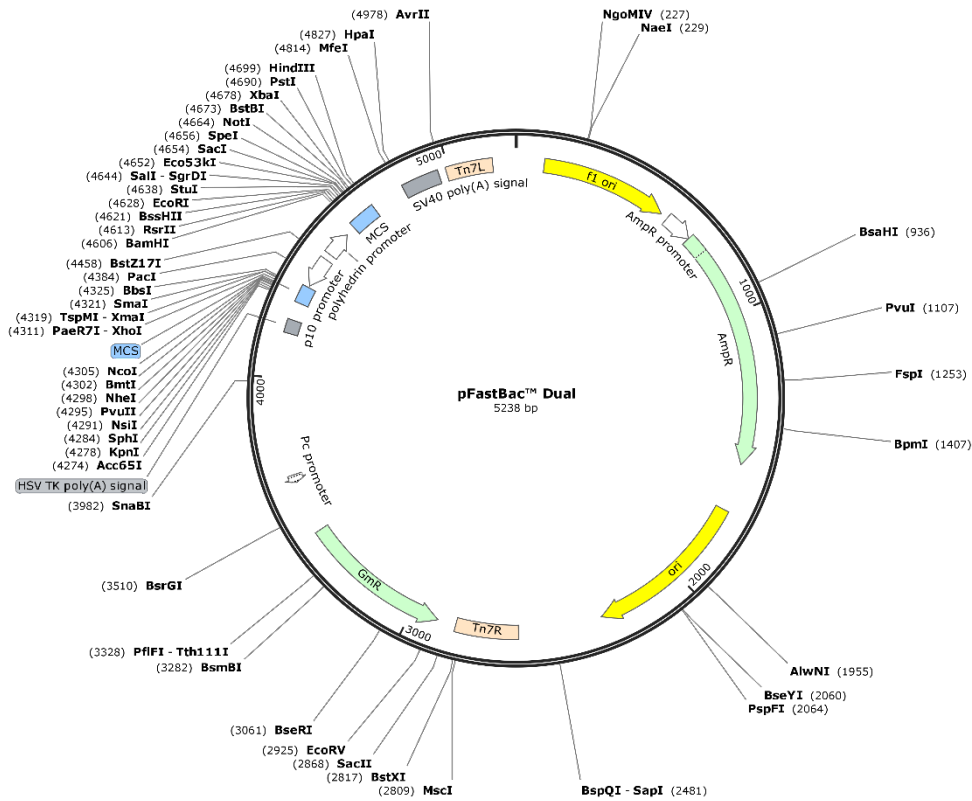
Figure 76: The pFastBac Dual vector was used for the expression of IgE antibodies and Fab fragments in *Sf*9 insect cells.

145

7.8 Oligonucleotides

Name	Sequence (5'-3')
Ig026D34Afwd	tttggtaattatgctatggcatgggtt
Ig026D34Arev	aacccatgccatagcataattaccaaa
Ig026R45Afwd	gcaccgggtaaagctccggaatgggtt
Ig026R45Arev	aacccattccggagctttacccggtgc
Ig026E109Afwd	ctgggtccgaatgcgtttgattattat
Ig026E109Arev	ataataatcaaacgcattcggacccag
Ig026D111Afwd	ccgaatgagtttgcttattatggtcag
Ig026D111Arev	ctgaccataataagcaaactcattcgg
Ig026Y113Afwd	gagtttgattatgctggtcagggcacc
Ig026T113Arev	ggtgccctgaccagcataatcaaactc
pFBD Lige sfi vh for long	gatcggcccattcggcctttgcgcaggtccagctggtgcagtctgggggct
pFBD Lige xho vh rev long	gatcctcgagacggtgaccagggttccctggccccagtagtcaaagta
pFBD Lige not vl for	gatcgcggccgcggctcactctgctttcgcggaaattgtgatgacgcag
pFBD Lige sgs vl rev	gatcggcgcgcccacagttcgtttgatctccacc

7.9 Sicherheit und Entsorgung

Folgende Reagenzien und Lösungsmittel waren mit Gefahrenhinweisen und Sicherheitsratschlägen gemäß §6 der Gefahrstoffverordnung versehen:

Substanz	Gefahrensymbol	H-Sätze	P-Sätze
ABTS		315-319-335	261-305+351+338
Acrylamid		301-312-315-317-319-332-340-350-361f.-372	201-280-301+352-305+351+338
Agar	Kein gefährliches Produkt im Sinne der Richtlinie 67/548/EWG		
Ammoniumpersulfat		272-302-315-317-319-334-335	220-261-280-305+351+338-342+311
Ampicillin		315-317-319-334-335	261-280-305+351+338-342+311
Bovines Serumalbumin (BSA)	Keine gefährlichen Produkte im Sinne der Richtlinie 67/548/EWG		
Bromphenolblau			
5-Brom-4-chlor-3-indoxylphosphat (X-Phos)			
Calciumchlorid-Dihydrat		319	305+351+338
Chloroform		302-315-351-373	302+352-314
Coomassie Brilliant Blau R-250	Keine gefährlichen Produkte im Sinne der Richtlinie 67/548/EWG		
Dimethylsulfoxid			
Dinatriumhydrogenphosphat			
Dithiothreitol (DTT)		302-315-319	302+350-305+351+338
EDTA-Dinatriumsalz-Dihydrat		319	305+351+338

Substanz	Gefahrensymbol	H-Sätze	P-Sätze
Essigsäure (100%)		226-314	280-301+330+331-305+351+338
Ethanol		225	210
Glucose	Keine gefährlichen Produkte im Sinne der Richtlinie 67/548/EWG		
Glycerin			
Imidazol		302-314-361d	280-301+330+331-305+351+338
Kanamycinsulfat		360	201-308+313
Kaliumchlorid	Kein gefährliches Produkt im Sinne der Richtlinie 67/548/EWG		
Magnesiumchlorid	Kein gefährliches Produkt im Sinne der Richtlinie 67/548/EWG		
Milchpulver			
Natriumchlorid	Keine gefährlichen Produkte im Sinne der Richtlinie 67/548/EWG		
Natriumdihydrogenphosphat			
Natriumdodecylsulfat (SDS)		228-302-311-315-319-335	210-280-302+352-403+235
Natriumhydroxid		314	280-305+351+338-310
Ni-NTA-Agarose	Keine gefährlichen Produkte im Sinne der Richtlinie 67/548/EWG		
Nitroblau-Tetrazoliumchlorid (NBT)			
Phenol		301+311+331-314-341-373	280-302+352-304+330+331-309-310-305+351+338
p-Nitrophenylphosphat	Kein gefährliches Produkt im Sinne der Richtlinie 67/548/EWG		
Polyethylenimin (PEI)		301	301+310

Substanz	Gefahrensymbol	H-Sätze	P-Sätze
2-Propanol		225-319-336	210-233-305+331+338
Salzsäure, konz.		314-335	261-280-305+351+338 310
Tetramethylethylendiamin (TEMED)		225-332-302-314	210-233-280-301+330+331-305+351+338
Triethylamin		225-332-312-302-314-335	210-280-301+330+331-302+352-305+351+338
Tris(hydroxymethyl)-aminomethan (Tris)		315-319	302+352-305+351+338
Trypton			
Trypsin	Keine gefährlichen Produkte im Sinne der Richtlinie 67/548/EWG		
Xylen Cyanol FF			
Zeocin			

Alle in dieser Arbeit verwendeten Chemikalien wurden entsprechend ihrer H- und P-Sätzen gehandhabt und nach der Gefahrgutverordnung entsorgt. Organische halogenfreie und halogenhaltige Lösungsmittel wurden getrennt in gekennzeichnete Behälter überführt. Kontaminierte Betriebsmittel wurden in dafür vorgesehenen Behältern gesammelt. Der Umgang mit humanen Zellen wurde ausschließlich auf Laboratorien der Sicherheitsstufe S1 nach §7 GenTG beschränkt. S1-kontaminierter Abfall wurde vor der Entsorgung in einem Autoklav durch unter Druck (5 bar) stehenden Wasserdampf 20 Minuten bei 120 °C hitzesterilisiert.

7.10 Curriculum vitae

Name: Frederic Jabs

Date of Birth: 14th February 1989

Place of Birth: Münster, Germany

Education and Qualifications

Since 06/2014	**University of Hamburg**, Hamburg (Germany)/ **Aarhus University**, Aarhus (Denmark)
	PhD student at Dep. of Organic Chemistry/Dep. of Engineering
	Thesis: "*Molecular basis of IgE specificity and effector functions in allergic diseases.*"
	Supervisor: Prof. Dr. B. Meyer and Assoc. Prof. Dr. Edzard Spillner
2011 - 2014	**University of Hamburg,** Hamburg (Germany)
	Chemistry (M. Sc.)
	Thesis: "*Site-directed mutagenesis and functional characterization of CCD-specific antibodies.*"
	Supervisor: Prof. Dr. R. Bredehorst
2008 - 2011	**University of Hamburg,** Hamburg (Germany)
	Chemistry (B.Sc.)
	Focus on Biochemistry and Molecular Biology
	Thesis: "*Generation of a leporid antibody-library targeting CD137.*"
	Supervisor: Prof. Dr. R. Bredehorst
1999 - 2008	**Gymnasium Nottuln**, Nottuln (Germany)
	Diploma from German secondary school qualifying for university admission or matriculation
1995 - 1999	**St. Martinus Grundschule Nottuln**, Nottuln (Germany)

Conference Contributions

EAACI Congress 2016 in Vienna

Oral Presentation: "Analyses of fine specificity and recognition of alpha-Gal by a monoclonal human IgE."

11. Danish Conference on Biotechnology and Molecular Biology in Vejle

Poster: "Fine specificity and recognition of alpha-Gal by a monoclonal IgE and sera of meat allergic patients."

EAACI Congress 2017 in Helsinki

Oral Presentation: "An anti-IgE single domain antibody disrupts the interaction of IgE with FcεRI by acting as functional high affinity mimic of CD23."

Supervised master theses

The following master theses were (partly) prepared under my supervision and published:

"Functional and structural analysis of therapeutic anti-IgE antibodies."
Brian Mølgaard, Aarhus University, **2016**.

"Facilitated allergen binding by carbohydrate-specific immunoglobulin E."
Marco Mandolesi, Aarhus University, **2017**.

8. Danksagung

9. Eidesstattliche Versicherung

Hiermit versichere ich an Eides statt, die vorliegende Dissertation selbst verfasst und keine anderen als die angegebenen Hilfsmittel benutzt zu haben. Die eingereichte schriftliche Fassung entspricht der auf dem elektronischen Speichermedium. Ich versichere, dass diese Dissertation nicht in einem früheren Promotionsverfahren eingereicht wurde.

_____   _____

Datum, Ort   Frederic Jabs